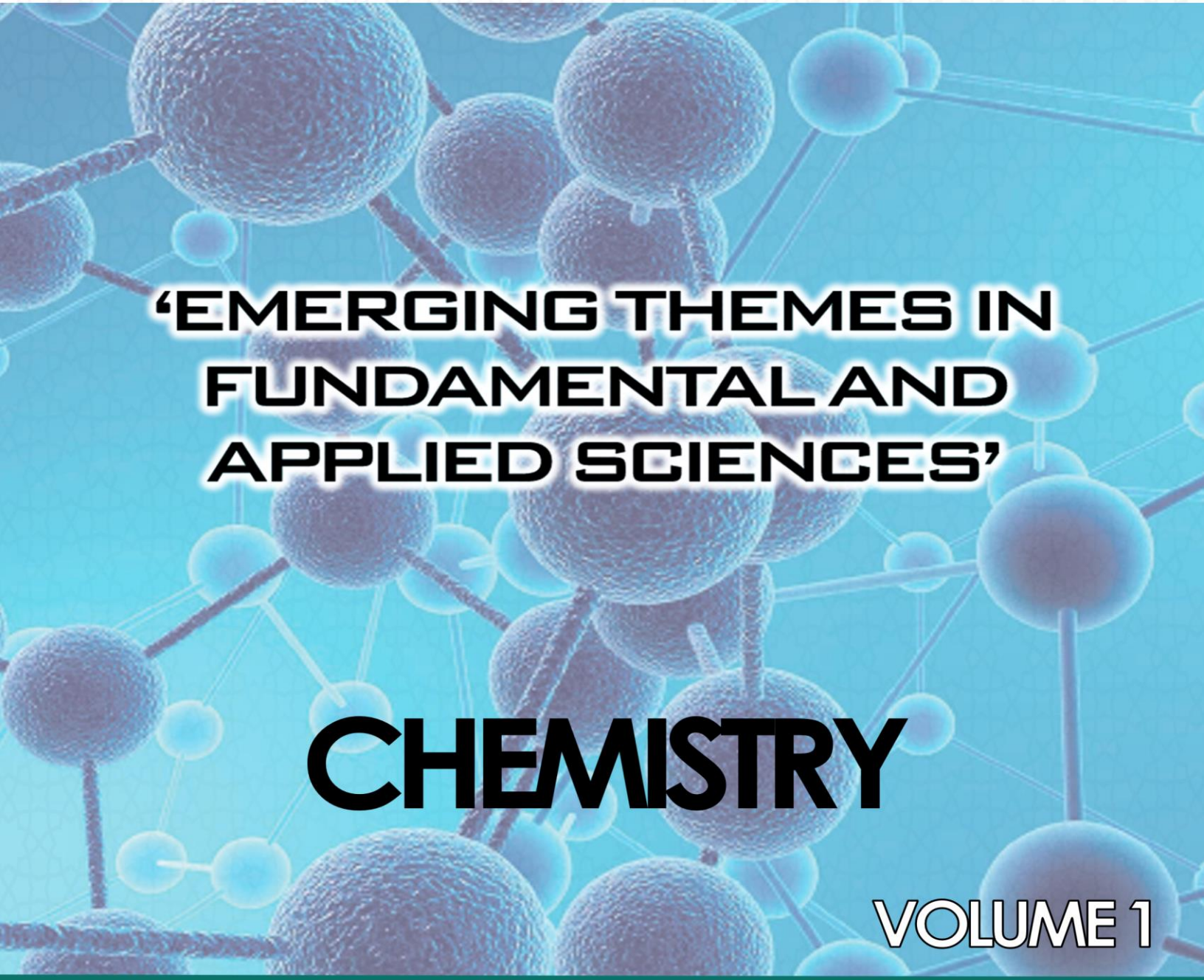

'EMERGING THEMES IN FUNDAMENTAL AND APPLIED SCIENCES'

CHEMISTRY

VOLUME 1

EDITORS

GWENDOLINE EE CHENG LIAN

SHAHRUL AINLIAH ALANG AHMAD

EMERGING THEMES IN FUNDAMENTAL AND APPLIED SCIENCES

Edited by

Gwendoline Cheng Lian Ee

Shahrul Ainliah Alang Ahmad

Faculty of Science
Universiti Putra Malaysia
Serdang
Selangor
Malaysia

UPM Press
Universiti Putra Malaysia
Serdang
Selangor
Malaysia

Volume Pertama /First volume 2017

Diterbitkan di Malaysia oleh/Published in Malaysia by

Penerbit UPM

Universiti Putra Malaysia

43400 UPM, Serdang Selangor

Perpustakaan Negara Malaysia Data pengkatalogan-dalam- Penerbitan

Emerging Themes in Fundamental and Applied Sciences

Editor: Gwendoline Cheng Lian Ee dan Shahrul Ainliah Alang Ahmad

eISBN 978-967-334-778-7

CONTENTS

PREFACE

This book is the first volume of research papers presented at the Fundamental Science Congress 2017 at Universiti Putra Malaysia on November 21-22, 2017.The congress served as a platform for researchers from different parts of Malaysia to share their knowledge and initiate collaboration among themselves. This book presents important research findings in various fields of chemistry ranging from organic, inorganic, environmental, food and physical chemistry. All the authors are researchers in various universities from Malaysia as well as from overseas.

Chapter 2 comprises papers on organic chemistry which cover topics on natural product chemistry, the chemistry of metabolite products of plants, animals, insects, marine organisms and microorganisms. Ionic liquids which have been reported to show excellent antimicrobial properties, by destroying or inhibiting the growth of microorganisms is being investigated as well and the findings is presented in this chapter.

Chapter 3 covers papers related to functional food products one of which is chocolate fortified with pumpkin and taro powders as well as cookies incorporated with breadfruit *(Artocarpus altilis)* flour and nutritional values of yogurt containing breadfruit resistant starch.

Chapter 4 consists of findings from environmental studies on the Selinsing Gold Mine in Pahang, Malaysia. The papers cover mainly the mineralogy of waste dump and stockpile, water quality of gold mine-impacted water and assessment of the compositions of major and trace elements in the soil of this gold mining area in Selinsing, Pahang.

Chapter 5 comprises metal complex reactions in the search for cancer therapeutics comprising transition metal-based complexes as potential leads for anticancer agents to be used in the treatment of cancer.

Chapter 6 covers a paper related to sensor application involving Immobilization of functionality complex on different surfaces which can serve as a good platform to construct redox-active interface for various purposes especially in sensing applications.

CONTRIBUTORS

Preface

Gwendoline Cheng Lian Ee**,** Chemistry Department, Faculty of Science, Universiti Putra Malaysia, 43400 Serdang,
Selangor, Malaysia

Chapter 1 Introduction

Gwendoline Cheng Lian Ee, [1]Chemistry Department, Faculty of Science, Universiti Putra Malaysia, 43400 Serdang,
Selangor, Malaysia

Chapter 2 Biological activities of organic compounds

2.1 A. Muniandy Arumugam[1], Gwendoline Cheng Lian Ee[1]*, Thiruventhan Karunakaran[1], Ka Woong Wong[1], Lim Chan Kiang[2] and Vivien Yi Mian Jong[3]

[1]Chemistry Department, Faculty of Science, Universiti Putra Malaysia, 43400 Serdang, Selangor, Malaysia
[2] Department of Chemical Science, Faculty of Science, Engineering & Technology, Universiti Tunku Abdul Rahman, Kampar, 31900, Perak, Malaysia
[3]Centre of Applied Science Studies, Universiti Teknologi MARA, Kuching, 94300 Sarawak, Malaysia
email: gwen@upm.edu.my

2.2 Nor Hisam Zamakshshari[1*], Gwendoline Cheng Lian Ee[1], Siau Hui Mah[2], Soek Sin Teh [3] and Shaari bin Daud[4]

[1] Chemistry Department, Faculty of Science, Universiti Putra Malaysia, 43400 Serdang, Selangor, Malaysia.
[2] School of Biosciences, Taylor's University (Lakeside Campus), 1, Jalan Taylor's, 47500 Subang Jaya, Selangor, Malaysia.
[3] Energy and Environment, Engineering & Processing Division, Malaysia Palm Oil Board, Bandar Baru Bangi, 4300 Kajang, Selangor, Malaysia.
[4] Faculty of Applied Science, Mara University of Technology Pahang Campus, Bandar Jengka, Pahang Malaysia.
email: shamcute87@gmail.com

2.3 Nur Kartinee Kassim[1*], Lim Pei Cee[1], Amin Ismail[2], Gwendoline Cheng Lian Ee[1] and Khalijah Awang[3]

[1]Chemistry Department, Faculty of Science, Universiti Putra Malaysia, 43400 UPM Serdang, Selangor, Malaysia,
[2]Department of Nutrition and Dietetics, Faculty of Medicine and Health Sciences, Universiti Putra Malaysia, 43400 UPM Serdang, Selangor, Malaysia,
[3]Department of Chemistry, Universiti Malaya, 50603 Kuala Lumpur, Malaysia
email: kartinee@upm.edu.my

2.4 N. N. Abdul Majid[1], H. Ahmad[1*], M. B. A. Rahman[1] and K. Jumbri [2, 3]
[1] Chemistry Department, Faculty of Science, Universiti Putra Malaysia,
43400 UPM Serdang, Selangor, Malaysia
[2] Centre of Research in Ionic Liquids, Universiti Teknologi PETRONAS, 32610 Seri Iskandar, Perak
[3] Department of Fundamental and Applied Sciences, Universiti Teknologi PETRONAS, 32610 Seri Iskandar, Perak
email: haslina_ahmad@upm.edu.my

2.5 Y.Abdulmumin[1] A.M Wudil[2] , A.J Alhassan[2] , A.A Imam[2], I.U Muhammad[2] and K.I Matazu[3]
[1]Department of Science Laboratory Technology, Hussaini Adamu Federal Polytechnic, Kazaure Jigawa State, Nigeria
[2] Department of Biochemistry, Bayero University, Kano,Nigria
[3] Department of Biochemistry, Umar Musa Yaradua University,Katsina
email: yabdulmumin@yahoo.com

Chapter 3 Functional food products

3.1 Shahidan, N., Kahar, N.K., Zakaria, Z., Rois Anwar, N.Z.
Faculty of Bioresources and Food Industry, University Sultan Zainal Abidin, Besut Campus, 22200, Besut, Terengganu, Malaysia
email: norshazila@unisza.edu.my

3.2 Z. Zarinah[1] *, M. Nur Amirah Adilah[2], H.Napisah[3],S.Norshazila[4] & M.N. Siti Nuriah[5]
[1,2,4]Faculty of Bioresources and Food Industry, Kampus Tembila, Universiti Sultan Zainal Abidin, 22200 Besut, Terengganu Darul Iman, Malaysia.
[3,5] Faculty of Health Sciences, Kampus Gong Badak, Universiti Sultan Zainal Abidin, 21300 Kuala Terengganu, Terengganu Darul Iman, Malaysia.
email: napisah@unisza.edu.my

3.3 Z. Zarinah[1] *, S. Noor Aidawati[2], H.Napisah[3],S.Norshazila[4] & M.N. Siti Nuriah[5]
[1,2,4,5] Faculty of Bioresources and Food Industry, Kampus Tembila, Universiti Sultan Zainal Abidin, 22200 Besut, Terengganu Darul Iman, Malaysia.
[3] Faculty of Health Sciences, Kampus Gong Badak, Universiti Sultan Zainal Abidin, 21300 Kuala Terengganu, Terengganu Darul Iman, Malaysia..
email: napisah@unisza.edu.my

Chapter 4 Environmental studies of a gold mine

4.1 S.N.M.S. Hasan[1], F.M. Kusin[1,2], N. Nurnabihah[1], S. Azmin[1], J. Shamshuddin[1], and F.M. Yusuff[3]
[1]Department of Environmental Sciences, Faculty of Environmental Studies, Universiti Putra Malaysia, 43400 UPM Serdang, Selangor, Malaysia

[2]Environmental Forensics Research Unit (ENFORCE), Faculty of Environmental Studies, Universiti Putra Malaysia, 43400 UPM Serdang, Selangor, Malaysia
[3]Department of Land Management, Faculty of Agriculture, Universiti Putra Malaysia, 43400 UPM Serdang, Selangor, Malaysia
email: muniraleeshara@gmail.com

4.2 Hairiyatul Aliyah Abdul Rahim [1], Faradiella Mohd Kusin [2], Noratiqah Masri[3], Sharifah Nur Munirah Syed Hasan[4]

[1,2,3,4]Department of Environmental Sciences, Faculty of Environmental Studies, Universiti Putra Malaysia, UPM, 43400 Serdang, Selangor, Malaysia
email: faradiella@upm.edu.my

4.3 Nor Hayati Che Awang[1], Faradiella Mohd Kusin[2], Sharifah Nur Munirah Syed Hasan[3], Noratiqah Masri[4]

[1]Department of Environmental Sciences, Faculty of Environmental Studies, Universiti Putra Malaysia, 43400 UPM Serdang, Selangor
email: faradiella@upm.edu.my

Chapter 5 Metal complexes reactions

5.1 B. Ahmad, H. Ahmad[*] and S. N. Harun

Chemistry Department, Faculty of Science, Universiti Putra Malaysia, 43400 UPM Serdang, Selangor, Malaysia
email: haslina_ahmad@upm.edu.my

Chapter 6 Sensor applications

6.1 Siti Fatimah Nur Abdul Aziz[1] and Shahrul Ainliah Alang Ahmad[1,2]

[1] Department of Chemistry, Faculty of Science, Universiti Putra Malaysia, 43400 UPM Serdang, Malaysia
[2] Institute of Advanced Technology, Universiti Putra Malaysia, 43400 UPM Serdang, Selangor Malaysia
email: ainliah@upm.edu.my

CHAPTER 1

INTRODUCTION

This multidisciplinary book on applications of different fields of Chemistry ranges from biological activities of organic compounds, to functional food products, environmental studies on water and air and metal complex synthesis and sensor applications.

Natural product chemistry is the chemistry of metabolite products of plants, animals, insects, marine organisms and microorganisms. Plants have been and always will be an important source of new drugs and new drug leads. Drug discovery based on plants have resulted in the development of anticancer agents and continues to contribute to new leads in clinical trials.

DNA was a target for many clinical anticancer drugs before its structure was even discovered. However, research centred on nucleic acids as drug targets have less attraction due to limited structural information on DNA-drug interaction. Since the discovery of nucleic acids structure by Watson and Crick in 1953, enormous progresses in nucleic acid studies have aroused. As a result, many complicated DNA structures have been solved, and this play important roles in providing insights into DNA-drug interactions, especially when DNAs complexes with small molecules. An understanding of the types of chemical interactions that occur between small molecules and DNA is important for predicting the potential physiological and/or therapeutic consequences of such interactions.

Ionic liquids are a novel class of molten salts with melting points below 100 °C. The different combination of cations and anions give ionic liquids unique properties that set driving their widespread application across diverse research areas. Since the late 1970s, ionic liquids have been reported to show excellent antimicrobial properties, by destroying or inhibiting the growth of microorganisms. However, the complete mechanism of action for ionic liquids as antibacterials remains unknown.

Functional foods are increasing in popularity owing to their ability to confer health and physiological benefits. Functional foods are food or food components which may provide health benefits beyond basic nutrition. These food may also play a role in reducing or minimizing the risk of certain diseases. Fruits and vegetables, whole grains, fortified foods and beverages and some dietary supplements are examples of functional food. Recently, new food products which include beneficial components are being developed.

The atmospheric concentrations of key greenhouse gases has increased due to human activities. Climate change resulting from increase in carbon dioxide concentration is mostly irreversible for thousands of years even after carbon dioxide emissions stop. Removal of atmospheric carbon dioxide after emissions has stopped, decreases radiative forcing and slower loss of heat to the ocean, hence, no significant drop of atmospheric temperatures. Other irreversible impacts resulting from increased

atmospheric carbon dioxide concentration from its current levels to a peak level over the coming years are dry-season rainfall reductions. Mining activities can result in water pollution. Distribution of major and trace elements in mine-impacted soil varies according to the different mining activities. It is important to check the water quality and physico-chemical characteristic of water to ensure the safety of the consumer.

CHAPTER 2

BIOLOGICAL ACTIVITIES OF ORGANIC COMPOUNDS

INTRODUCTION

Antibiotic resistance develops as a result of increasing resistance of microbes to present antimicrobial agents. Many researches have been devoted to searching for novel antibacterial and antifungal agents as well as antioxidants. Natural product compounds from plants can be a source of antimicrobials as well as antioxidant agents. Ionic liquids (ILs) which are known as designer liquids have also now increased attention as they can exert a broad spectrum of antimicrobial activity.

2.1 Natural Products from *Garcinia beccarii* and *Garcinia cuneifolia*

Abstract

Our detailed study on the phytochemistry of the stem bark of *Garcinia beccarii* and *Garcinia cuneifolia* resulted in the isolation of six xanthones and two common terpenes. Four xanthones, rubraxanthone, trapezifolixanthone, α-mangostin and *β*-mangostin were isolated from *Garcinia beccarii* while two other xanthones, dulxanthone C and osajaxanthone were obtained from *Garcinia cuneifolia*. Stigmasterol was also found in both plants while -sitosterol was only obtained from *Garcinia cuneifoila*. The structures of these compounds were elucidated using spectroscopic analysis such as 1D and 2D-NMR, GCMS and IR. The hexane extracts of *Garcinia beccarii* and *Garcinia cuneifolia* demonstrated good cytotoxic activities against MCF 7 and HL-60 cancer cell lines.

Keywords: *Garcinia beccarii*; *Garcinia cuneifolia*; xanthones; cytotoxic activities

Introduction

The genus *Garcinia* is a member of the family Clusiacea with over 400 plant species found worldwide (Perry and Metzger, 1980). It is a tropical evergreen tree distributed mainly in Southeast Asia and South America (Obolskiy, 2009). In peninsular Malaysia, there are 49 species found in all types of lowland forests (Nazre, et al, 2009). In Borneo Island inclusive of Sabah and Sarawak this species is found abundantly. This genus possesses phytochemicals with pharmacological effects. It was reported that compounds isolated are mostly xanthones (39%), flavonoids (27%), triterpenoids (10%), benzophenones (8%) and other classes of compounds (16%). Previously *Garcinia* plants have become familiar in the field of ethnomedicine with a recent report of the active principles being used in the treatment of advanced or terminal stage cancer (Al Qathama *et al*.,2016). It is reported that over 30 natural active compounds show good pharmacological effects as anti-migratory compounds for metastasis of melanoma cells. (Al Qathama *et al*., 2016).

Materials and methods

Plant Material

The stem bark of *Garcinia beccarii* (RG5031) and *Garcinia cuneifolia* (RG5034) were collected from Kuching, Sarawak and identified by Dr. Vivien Jong Yi Mian from the Centre of Applied Science, UiTM, Kuching, Sarawak.

Analysis Instrumentation

Infrared spectra were measured using universal attenuated total reflection (UATR) technique on Perkin-Elmer 100 Series FT-IR spectrometer. EIMS were recorded on a Shimadzu GCMS-QP 5050A spectrometer (column, SGE BPX5 30 meter x 0.25 mm I.D x 0.25 µm film thickness, temperature, 200 ^{o} C). NMR spectra were obtained using a JEOL 500 MHz FTNMR spectrometer using $CDCI_3$ as a solvent and tetramethylsilane (TMS) as internal standard. UV spectra were recorded in EtOH on a Shimadzu UV-160A, UV Visible Recording Spectrophotometer. Melting points were obtained on a Leica Galen III instrument.

Extraction and Isolation

The stem bark of *Garcinia beccarii and Garcinia cuneifolia* was dried and ground into fine powder. A total of 2 kg of powder was obtained and used in the extraction process. Hexane, chloroform, ethyl acetate, and methanol were used as the solvents for *Garcinia beccarii* extractions. However only hexane and chloroform were used for the extraction of *Garcinia cuneifolia*. The extractions were 72 hours for each solvent, three times before introducing the next solvent by increasing polarity. After the extractions, the crude extracts obtained were dried by using a rotary evaporator. Column chromatographic techniques were performed on the extracts using silica gel and eluting with different solvent system in increasing polarities. The eluents were dried with a rotary evaporator under reduced pressure. The fractions were monitored with TLC and fractions that show similar spots and characteristics were combined and proceed with further column chromatographic separation and purification to enable the discovery of pure secondary metabolites present in the plant. The separation and purification of the *Garcinia beccarii* extracts led to the isolation of six pure compounds. Four xanthones which are rubraxanthone **(1)**, α-mangostin **(2)**, ß-mangostin **(3)**, trapezifolixanthone **(4)** and two terpenes which are stigmasterol **(5)** and *β*-sitosterol **(6)** were obtained from the extracts. Meanwhile, the separation and purification of the *Garcinia cuneifolia* extracts led to the isolation of two pure xanthone compounds namely dulxanthone C **(7)** and osajaxanthone **(8)** which were obtained from the extracts.

Rubraxanthone (1). Yellow powder; m.p. 208-209^{o}C (Lit. 205-206^{o}C, Lee and Chan, 1977). EIMS m/z (% intensity): 410 ([M^{+}], 15), 341 (100), 311 (20), 299 (35), 288(20), 273(15), 69 (15). IR λ_{max} cm^{-1}, uATR) 3244, 2936, 1599, 1459, 1276. ^{1}H NMR (400 MHz, Acetone-d_6) and ^{13}C NMR (125 MHz, Acetone-d_6) refer Table 1.

α-Mangostin (2). Fine orange crystal; m.p. 180-181˚C (Lit. 182-183 C, Yates *et al*., 1958). IR ν_{max} cm^{-1}: 5423, 3428, 2936, 1706, 1604, 1453, 1284. EIMS m/z (% intensity): 410[M+] (78), 367 (53), 354 (53), 339 (100), 323 (53), 285 (31), 162 (29). ^{1}H NMR (400 MHz,$CDC1_3$): 13.28 (s, 1H, OH-1), 6.79 (s, 1H, H-5), 6.37 (s, 1H, H-4), 5.25 (t, 2H, *J* =

6.9Hz, H-2', 2''), 4.09 (d, 2H, *J* = 6.9Hz, H-1''), 3.77 (s, 3H, OCH_3-7), 3.33 (d. 2H, *J* = 6.9Hz, H-1'), 1.80 (s, 3H, H-5'), 1.75 (s, 3H, H-5''), 1.62 (s, 6H, H-4', 4''). ^{13}C NMR(100 MHz,$CDC1_3$):160.5 (C-1), 110.0 (C-2), 162.4 (C-3), 92.2 (C-4), 154.9 (C-4a), 101.8 (C-5), 155.4 (C-5a), 160.5 (C-6), 143.8 (C-7), 137.0 (C-8), 110.7 (C-8a), 181.9 (C-9), 102.7 (C-9a), 21.1 (C-1'), 122.6 (C-2'), 130.5 (C-3'), 25.0 (C-4') 17.0 (C-5'), 26.0 (C-1''), 124.0 (C-2''), 130.5 (C-3''), 25.1 (C-4''), 17.4 (C-5''), 60.3 (7-OCH_3).

β-mangostin (3). Fine yellow crystal from chloroform; m.p. 172-173 ˚C (Lit. 175-176^o C, Ee *et al*. , 2006). IR λ_{max} cm^{-1} : 5423, 3428, 2936, 1706, 1604, 1453, 1284. EIMS m/z (% intensity):424 [M^+] (53), 381 (16), 369 (20), 353 (100), 335 (17), 299 (21), 169 (10). ^{1}H NMR (400 MHz,$CDC1_3$): 6.48 (s, 1H, H-4), 6.82 (s, 1H, H-5), 3.28 (d, 2H, *J* = 7.3Hz, H-1') 5.24 (t, 1H, *J* = 7.3Hz, H-2'), 1.74 (s, 3H, H-4'), 1.61 (s, 3H, H-5'), 4.09 (d, 2H, *J* = 6.4Hz, H-1''), 5.18 (t, *J* = 6.4Hz, H-2"), 1.80 (s, 3H, H-4''),1.62 (s, 3H, H-5''), 13.61 (s, 1H, OH-1), 3.94 (s, 3H, OCH_3-3), 3.77 (s, 3H, OCH_3-7). ^{13}C NMR (100 MHz,$CDC1_3$): 159.7 (C-1), 111.0 (C-2), 163.7 (C-3), 89.0 (C-4), 155.7 (C-4a), 101.8 (C-5), 155.2 (C-5a), 154.4 (C-6), 143.7 (C-7), 137.3 (C-8), 111.2 (C-8a), 182.1 (C-9), 103.3 (C-9a), 21.0 (C-1'), 122.4 (C-2'), 130.6 (C-3'),17.0 (C-4') 25.1 (C-5'), 26.0 (C-1''), 123.8 (C-2''), 130.7 (C-3''), 17.4 (C-4''), 25.1 (C-5''), 55.7 (3-OCH_3), 60.5 (7-OCH_3)

Trapezifolixanthone (4). Yellow crystals; m.p. of 171-172 ˚C (Lit. 171-172 ˚C, Somanathan *et al*., 1974). IR λ_{max} cm^{-1}: 3364, 2924, 1641, 1584 ; EIMS [M^+] m/z : 378, 364, 363, 335, 305, 174, 154, 137, 81, 69, 55 ; ^{1}H NMR(500 MHz,$CDC1_3$) 7.27 (d, *J*=8.6Hz, H-6), 7.25 (t, *J*=8.6Hz, H-7), 7.35 (d, *J*=8.6Hz, H-8), 6.69 (d, *J*=10.3Hz, H-10), 1.47 (s)H-13, 3.52 (d, *J*=6.9Hz, H-1'), 5.27 (t, *J*=6.9Hz, H-2'), 1.86 (s)H-4', 1.64 (s) H-5', 13.31 (s, 1-OH), 5.73 (s,5-OH). ^{13}C NMR (125 MHz,$CDC1_3$) 155.7 (C-1), 104.2 (C-2), 158.3 (C-3), 107.7 (C-4), 154.0 (C-4a), 146.3 (C-5), 145.5 (C-5a), 120.6 (C-6), 124.0 (C-7), 115.5 (C-8), 121.3 (C-8a), 181.3 (C-9), 103.1 (C-9a), 115.2 (C-10), 127.9 (C-11), 78.2 (C-12), 27.6 (C-13), 27.6 (C-14), 21.1 (C-1'), 122.4 (C-2'), 131.0 (C-3'), 17.3 (C-4'), 25.1 (C-5')

Dulxanthone C (7). Pale yellow powder; m.p. 244-245 ^{o}C (Lit. 245-248 ^{o}C, Chang et al., 1989). IR λ_{max} (cm^{-1}, KBr disc) :3173, 2974, 1646, 1611, 1461, 1126. EIMS m/z (% intensity): 310 ([M^+], 15), 295 (100), 147 (15). ^{1}H NMR(500 MHz, $CDC1_3$) 6.10 (1H, s, H-4), 7.40 (1H,d, *J*=9.2Hz, H-5), 7.44 (IH, dd, *J*=9.2, 2.8, H-6), 7.43 (IH, d, *J*=2.8Hz, H-8), 6.52 (1H, *J*=10.1Hz, H-4'), 5.41 (1H, *J*=10.1 Hz, H-5'), 1.42 (3H, s, H-7'), 1.42 (3H, s, H-8'), 13.05 (OH, s, 1-OH), 8.36 (OH, s, 7-OH). ^{13}C-NMR (125 MHz, $CDC1_3$)162.3 (C-1), 94.19 (C-2), 183.54 (C-3), 56.05 (3OCH-3), 107.07 (C-4), 153.28 (C-4a), 150.21 (C-5),133.03 (C-6), 108.85 (C-7), 136.51 (C-8), 112.47 (C-8a), 181.0 (C-9), 103.64 (C-9a), 21.73 (C-1'), 122.79 (C-2'), 131.57 (C-3'), 18.16 (C-4'), 25.93 (C-5'), 33.52 (C-1''), 122.99 (C-2''), 131.86 (C-3''), 17.85 (C-4''), 25.81 (C-5''), 56.37 (5 OCH_3)

Osajaxanthone (8). Yellow needles with m.p. 247-248^{0}C (Lit, 245-248^{0}C, Chang et al., 1989). IR λ_{max} (cm^-1, KBr disc): 3523, 2924, 1734, 1577, 1271. EIMS m/z (% intensity):310 ([M+], 15), 295 (100), 147 (15). ^{1}H-NMR (500 MHz.$CDC1_3$) 6.33 (s) H-2, 6.72 (s) H-7, 3.50 (2H,d,*J*=6.9Hz, H-1'), 5.25(1H,t, *J*=6.9Hz,H-2'), 1.74 (6H,s H-4'), 1.68 (3H,s H-5'), 3.99 (2H,d H-1"), 5.34 (1H, *J*=6.9, H-2"), 1.83 (3H,s H-5"), 13.39 (s) 1-OH,

3.89 (3H,s 3-OCH_3), 3.98 (3H,s 5-OCH_3). ^{13}C- NMR(100 MHz, acetone-d_6) 157.1 (C-1), 104.0 (C-2), 160.5 (C-3), 94.6 (C-4), 157.4 (C-4a), 119.6 (C-5), 124.1 (C-6), 153.3 (C-7), 108.7 (C-8), 120.8 (C-8a), 180.5 (C-9), 103.2 (C-9a), 149.8 (C-10a), 115.2 (C-4'), 127.3 (C-5'), 77.2 (C-6'), 29.8 (C-7'), 29.8 (C-8')

Results and discussion

Rubraxanthone **(1)**, a yellow powder with melting point of 208-209˚C (Lit. 210˚C, Ampofo and Waterman, 1986) was successfully isolated. This pure compound was obtained from the chloroform, ethyl acetate and methanol extracts. The fractions that exhibit the same characteristics and R_f value of this compound were combined and column chromatographed several times to yield the pure compound and in a larger amount. The mass spectroscopic analysis showed the occurrence of a molecular ion peak at *m/z* 410 which resembles a molecular formula of $C_{24}H_{26}O_6$. The presence of a geranyl unit was confirmed by the fragment ion, $[M - 69]^+$ and $[M - 123]^+$ while its position at C-8 was indicated by $[M - 111]^+$, a fragment typical of 8-geranyl-7-methoxy xanthone (Ampofo and Waterman, 1986).

The FTIR spectrum exhibited a strong band at 3244 cm^{-1} (phenolic hydroxyl), 1276 cm^{-1} (chelated carbonyl), 1599 cm^{-1} (conjugated C=C), and 1439 cm^{-1} (carbonyl functionalities).

In the ^{1}H-NMR spectrum , the existence of a pair of meta-coupled aromatic protons were observed at *δ*6.17 (1H, *d*, *J* = 1.8 Hz) and *δ*6.29 (1H, *d*, *J* = 1.8 Hz). Moreover, the presence of a chelated hydroxyl group was indicated at a signal *δ*13.48 in the spectrum. The singlet peaks at signals *δ*6.82 and *δ*3.78 reveal the presence of a lone aromatic proton and a methoxyl group.

The ^{13}C-NMR spectral data experiment showed a total of 24 carbon signal indicative of four sp^3 methyl, three sp^2 methylene, five sp^3 methine and twelve quaternary carbons with the aid from the DEPT NMR. The ^{13}C – ^{1}H correlations for all protonated carbons of rubraxanthone **(1)** were observed in the HMQC spectrum.

From the HMBC spectrum, the chelated hydroxyl group, *δ* 13.48 (OH-1) gave a ^2J correlation with C-1 (*δ* 164.7) and ^3J correlations with C-2 (*δ* 97.9) and C-9a (*δ* 102.8) which confirms the position of OH-1. The methylene proton of H-1' from the geranyl moiety gave ^2J correlations with C-8 (*δ* 137.4) and C-2' (*δ* 123.9) while ^3J correlations were observed for C-8a (*δ* 111.1), C-7 (*δ* 143.8) and C-3' (*δ* 134.3) which confirmed the position of the geranyl moiety at C-8 (*δ* 137.4). The assignments of the substituents to the xanthone nucleus were carried out by analysing the correlations in the HMBC spectrum and confirmed by comparison of rubraxanthone **(1)** physical data with the literature values. Rubraxanthone **(1)** was therefore identified as 8-geranyl-7-methoxy-1,3,6-trihydroxyxanthone and the assignments of rubraxanthone **(1)** along with spectral data are summarized in Table 1. This compound **(1)** was reported to have been previously isolated from the pericarp of *Garcinia mangostana* (Mohamed, *et al.*, 2014).

The hexane extract of *Garcinia becarii* was found to be active against MCF 7 (breast cancer) cell line with an IC_{50} value of 1.75 µg/ml and HL-60 (leukemia) cell line with an IC_{50} value of 4 µg/ml. Meanwhile the chloroform and methanol crude extract

demonstrated moderate cytotoxic activities against the MCF 7 and HL-60 cell lines. However, the methanol extract was found to be moderately active against HL-60 cell line with an IC_{50} value of 16.60 µg/ml but was not active against MCF 7 cell line. The hexane and chloroform extracts of *Garcinia cuneifolia* was subjected to cytotoxic analysis against the HL-60 and MCF 7 cell lines as well. It resulted in the hexane extract giving IC_{50} values of 11.37 µg/ml and 10.14 µg/ml against MCF 7 and HL-60 cell lines respectively. However there was no activity for the chloroform extracts on both cell lines under investigation. The antimicrobial activity test was also carried out using six pathogenic bacteria, namely, *Bacillus Subtilis B29, Bacillus Subtilis B145, Staphylococcus aureus S276, Staphylococcus epidermidis S273, Methicilin Resistant Staphylococcus aureus and Streptococcus sp*. However, only moderate inhibitions on these bacteria were observed for the extracts.

Conclusion

Phytochemical and biological studies on *Garcinia becarii* and *Garcinia cuneifolia* discovered the presence of several triterpenoids and xanthones. *Garcinia Beccarii* (stem bark) afforded *stigmasterol, β-sitosterol, α-mangostin, β-mangostin and trapezfolioxanthone.* Meanwhile, studies on *Garcinia cuneifolia* (stem bark) revealed the presence of two xanthones, *dulxanthone C and osajaxanthone.* This is the first report on the phytochemistry of *Garcinia beccarii*. The hexane extracts of *Garcinia beccarii* and *Garcinia cuneifolia* demonstrated good activity against MCF 7 and HL-60 cancer cell lines suggesting that these two plants could be a good source of lead compounds to be used as drug candidates in the treatment of breast cancer and leukemia. Also in this investigation rubraxanthone and *α*-mangostin were found abundantly from *Garcinia beccarii.* It is recommended that for the future studies, these compounds can be used for semi synthesis modification of the structures to get good or better activities. Therefore this is an opportunity to isolate natural compounds from this species and modify them to get more lead compounds for drug discovery.

Acknowledgements

The authors express gratitude to the Malaysian Ministry of Higher Education for providing financial support under the FRGS research grant and Universiti Putra Malaysia for providing research facilities and technical support. The Sarawak Biodiversity Centre (SBC) is acknowledged.

References

Al-Qathama, A. J., Ezuruike, A. F., Mazzari, A., Yombawi, A., Lopez-Soriano, C., Fuchs, M., & Prieto, J. M. (2016). Cytotoxic and antimigratory properties of popular Nigerian medicinal plants. *Planta Medica*, *81*(S 01), 313.

Ampofo, S. A., & Waterman, P. G. (1986). Xanthones from three *Garcinia* species. *Phytochemistry, 25*(10), 2351-2355.

Chang, C.H., Lin, C.C., Hattori, M., & Namba, T. (1989). Four prenylated xanthones from *Cudrania cochinchinensis*. *Phytochemistry*, 28, 595–598.

Ee, G. C. L., Daud, S., Taufiq-Yap, Y. H., Ismail, N. H., & Rahmani, M. (2006). Xanthones from *Garcinia mangostana* (Guttiferae). *Natural Product Research, 20*(12), 1067-1073.

Lee, Y., & Chan, S. I. (1977). Effect of lysolecithin on the structure and permeability of lecithin bilayer vesicles. *Biochemistry*, *16*(7), 1303-1309.

Mohamed, G. A., Ibrahim, S. R., Shaaban, M. I., & Ross, S. A. (2014). Mangostanaxanthones I and II, new xanthones from the pericarp of *Garcinia mangostana*. *Fitoterapia*, *98*, 215-221.

Nazre, M., Latiff, A., & Mohamad-Roslan, M. K. (2009). Effect of topography and soil on the distribution of under canopy trees of *Garcinia* (Guttiferae) in lowland forest of Peninsular Malaysia. *International Journal of Botany*, *5*(4), 287-294.

Obolskiy, D., Pischel, I., Siriwatanametanon, N., & Heinrich, M. (2009). *Garcinia mangostana* L.: a phytochemical and pharmacological review. *Phytotherapy Research*, *23*(8), 1047-1065.

Perry, L. M., & Metzger, J. (1980). *Medicinal plants of East and Southeast Asia: attributed properties and uses*. MIT press.

Somanathan, R., & Sultanbawa, M. U. S. (1974). Chemical investigation of ceylonese plants. Part VIII. Trapezifolixanthone, a new di-isoprenylated xanthone from the bark of *Calophyllum trapezifolium* Thw.(Guttiferae). *Journal of the Chemical Society, Perkin Transactions 1*, 2515-2517.

Table 1

^{1}H-NMR (400MHz, Acetone-d_6), ^{13}C-NMR (100MHz, Acetone-d_6) and HMBC assignments for rubraxanthone **(1)**.

Position	^{1}H (δ)	^{13}C (δ)	HMBC
1	13.48 (*s*, OH)	164.1 (C)	C-2, C-1 C-9a
2	6.17 (1H, *d*, *J* = 1.8Hz)	97.9 (CH)	C-9a
3	-	164.7 (C)	-
4	6.29 (1H, *d*, *J* = 1.8Hz)	92.9 (CH)	C-4a
5	6.82(1H, *s*)	101.9 (CH)	C-5a, C-6a, C-8a
6	-	156.8 (C)	-
7	-	143.8 (C)	-
8	-	137.4 (C)	-
9	-	181.9 (C=O)	-
4a	-	157.2 (C)	-
5a	-	155.5 (C)	-
8a	-	111 .1 (C)	-
9a	-	102.9 (C)	-
1’	4.10 (2H, *d*, *J* = 6.72Hz)	25.9 (CH_2)	C-7, C-8, C-2’, C-3’, C-8a
2’	5.25 (1H, *t*, *J* = 6.72Hz)	123.9 (CH)	C-8’
3’	-	134.3 (C)	-
4’	1.97 (2H, *d*, *J* = 6.72Hz)	39.6 (CH_2)	C-2’, C-3’, C-5’, C-8’
5’	1.95 (2H, *d*, *J* = 6.72Hz)	26.5 (CH_2)	C-4’, C-2’, C-3’
6’	5.02 (1H, *t*, *J* = 5.48Hz)	124.3 (CH)	-
7’	-	130.8 (C)	-
8’	1.81 (*s*, 3H)	15.7 (CH_3)	C-2’, C-3’
9’	1.53 (*s*, 3H)	29.9 (CH_3)	C-10’
10’	1.30 (*s*, 3H)	16.8 (CH_3)	C-9’
7-OCH_3	3.78 (*s*, OCH_3)	60.5 (O-CH_3)	C-7

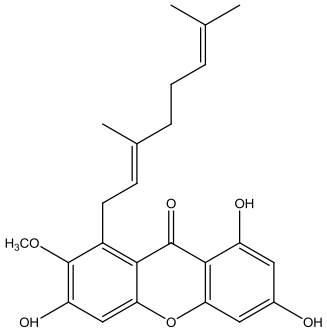

(1)

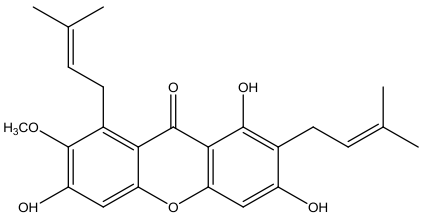

(2)

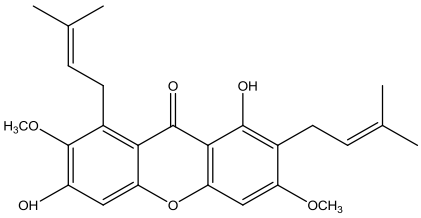

(**3**)

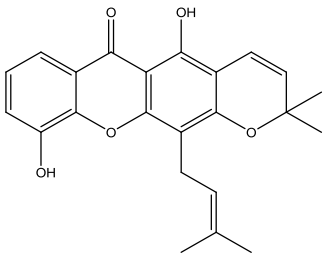

(**4**)

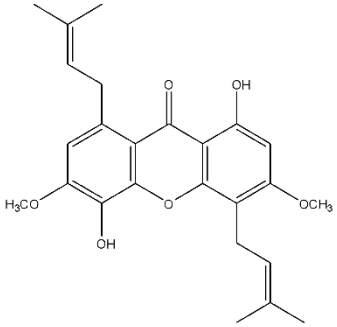

(**7**)

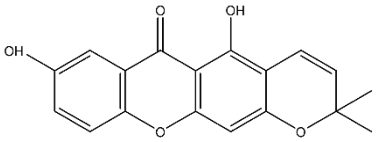

(**8**)

Figure 1: Structures of xanthones

2.2 Anti-oxidant activities of *Morinda citrifolia* and their phytochemical studies

Abstract

An investigation on the antioxidant activities of different extracts of *Morinda citrifolia* were carried out using 3 different assays, beta-carotene bleaching and Ferric reducing antioxidant power (FRAP) and nitric oxide scavenging activity assays . In beta-carotene bleaching assay, the dichloromethane extract gave the highest percentage of β-carotene bleaching which is 13.58 % at 100 µg/ml. The FRAP assay also showed the dichloromethane extract to possess the highest FRAP value which is 3.03 GAE compared to the other extracts. Meanwhile, good nitric oxide scavenging activity was shown by the dichloromethane extract with an IC_{50} value of 165.59 µg/ml. The total phenolic content (TPC) test to determine the amount of phenolic compound content in each extract indicated the highest total phenolic content in the dichloromethane extract which is 122.79 GAE. Phytochemical studies on each extract resulted in the isolation of four anthraquinone compounds, nordamnacanthal (**1**), sorendidiol (**2**), 1,3-dihydroxy-2-methoxy anthraquinone (**3**) and lucidin-ω-methyether (**4**). The structures of these compounds were elucidated using spectroscopic analysis such as GCMS, IR, UV ^{1}D and ^{2}D-NMR.

Keywords: Antioxidant activities; total phenolic content; *Morinda citrifolia*, anthraquinones

Introduction

Plants are significantly important for human beings such as for respiration, food, medicine and many more. Plants have been used in medicine for a long time by human civilization in treatments to cure diseases. Previous scientific studies have shown that several therapeutic properties of plants that are usually used in old folk medicines have contributed to the development of drugs which are obtained from isolation from plants (Filho et al, 2009). *Morinda* species are known as traditional folk medicine for the treatment of many diseases including diabetes, hypertension, and cancer (Kamiya et al, 2004). *Morinda citrifolia* is known as *mengkudu* by locals in Malaysia. It is a small tree (3 to 8 meters tall). The fruit it soft and have a strong smell. This species grow on a wide range of soils and harsh environmental condition like brackish tide pools, lime stone soils or outcroppings on coral atolls (Selvan, 2007). Reactive oxygen and reactive nitrogen species are generated in the human body by energy transfer processes and enzymatic reactions (Schulz, 2005). An increase in the level of reactive oxygen species will lead to disorders and diseases such as atherosclerosis, neurodegenerative disorder, aging and cancer (Apea-Bah, 2016). Inhibiting reactive oxygen species and radical molecules might reduce these disorders and diseases. Phenolic compounds are known to have antioxidant properties which will protect cells from reactive oxygen and reactive nitrogen species. These phenolic compounds usually exhibit oxidative activities via several mechanisms of action. The mechanisms involve singlet oxygen quencher,

hydrogen donating antioxidant, free radical scavenger and metal ions chelator (Ruhomally et al, 2015). Activities of extracts might be due to the phenolic compounds in the extracts (Saeed et al, 2012).

Materials and methods

Plant Collection

The root bark of *Morinda citrifolia* was collected from Negeri Sembilan, Malaysia and identified by Professor Dr. Rusea Go from biology department, University Putra Malaysia. A voucher specimen was deposited in the Herbarium of Biology Department, Faculty of Science, University Putra Malaysia.

Plant Extraction

The collected plant sample was dried under open air and ground into fine powder. The powdered root bark of *Morinda citrifolia* (0.9 kg) was macerated three times in four different solvents such as hexane, dichloromethane, ethyl acetate and methanol for 72 hours. The macerated sample was filtered and evaporated under reduced pressure to obtain dry extracts of methanol (35 g), ethyl acetate (19 g), dichloromethane (18 g) and hexane (11 g). Two techniques were used to obtain twelve anthraquinone compounds which are column chromatography (vacuum and gravity) and preparative thin layer chromatography. Nordamnacanthal (**1**) was successfully isolated from the hexane extract. Meanwhile, sorendidiol (**2**) was successfully isolated from the semi polar extracts (ethyl acetate and dichloromethane). Finally, the methanol extract gave 1,3-dihydroxy-2-methoxy anthraquinone (**3**) and lucidin-ω-methyether (**4**). The structures of these compounds were elucidated using spectroscopic analysis such as GCMS, IR, UV ^{1}D and ^{2}D-NMR.

Total Phenolic Content (TPC)

The total phenolic content was determined using the Folin-Ciocalteu assay, conducted according to a protocol of Kahkonen *et al.* (1999).

Antioxidant assays

The β-carotene bleaching (BCB) assay was conducted according to a protocol of Kassim et al (2013). The Ferric Reducing Power (FRAP) of the extracts and gallic acid were determined according to Ozturk *et al.* (2007). The Nitric oxide scavenging activities of the extracts and gallic acid were determined using a method by Tsai *et al.* (2007).

Statistical Analysis

The anti-oxidant test and phytochemical analysis data were represented as mean ± standard deviation and were carried out in triplicate independent analyses. The graphs were generated using Microsoft Excel Software (Version 2010). Data were analysed using one-way ANOVA by turkey post hoc test (SPSS 14.0) while independent sample T-test (SPSS 14.0) was used to determine any significant difference between samples and standard drugs. Pearson correlation (SPSS 14.0) was used to determine the relationship between phytochemical analyses with anti-oxidant activities. The significance level was set at $p < 0.05$.

Results and discussion

In the total phenolic content test, gallic acid was used as a standard. The standard curve for gallic acid was obtained from the calibration equation, y = 0.00458x + 0.0457(R^2 = 0.9997) where y is the absorbance and x is the weight of gallic acid present. The highest total phenolic content was found in the dichloromethane extract which is 122.789 GAE. Meanwhile, the methanol extract had the lowest value of total phenolic content which was 21.431 GAE. Results are shown in Figure 2. Meanwhile, in β-carotene bleaching, BHT is used as a standard drug in order to compare with the samples. The extract with the highest percentage of β-Carotene bleaching was dichloromethane extract which is 13.58 % at 100µg/ml. Compared to the standard drug, all the *Morinda citrifolia* extracts showed weak activities in inhibiting lipid peroxidation (see Figure 2). In Frap assay, the methanol extract gave the lowest reducing power activity compared to the hexane, dichloromethane and ethyl acetate extracts. This may be due to less phenolic compounds present in the methanol extract. The highest reducing power activity was shown by the dichloromethane extract. The nitric oxide scavenging activities were carried out for all the extracts of *Morinda citrifolia.* The IC_{50} values for all the extracts and gallic acid are listed in Table 1. The results reveal that the non-polar and polar extracts showed weak inhibition towards nitric oxide radicals as compared to the semi polar extract. The dichloromethane extract is the most potent inhibitor as it removed the nitric oxide at a lower concentration compared to the other extracts. Surprisingly, the dichloromethane extract showed a nitric oxide scavenging activity as good as water extract of *Camella sinensis* (Tsai et. al., 2007).

Table 1: IC_{50} values of extracts and gallic acid against nitric oxide radical scavenging activity.

Plant Species	Extract	IC_{50} (µg/mL)
Morinda citrifolia	Hexane	>1000
	Dichloromethane	165.5916 ± 1.3706*
	Ethyl acetate	172.3612 ± 1.0807*
	Methanol	>1000
Standard drug	Gallic Acid	26.621 ± 1.3835

* denotes significant difference between samples and standard drug ($p<0.05$).

Correlation studies were carried out to determine the role or mechanism of phenolic compounds in extracts towards antioxidant activities. Strong correlations were observed between the total phenolic content and ferric reducing power ($r^2(4) = .962$, $p = 0.038$). Most of the phenolic compounds present in these extracts can reduce the Fe^{3+} complex to Fe^{2+} complex. Similarly, the strong correlations observed between the total phenolic content and nitric oxide scavenging assay proved that the inhibition of nitric oxide production was contributed by phenolic compounds ($r^2(4) = -.927$, $p = 0.073$). Unfortunately, the weak correlation between the total phenolic content and β- carotene bleaching showed that not all phenolic compounds in this species have the ability to inhibit lipid peroxidation ($r^2(4) = .254$, $p = 0.746$). Each antioxidant assay measures the antioxidant activity based on different reaction mechanisms leading to different

antioxidant results. The differences in antioxidant activities from their phytochemical analysis are due to the properties of the individual compounds in the mixture. The differences in antioxidant activities may also be due to several effects such as combination, synergistic and antagonism effect. Combination effect from two or more compounds in an extract may increase the antioxidant activities or vice versa. Meanwhile, the diverse types of compounds that have antioxidant and pro-oxidant properties will lead to changes in activities caused by synergies and antagonism effect (Hincapie *et al,* 2011).

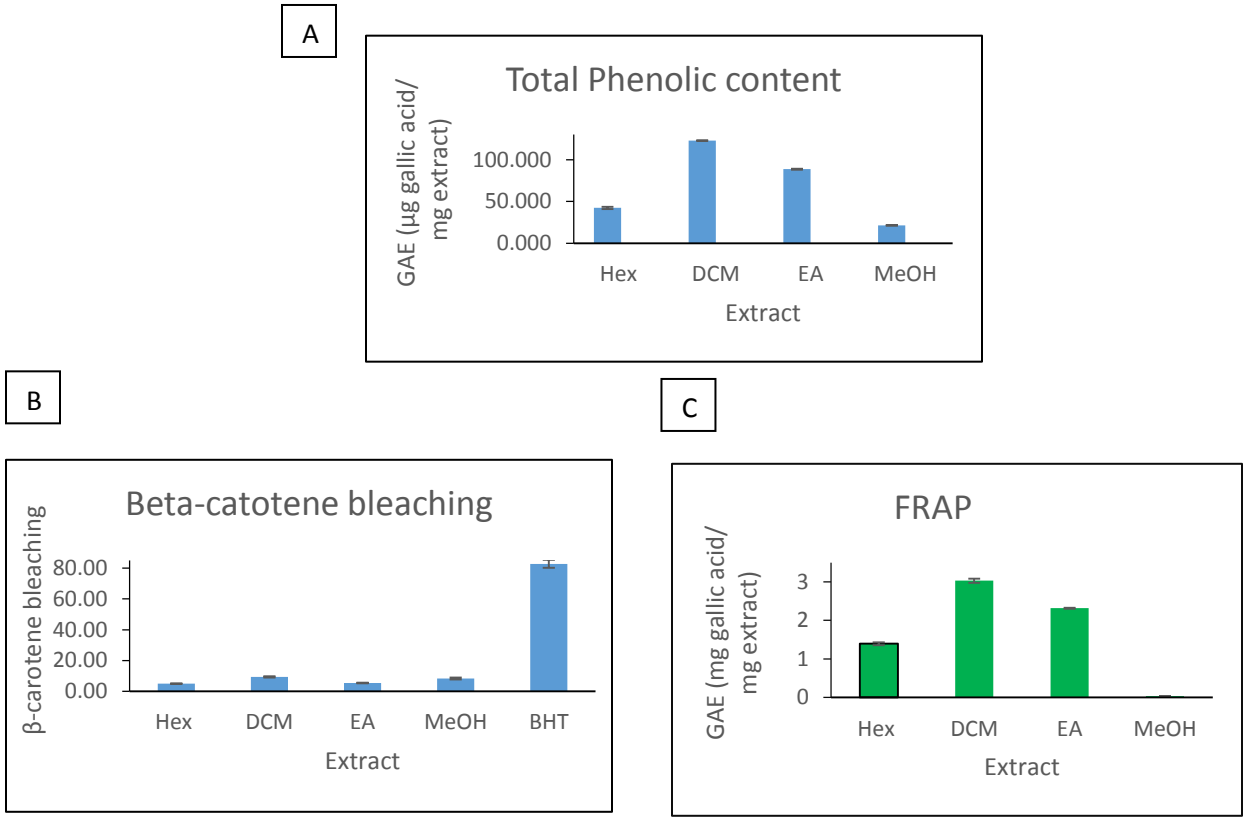

*a-d denote a significant difference between samples ($p<0.05$).
* denotes significant differences between samples and standard drug ($p<0.05$)
*Hex=hexane, DCM = dichloromethane, EA=ethyl acetate, MeOH=methanol

Figure 2: A) Total phenolic content of crude extract in GAE, B) Beta-Carotene Bleaching activities of extracts and standard drug at 100 µg/mL, C) Ferric reducing antioxidant power (FRAP) of extracts.

Isolation work on *Morinda citrifolia* resulted in the isolation of 4 antraquinones. They are nordamnacanthal (**1**), sorendidiol (**2**), 1,3-dihydroxy-2-methoxy anthraquinone (**3**) and lucidin-ω-methyether (**4**).

Nordamnacanthal (1), Yellow needle crystal; m.p: 219-222ºC (literature 218-220ºC, Prista et. al., 1965) IR ν_{max} cm^{-1}: 2928, 1734, 1649, 1356, 1274; UV (EtOH) λmax 290 and 246nm; EI-MS m/z: 268, 240, 212, 184, 128, 69. ^{1}H and ^{13}C- NMR spectra are consistent with literature (Kamiya et. al., 2010).

Sorendidiol (2), Yellow needle crystal; m.p: 286-288ºC (literature 287-288ºC, Briggs et. al., 1952) IR ν_{max} cm^{-1}:3295, 2930, 1740, 1561, 1440, 1294 and 1108; UV (EtOH) λmax nm: 412 and 320; EI-MS m/z: 254, 225, 197, 139, 115 . ^{1}H and ^{13}C- NMR spectra are consistent with literature (Kamiya et. al., 2010).

1,3-dihydroxy-2-methoxy anthraquinone (3), Yellow needle crystal; m.p: 218-220ºC (literature 219-220ºC, Roberge and Brassard, 1981); IR ν_{max} cm^{-1}: 3410, 2926, 1639, 1581, 1452, 1382 and 1276; UV(EtOH) λmax nm: 411, 245 and 205; EI-MS m/z: 270, 252, 227, 196, 115. ^{1}H and ^{13}C- NMR spectra are consistent with literature (Roberge and Brassard, 1981).

Lucidin-ω-methyether (4), Orange-Yellow powder; m.p: 170-173ºC (literature 170ºC, Chang and Lee, 1984) IR ν_{max} cm^{-1}: 3142, 2924, 1672, 1573, 1367, 1332 and 1273 ; UV(EtOH) λmax nm: 419, 325 and 226; EI-MS m/z: 284, 252, 196, 168. ^{1}H and ^{13}C-NMR spectra are consistent with literature (Chang and Lee, 1984).

Conclusion

The semi polar extract of this species demonstrates a good antioxidant activity. The pure compounds present in *Morinda citrifolia* will be tested for their antioxidant activities to determine any potential lead compounds which can be drug candidates for antioxidant drugs.

Acknowledgements

The authors would like to acknowledge financial support from UPM under the PUTRA grant and research facilities.

References

Apea-Bah, F. B., Minnaar, A., Bester, M. J., and Duodu, K. G., (2016). Sorghum–cowpea composite porridge as a functional food, Part II:Antioxidant properties as affected by simulated in vitro gastrointestinal digestion, *Food Chemistry* 197:307–315.

Briggs, L. H., Nicholls, G. A., and Peterson, R. M. L., (1952). Chemistry of the Coprosma genus. VI Minor antraquinone coloring matters from *Cosprosma australlis. Journal of Chemistry Society*, 1718-1722.

Chang, P., and Lee, K. H., (1984). Cytotoxic antileukimic antraquinones from *Morinda parvifolia*. *Phytochemistry*, 23:1733-1736.

Filho, C., Meyre, V., Silva, C., & Niero, R. (2009). Chemical and pharmacological aspects of the genus *Calophyllum*. *Chemistry & Biodiversity,* 6: 313-327.

Hincapie, C. A., Monsalve, Z., Seigler, D. S., Alarcon, J., and Cespedes, C. L., (2011). Antioxidant activity of *Blechnum chilense* (Kaulf.) Mett., *Curcuma domestica* Valeton and *Targetes verticillata* Lag. and Rodriquez. *Buletin Latinoamericano y del Caribe de Plantas Medicinales y Aromaticas 10:* 315-324.

Kamiya, K., Tanaka, Y., Endang, H., Umar, M., and Satake, T., (2004). Chemical Constituents of *Morinda citrifolia* Fruits Inhibit Copper-Induced Low-Density Lipoprotein Oxidation*, J. Agric. Food Chem. 52*: 5843-5848.

Kahkonen, M.P., Hopia, A.I., Vuorela, H.J., Rauha, J.P., Pihlaja, K. and Kujala, T.S., (1999). Antioxidant activity of plant extracts containing phenolic compounds*. Journal of Agricultural and Food Chemistry, 47*:3954-3962.

Kassim, N. K., Rahmani, M., Ismail, A., Sukari, M. A., Ee, G. C. L., Nasir, N. M., and Awang, K., (2013). Antioxidant activity-guided separation of coumarins and lignan from *Melicope glabra* (Rutaceae). *Food Chemistry, 139*: 87–92.

Öztürk, M., Aydoğmus-Öztürk, F., Duru M. E., and Topçu, G., (2007). Antioxidant activity of stem and root extracts of Rhubarb (*Rheum ribes*): an edible medicinal plant. *Food Chem, 103*: 623-630.

Prista, L. N., Roque, A. S., Ferreira, M.A. and Alves, A. C., (1965). Chemical study of *Morinda geminates*. I. Isolation of morindone, damnacanthal, nor-damnacanthal and rubiadin-1-methyl ether. *Garcia de Orta 13*: 19-38.

Ruhomally, Z., Somanah, J., Bahorun, T., and Neerghee-bhujun, V. S., (2015). *Morinda citrifolia* L. fruit extract modulates H_2O_2 – induced oxidative stress in human liposarcoma SW872cell. *Journal of traditional and complementary medicine, 6:* 299-304.

Roberge, G., and Brassard, P., (1981). Reactions of ketene acetals13. Synthesis of contiguously trihydroxylated naphtha and Antraquinones*. J. org. Chem., 46:*4161-4166.
Selvan, V., (2007). Trees and shrubs of the Maldives, Thammada Press Co., Ltd., Bangkok, 2007, ©FAO regional office for Asia and the pacific.

Schulz, W.A., (2005). Molecular biology of human cancer: An advanced student's textbook, Springer Science + Business media, Inc, United States of America.

Saeed, N., Khan M. R, and Shabbier, M., (2012). Antioxidant activity, total phenolic and total flavonoid content of whole plant extract *Torilis leptophylla* L. *Complementary and alternative medicine, 12:*221.

Tsai, P.-J., Tsai, T.-H., Yu C.-H., and Ho, S.-C., (2007). Comparison of NO-scavenging and NO-suppressing activities of different herbal teas with those of green tea*, Food Chemistry, 103*:181–187.

2.3 New Antioxidant Glycoside from *Melicope glabra* (*Rutaceae*)

Abstract

Bioassay-guided chromatographic separation of the active ethyl acetate extract of *Melicope glabra* bark has resulted in the isolation of a new glycosides (1). The structure was elucidated by a combination of spectroscopic techniques including UV, IR, MS, 1D-NMR and 2D-NMR. The antioxidant activity of eluted fraction and pure compound were evaluated using *β*-carotene bleaching antioxidant assays. The inhibition of lipid peroxidation of the new compound was comparable to the standard used in *β*-carotene bleaching antioxidant assays.

Keywords: *Melicope glabra*; antioxidant; glycoside; *β*-carotene bleaching

Introduction

Oxidative damage to DNA by free radicals has long been associated with the onset of cancer as well as cardiovascular and neurodegerative diseases (Moon & Shibamoto, 2009; Paz-Elizur *et al.,* 2008). Antioxidants are capable of interrupting free radical chain reactions, hence preventing oxidative damage thereby reducing the risk of onset of these diseases (Stanner, Hughes, Kelly & Buttriss, 2004). Plant-derived antioxidants such as vitamin E (tocopherol and tocotrienol), ascorbic acid, carotenoids (Sies, Stahl & Sundquist, 1992) and anthocyanins (Tsuda, Kato & Osawa, 2000) have shown significant ability to scavenge free radicals. The genus *Melicope* within the *Rutaceae* family is known to produce a variety of flavones, benzopyrans, phenolics and triterpenoids, some with interesting biological activities (Johnson *et al*, 2010; Komala *et al.,* 2006; Barrows, Powan, Pond, & Matainaho, 2007). We report herein the isolation of a new glycoside from the active ethyl acetate extract of this plant, adding to the previously reported glabranin, umbelliferone, scopoletin and sesamin isolated from its methanolic extract (Kassim *et al.,* 2013) and the structures of the new glycoside were elucidated using spectroscopic methods. The glycoside exhibited good inhibitory activities against *β*-carotene peroxidation.

Materials and methods

Plant Material

The bark of *M*. *glabra* (1 kg) was collected from Kedah, Malaysia and a voucher specimen (No. 4563) has been deposited at the Department of Biology, Universiti Malaya, Malaysia.

Analysis Instrumentation

^{1}H-NMR,^{13}C-NMR, COSY, DEPT, HMQC and HMBC spectra were recorded on a BRUKER AVANCE 600 or JEOL JNM CRX 400 NMR spectrometer using $CDCl_3$ as

solvent and tetramethylsilane (TMS) as internal standard. The IR spectra were recorded using Perkin Elmer 1275X FTIR spectrophotometer. The ultraviolet spectra were recorded on a Shimadzu UV -2100 spectrophotometer in methanol. EIMS and HRESI-MS were recorded on Shimadzu GCMS-QP5050A and microOTOF-Q86 spectrometers, respectively. The antioxidant assay was performed using Bio-Tek precision and Fluostar Omega-BMG Labtech microplate readers.

Extraction and isolation

The extraction procedure for air-dried bark of *M. glabra* was previously reported (Kassim *et al*, 2013). The ethyl acetate extract (33 g) was fractionated using flash column chromatography on silica gel and eluted with mixtures of n-hexane, ethyl acetate and methanol to afford 52 fractions of 200 mL each. The fractions with similar TLC profiling were combined and subjected to *β*-carotene assay. The active fraction, ME24 (fractions 23-24) was purified using silica gel column chromatography. Elution with n-hexane-ethyl acetate gave 48 sub-fractions of 70 mL each. Sub-fractions 24-48 were combined and chromatographed using chromatotron with solvent mixtures of chloroform and acetone to afford compound 1 (7 mg) as a yellowish oil.

Compound 1: Obtained as yellowish oil; UV λ_{max} (MeOH) nm (log ε): 307 (3.13), 302 (3.01), 285 (3.52),; IR (KBr) λ_{max} cm^{-1}: 3500, 2923, 1730, 1458; EIMS *m/z* (relative intensity %): 370 ([$C_{16}H_{18}O_{10}$], 30%) , 203 ([$C_7H_9O_7$]$^+$, 15%), 164 ([Glu-O, $C_6H_{12}O_5$], 19%), 149 ([$C_8H_5O_3$], 100%); HRESI-MS m/z: 763.1766 ([2M+Na]$^+$, calcd. for $C_{32}H_{36}O_{20,}$ 763.1696), 393.0822 (calc. for [$C_{16}H_{18}O_{10}$+Na]$^+$, 393.0797); ^{1}H-NMR (400MHz, $CDCl_3$) and ^{13}C-NMR (100 MHz, $CDCl_3$) – see Table 1.

***β*-Carotene bleaching assay**

Antioxidant potential of the extracts, fractions as well as the isolated compound were determined using a published method (Zubia *et al*, 2009; Kassim *et al*, 2013) with slight modification. *β*-carotene solution (210 µL, 1 $mgmL^{-1}$ in chloroform) was added to linoleic acid (5 µL) and Tween 20 (42 µL) in a round bottom flask. After the chloroform was removed by rotary evaporation at 40°C, distilled water (10 mL) was added with vigorous shaking to form an emulsion. A 200 µL aliquot of the emulsion was transfered into each well of a 96-well microplate containing test samples (50 µL, 100 $ugmL^{-1}$). BHT, vitamin C and vitamin E were used as positive controls. The plates were incubated at 50°C in the dark for 180 mins. Absorbance was read at 470 nm at the start (t = 0 min) and at 30 mins intervals. The antioxidant activity (AA) was calculated according to the formula given below:

$$AA\% = 1-[(A_{t=0} – A_{t=2}) / (A_{c=0} – A_{c=2})] \times 100$$

where $A_{t=0}$ and $A_{t=2}$ = Absorbance of the test samples measured at 0 and 180 minutes respectively, $A_{c=0}$ and $A_{c=2}$ = Absorbance of control (*β*-carotene-containing emulsion and methanol only) measured at 0 and 180 mins respectively.

Results and discussion

Structural determination of compound 1

Compounds 1 (Figure 1) was isolated from ethyl acetate extract as yellowish oil. A broad band (3500 cm^{-1}) and a sharp peak (1730 cm^{-1}) observed in the IR spectrum were assigned to hydroxyl and carbonyl groups, respectively. EIMS showed a molecular ion peak at m/z 370 with the base peak at m/z 149, and in combination with ^{1}H-NMR and ^{13}C-NMR spectra, the compound was deduced to have a molecular formula $C_{16}H_{18}O_{10}$. Accurate mass of compound 1 was determined by HRESI-MS with peaks showed at m/z 393.0822 ($C_{16}H_{18}O_{10}$[370.0924+Na]$^{+}$, calculated 370.0900 and m/z 763.1766 indicated the dimer adduct ion of (1). Only six protons were observed in the low field region of the ^{1}H-NMR spectrum which was made up of a set of doublet at δ 7.56 and 6.85 with common coupling constant value of 8.2 Hz indicating *cis* orientation of the double bond between C-7 and C-8 (Table 1) (Jacobsen, 2007). The aromatic ring was 1,2,4,5-tetrasubstituted with two singlets at δ 7.44 (H-6) and 6.94 (H-3). A two-proton singlet at δ 6.04 was assigned to the methylenedioxy group. The ^{2}J and ^{3}J HMBC correlations between H-6 to C-5, C-4 and C-1, and between H-3 to C-4 and C-2 further substantiated the proposed substitution pattern in the aromatic ring. The remaining signals were attributed to the sugar moiety with an anomeric proton doublet at δ 4.65 (J = 9.2 Hz) indicating *β*-configuration (Table 1) (Jacobsen, 2007). The series of resonances with chemical shifts at δ 4.65 (*d*, 9.2 Hz), 4.43 (*dd*, 9.2, 11.9 Hz), 4.27 (*dd*, 11.9, 8.2 Hz), 4.11 (*dd*, 8.2, 2.7 Hz), 2.84 (*m*) and 3.65 (*dd*, 11.0, 4.6 Hz), 3.76 (*dd*, 11.0, 5.5 Hz) are the typical diagnostic signals for H-1' to H-6' of a sugar unit. The ^{13}C-NMR spectrum revealed the presence of 16 carbons made up of two methylene, nine methine and five quarternary groups. The signal most downfield (δ 197.2) was assigned to the carbonyl group. The methylenedioxy group was observed at δ 101.1. Other downfield frequencies due to aromatic and double bond carbons at δ 152.1, 147.4, 108.5, 147.9, 148.4, 108.2 124.8 and 107.1 were assigned to C-1, C-2, C-3, C-4, C-5, C-6, C-7 and C-8, respectively. The remaining signals at δ 83.6, 52.2, 77.2, 70.8, 76.6 and 61.2 were assigned to C-1', C-2', C-3', C-4', C-5' and C-6', respectively. However, the absence of usual *O*-glycosidic anomeric carbon and the appearance of characteristic *C*-glycoside carbon signal at δ 83.6 in the ^{13}C spectrum is evidence of the possible occurance of *C*-glycosylation in the structure. The *C*-glycosidic lingkage with aglycone was supported by ^{3}J HMBC correlation between H-3' (δ 4.27) and the carbonyl of C-9 (δ 197.2) (Figure 2). This lingkage could induce deshielding of C-2' followed by an upfield shift of the anomeric carbon signal. COSY correlation also showed the coupling between H-7/ H-8, H-1'/H-2', H-3' /H-4' and H-6'/H-5'. Mass spectral fragmentation of (1) gave the aglycone ion (m/z 194 [$C_{10}H_{10}O_4$]$^{+}$) due to loss of sugar. Based on available spectral data (Table 1), the structure of the compound (1) was given the trivial name 'glabresmin'.

β-carotene-linoleate bleaching

β-carotene bleaching assay measures the ability of an antioxidant to inhibit lipid peroxidation. The free radicals generated from the coupled oxidation reaction of linoleic

acid attacking and degrading *β*-carotene molecules results in discoloration. The presence of an antioxidant in the sample will minimize *β*-carotene destruction by neutralizing the linoleate free radicals and other free radicals present in the system.

Figure 3 clearly shows that pure compounds 1 is more potent than its fraction (ME24). The antioxidant activity for the fraction only lasted for 30 minutes and continued to decrease after whereas the antioxidant activity of (1) remained as 100% even after 60 minutes incubation time. The ethyl acetate extract and compound 1 exhibited comparable antioxidant activity to ascorbic acid as its antioxidant activity started to decrease only after 60 minutes incubation and displayed pro-oxidant activity after 180 minutes. However, compound 1 showed weaker activity compared to the other two standards, α-tocopherol and BHT. Thus, the antioxidant ability decreases in the order of α-tocopherol > BHT > ethyl acetate extract > compound 1 > ascorbic acid > ME 24. The higher antioxidant activity of compound 1 may be explained by the presence of a phenolic moeity since it has the ability to donate protons to free radicals thus terminating the chain reaction.

Results obtained in this study suggest that the bioactive molecule extracted from *M. glabra behave* as either antioxidants or pro-oxidants depending upon the duration of incubation. The pro-oxidant behaviour of ascorbic acid in the *β*-carotene bleaching system has been previously reported and was proposed to be due to the formation of ascobyl radicals during oxidation (Rufino, Alves, de Brito, Pérez-Jiménez, Saura-Calixto, & Mancini-Filho, 2010). It should be useful to investigate the mechanisms of action of compounds 1.

Conclusion

In this work, activity assay–guided isolation technique was employed in isolating a new antioxidant glycosides identified as glabresmin (1) from the ethyl acetate extract of *M. glabra*. The structure was elucidated by interpretation of spectral data. The compound displayed free radical scavenging and antioxidant activities. Phenolic moeity in compound 1 does enhance the antioxidant activity. The phenoxy radicals formed are stablised by resonance preventing further electron transfer, eventually retarding the chain propagation. Inhibition of lipid peroxidation in the *β*-carotene bleaching system was time dependant; the compound and ascorbic acid displayed a decrease in antioxidant activity after 90 minutes' incubation and they became pro-oxidant after longer incubation periods.

Acknowledgement

We would like to thank the Malaysian government for financial support and Universiti Putra Malaysia for providing research facilities. We also wish to thank Universiti Kebangsaan Malaysia for their kind assistance in performing part of the chemical assays. Lastly, thank you Prof. Karen Crouse for the editorial services.

References

Barrows, L.R., Powan, E., Pond, C.D., & Matainaho, T. (2007). Anti-TB activity of *Evodia elleryan*a bark extract. *Fitoterapia*, *78*, 250-252.

Hamburger, M., & Hostettmann, K. (1991). 7. Bioactivity in plants: the link between phytochemistry and medicine. *Phytochemistry*.

Jacobsen, N.E. (2007). NMR spectroscopy explained: simplified theory and applications and examples for organic chemistry and structural biology, John Wiley & Sons, Inc., Hoboken, New Jersey.

Johnson, A.J., Kumar, R.A., Rasheed, S.A., Chandrika, S.P., Chandrasekhar, A., Baby, S., & Subramoniam, A. (2010). Antipyretic, analgesic, anti-inflammatory and antioxidant activities of two major chromenes from *Melicope lunu-ankenda*. *Journal of Ethnopharmacology*, *130*, 267-71.

Kassim, N.K., Rahmani, M., Ismail, A., Sukari, M.A., Ee, G.C.L., Nasir, N. & Awang, K. (2013). Antioxidant activity-guided separation of coumarins and lignin from *Melicope glabra* (Rutaceae), *Food Chemistry*, *139*, 87

Komala, I., Rahmani, M., Sukari, M.A., Ismail, H.B.M., Ee, G.C.L., & Rahmat, A. (2006) Furoquinoline alkaloids from *Melicope bonwickii* (F. Muell.) T. Hartley. *Natural Product Research*, *20*,355-360.

Moon, J.K., & Sibamoto, T. (2009), Antioxidant assays for plant and food components, *Journal of Agricultural and Food Chemistry, 57,* 1655-1666.

Paz-Elizur, T., Sevilya, Z., Leitner-Dagan, Y., Elinger, D., Roisman, L.C., & Livneh, Z. (2008). DNA repair of oxidative DNA damage in human carcinogenesis: potential application for cancer risk assessment and prevention*. Cancer letter. 266,* 60-72.

Rufino, M.S.M., Alves, R.E., de Brito, E.S., Pérez-Jiménez, J., Saura-Calixto, F., & Mancini-Filho, J. (2010). Bioactive compounds and antioxidant capacities of 18 non-traditional tropical fruits from Brazil. *Food Chemistry, 121*, 996-1002.

Saliva, J. M. R., Darmin, N., Fernandez, Y. & Mitjavila S. (1991). Oxygen free radical scavenger capacity in aqueous models of different procyanidins from grape seeds. *Journal of Agricultural and Food Chemistry, 39,* 1549-1552.

Sies, H., Stahl, W., & Sundquist, A.R. (1992). Antioxidant functions of vitamins. Vitamins E and C, beta-carotene and other carotenoids. *Annals of the New York Academy of Sciences, 669*, 7-20.

Stanner, S.A., Hughes, J., Kelly, C.N., & Buttriss, J. (2004). A review of the epidemiological evidence for the 'antioxidant hypothesis, *Public Health Nutrition*, *7*, 407-422.

Tsuda, T., Kato, Y., & Osawa, T. (2000). Mechanism for the peroxynitrite scavenging activity by anthocyanins. *FEBS Letters, 484*, 207-210.

Zhang, D., Yasuda, T., Yu, Y., Zheng, P., Kawabata, T., Ma, Y., & Okada, S. (1996). Ginseng extract scavenges hydroxyl radical and protects unsaturated fatty acids from

decomposition caused by iron-mediated lipid peroxidation. *Free Radical Biology and Medicine, 20*, 145-150.

Zubia, M., Fabre, M.S., Kerjean, V., Lann, K.L., Stiger-Pouvreau, V., Fauchon, M., & Deslandes, E. (2009). Antioxidant and antitumoural activities of some *Phaeophyta* from Brittany coast. *Food Chemistry*, *116*, 693-701.

Table 1: ^{1}H-NMR ($CDCl_3$, 400 MHz) and ^{13}C-NMR ($CDCl_3$, 100 MHz) spectral data of compound **1**.

Position	δ_H	δ_C	HMBC	NOESY
1	-	152.1	-	-
2	-	147.4	-	-
3	6.94 (*s*)	108.5	C_4, C_2,	-
4	-	147.9	-	-
5	-	148.4	-	-
6	7.44 (*s*)	108.2	C_1, C_5, C_4	-
7	7.56(*d*, *J* = 8.2 Hz)	124.8	C_8	H-8
8	6.85 (*d*, *J* = 8.2 Hz)	107.1	C_9, C_7, C_1	H-7
9	-	197.2	-	-
10	6.04 (*s*)	101.1	C_5, C_4	-
1’	4.65 (*d*, *J* = 9.2 Hz)	83.6	$C_{2'}$, $C_{6'}$	H-3’, H-5’
2’	2.84 (*m*)	52.2	-	-
3’	4.27 (*dd*, *J* = 11.9, 8.2 Hz)	77.2	C_9, $C_{1'}$, $C_{2'}$	H-1’
4’	4.11(*dd*, *J* = 8.2, 2.7 Hz)	70.8	$C_{3'}$, $C_{2'}$	
5’	4.43 (*m*)	76.6	-	H-1’
6’	3.65 (*dd*, *J* = 11.0, 4.6 Hz) 3.76 (*dd*, *J* = 11.0, 5.5 Hz)	61.2	$C_{5'}$	H-6b’ H-6a’

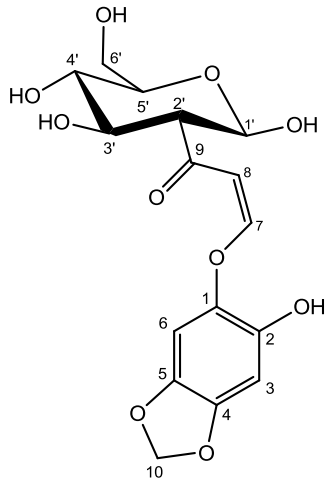

(**1**)

Figure 1: Structure of compound 1

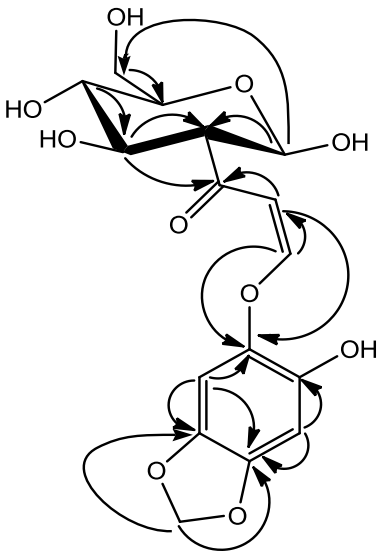

(**1**)

Figure 2: Key HMBC correlations of compound 1

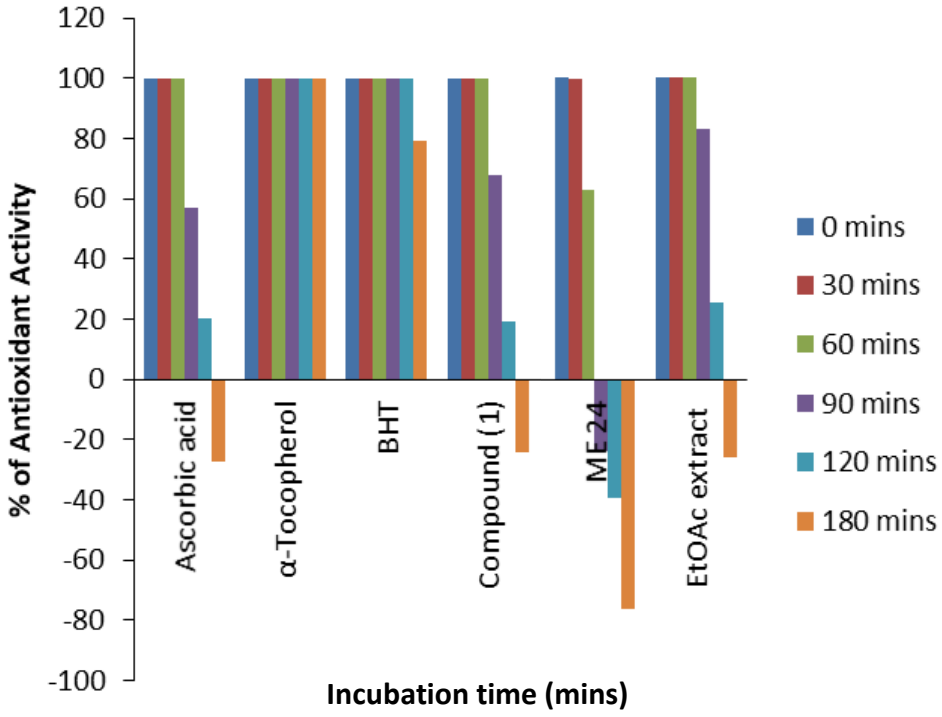

Figure 3: Percentage of antioxidant activity of compound 1, fraction (ME 24), ethyl acetate(EtOAc) extract, ascorbic acid, α-Tocopherol and BHT as assessed with β-carotene bleaching method at different incubation time.

2.4 Synthesis and Characterization of New Choline-based Ionic Liquids and Their Antimicrobial Properties

Abstract

Antibiotic resistance is a global public health concern due to increasing resistance of microbes to antimicrobial agents. Many researches have been devoted to formulate novel antibacterial and antifungal agents. Ionic liquids (ILs) which are known as designer liquids have raised particular attention as they can exert a broad spectrum of antimicrobial activity. Two new cholinium-based ionic liquids were synthesized by using simple neutralization reaction. The synthesized ILs were choline nonadecanoate and choline linoleate. Result obtained from FT-IR, ^{1}H and ^{13}C NMR, mass spectrometry, thermogravimetric and differential scanning calorimetry confirmed the formation of these cholinium-based ILs. These ILs were then tested for their antimicrobial properties towards three Gram-positive bacteria, two Gram-negative bacteria, and two types of yeasts. Interestingly, choline linoleate possesses excellent antimicrobial activity as good as the standard, Streptomycin towards Staphylococcus epidermidis S273.

Keywords: ionic liquids; antimicrobial; cholinium; neutralization reaction

Introduction

Antimicrobials

Antimicrobials are an important class of compounds which used to destroy and inhibit the growth of microorganisms. It was not until 1800s, the development of antimicrobials research has expanding due to the acceptance of the germ theory [1]. This theory included anti-biosis, disinfection, preservation, sterilization and modern infection control.

Ionic liquids

Ionic liquids (ILs) have found many applications due to their interesting properties. Commonly known as green solvents, ionic liquids have found many applications due to their interesting properties such as a low vapor pressure and non-flammability [2]. Ionic liquids composed of a combination of cation and anion which have low melting points below 100°C, high thermal stability and high conductivity. Ionic liquids have been used in various applications depends on the properties. Using a novel density functional theory (DFT) method, Garcia and coworkers reported the mechanism insights on the solvation of fullerene B80 with cholinium-based ILs [3]. ILs also find its way in separation processing, as electrolytes for lithium batteries and also as phase change materials for the storage of solar energy [4]. It was also reported that some cholinium-based ILs such as cholinium sacchrinate and cholinium dihydrogen phosphate have been successfully to biodegraded the azo dyes [5]. Recently, magnetic ILs was used to extract DNA and it was found that the extraction efficiencies was high in larger DNA molecules [6].

Choline hydroxide, which acts as important starting material for the production of

acetylcholine is a basic component of lecithin. It is usually found in many animal organs and even in plants. Choline hydroxide can be used in aqueous environment due to the miscibility of this compound in water. Some important applications of choline hydroxide in electronic field are as positive photoresist developing agents stripping photoresists, anisotropic etching agents, and washing agents for silicon wafers [7].

Results and Discussion

Properties of Synthesized Ionic Liquids

Choline nonadecanoate (1a): White solid (Yield: 68.5 %). The absorption peak at around 3373.29 cm^{-1} was assigned as -OH stretching of choline hydroxide [9]. Peaks at 1085.34 cm^{-1} is a characteristic of C-N of aliphatic amines while peak at 1647.96 cm^{-1} was assigned as C-O stretching of alcohols. C-H bending of choline hydroxide was observed at 953.02 cm^{-1} and this agree with report by Kalmode et al. [9]. The absorption peaks of nonadecanoate can be observed at 2916.3 cm^{-1} and 2850.75 cm^{-1}. ^{1}H NMR (500MHz, DMSO) δ (ppm): 3.97 (d, 2H), 3.47 (t, 2H), 3.30 (s, 1H), 3.17 (s, 9H), 2.16 (t, 2H), 1.51 (t, 2H), 1.24 (d, 22H), 0.85 (t, 3H). 13C NMR (500MHz, DMSO) δ (ppm): 14.19, 29.48, 32.03, 36.41, 54.29, 55.97, 67.98, 179.77. Mass spectrum for choline was at m/z 106 and for nonadecanoate was at m/z 298 and m/z 255, respectively.

Choline linoleate (1b): Dark brown liquid (Yield: 54.0%). A broad absorption band was found at 3386.19cm^{-1} which represent OH group. The other peaks of choline hydroxide are observed at 1080.36 cm^{-1} and this is a characteristic of C-N of aliphatic amines while peak at 1702.57 cm^{-1} was assigned as C-O stretching of alcohols. The absorption peaks of linoleate are at 2922.68, 2857.79, 1556.49, 1460.01, 1399.89 cm^{-1}. ^{1}H NMR (500MHz, Acetone) δ (ppm): 4.01 (s, 2H), 3.63 (s, 2H), 3.51 (s, 1H), 3.32 (s, 9H), 2.75 (t, 2H), 2.14 (t, 2H), 1.53 (d, 16H), 1.26 (d, 4H), 0.84 (s, 3H). 13C NMR (500MHz, Acetone) δ (ppm): 205.64, 129.89, 129.72, 127.95, 64.87, 60.70, 53.79, 55.89, 27.12, 22.46, 13.65. Mass spectrum for choline was at m/z 107 and for linoleate was at m/z 237.

Thermal Analysis

DSC was used to measure the melting temperature (T_m) of cholinium-based compounds and the results were tabulated in Table 1. It was reported before that different combinations of anions and cations will result in different characteristic and properties of ILs [10]. In this research, only choline nonadecanoate fulfill the characteristic of ILs with slightly low T_m which are below 100°C. Compound 1b showed melting temperature above 100°C and thus is classified as new choline-based salt. Decomposition of both cholinium-based compounds was observed using thermogravimetric analysis (TGA) at high temperature in a range of 200℃ to 350℃.

Table 1. Melting temperature (T_m) of choline-based ILs

Cholinium-based ILs	Melting temperature (T_m/°C)
1a	69.50 (±0.4)
1b*	225.03 (±0.8)

* Not considered as ILs due to high melting point (>100°C)

Antimicrobial Activity

Different types of bacteria were used in this studies: three Gram-positive, *Bacillus subtilis (B29)*, *Staphylococcus aureus (S276)*, *Staphylococcus epidermidis (S273)*, two Gram-negative, *Pseudomonas aeruginosa (ATCC 15422)* and Escherichia coli (E266) and two types of yeasts, Candida albicans (9002) and *Candida tropicalis (A3)* were used to assess the antimicrobial activity of the ILs that have been synthesized. The minimum inhibitory concentration (MIC) of this cholinium-based ILs cannot be determined due to low solubility of ILs in nutrient broth. Table 2 shows the inhibition zone diameter of ILs (mm) towards the microorganisms. For the sake of comparison, *Streptomycin* and *Nystatin* were tested as positive standards whereas water and DMSO as negative standards.

Interestingly, choline linoleate possesses excellent antimicrobial activity as good as the standard, *Streptomycin* towards *Staphylococcus epidermidis S273* with inhibition zone diameter of 22 mm. In contrast, choline linoleate was found to be inactive towards all microorganisms. This is very interesting as we can see that by changing the anion of the cholinium salts compounds will give a strike different in term of the antimicrobial activity.

Table 2. Inhibition zone diameter of choline-based compounds towards bacteria (mm)

Cholinium-based ILs	Inhibition zone diameter of choline-based ILs (mm) towards bacteria						
	B29	***S276***	***S273***	***ATCC 15422***	***E266***	***9002***	***A3***
1a	-	-	-	-	-	-	-
1b	10	8	**22**	7	9	7	10
Std (+ve) (1 mg/ml)	19	20	22	20	23	25	19
H_2O (-ve)	-	-	-	-	-	-	-

(1 mg/ml)							
DMSO (-ve) (1 mg/ml)	-	-	-	-	-	-	-

Experimental

Materials and Reagents

Choline hydroxide (45 wt% aqueous solution) was purchased from ACROS Organics. Nonadecanoic acid was purchased from Fluka. Linoleic acid was purchased from Sigma-Aldrich. The solvents, diethyl ether (99% purity) and chloroform (99% purity) were purchased from Merck. All chemicals and materials are commercially available and of higher analytical grade unless otherwise specified. The chemicals were used without purification, unless otherwise stated.

Synthesis of Cholinium-based Ionic Liquids

Cholinium-based ILs were synthesized through neutralization of choline hydroxide with two types of carboxylic acids. These ILs were synthesized according to the procedures reported by Taha et al., [11]. They reported the synthesis of choline hydroxide with Good's buffers. Scheme 1 shows the reaction mechanism of cholinium-based ILs. The product formed is choline carboxylate and water. Figure 1 shows the structure of two cholinium-based ILs.

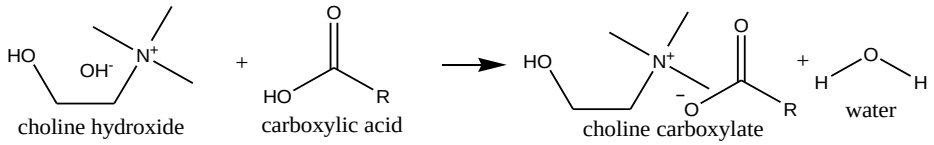

Scheme 1: Reaction mechanism of choline-based ILs

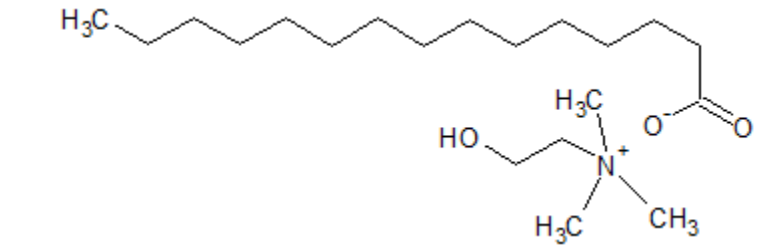

(a)

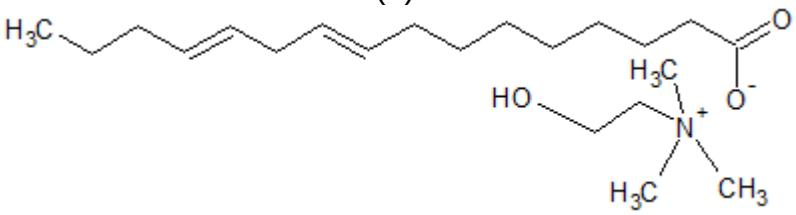

(b)

Figure 1. Structure of new cholininium-based compounds (a) Choline nonadecanoate, (b) Choline linoleate

Choline nonadecanoate (1a): Choline nonadecanoate was synthesized through neutralization of choline hydroxide with nonadecanoic acid. Nonadecanoic acid (0.025 mol) was dissolved in 60 mL of distilled water with heat. It was added slowly into 0.025 mol of choline hydroxide. The mixture was stirred continuously for 12 hours at room temperature. The solvent was removed using rotary evaporator, followed by vacuum drying at 70°C for 24 hours. For purification, the sample was washed with toluene for three times. Then, the solvent was removed by vacuum drying at 65°C for 24 hours

Choline linoleate (1b): Choline linoleate was synthesized by using method in 1a but replacing nonadecanoic acid with linoleic acid. For purification, the sample was washed with toluene for three times. Then, the solvent was removed by vacuum drying at 65°C for 24 hours.

Characterization and Instrumentations

The instruments used for characterization are Shimadzu Europe-GCMS-QP5050A for mass spectrometry, Perkin Elmer-FTIR Spectrometer Spectrum RX1, Varian 500 MHz NMR spectrometer, Differential Scanning Calorimeter (DSC) Mettler Toledo DSC823 and Thermogravimetric Analysis (TGA). Temperature range used for DSC and TGA was 25-400°C.

Antimicrobial Activity

Antimicrobial or antifungal test was carried to determine the effectiveness of choline-based ILs in treating bacteria or fungal infections. The response (sensitivity/resistance) of microbes against antimicrobial compounds various to each other. The test was carried out by placing 6mm diameter of paper disc containing IL sample onto a plate which microbes grew. The microbe culture was standardized to 0.5 Mc Farland standard which was approximately 10^8 cells. Streptomycin standard were used for each bacteria. Nystatin standard were used for yeast. The plates were inverted and incubated at 30-37°C for 18-24-48 hours or until sufficient growth has occurred. After incubation, each plate was examined. The diameters of the zones of complete inhibition (as judged by the unaided eye) were measured, including the diameter of the disc. Zones were measured to the nearest whole millimeter, using sliding calipers or a ruler, which was held on the back of the inverted petri plate. The ILs samples were tested against *Bacillus subtilis (B29)*, *Staphylococcus aureus (S276)*, *Staphylococcus epidermidis (S273)*, *Pseudomonas aeruginosa (ATCC 15442)*, *Escherichia coli (E266)*, *Candida albicans (9002)* and *Candida tropicalis (A3)*.

Conclusion

Two new cholinium-based compounds were successfully synthesized by neutralization reaction. The synthesized cholinium-based compounds were cholinium nonadecanoate and cholinium linoleate. All the synthesized cholinium-based compounds were characterized by using infrared spectroscopy, ^{1}H and ^{13}C NMR spectroscopy, mass spectrometry, thermogravimetric and differential scanning chromatography. Result obtained from all characterization techniques confirmed the formation of these choline-

based compounds. One of the synthesized cholinium-based compounds, cholinium nonadecanoate shows excellent antimicrobial properties towards *Staphylococcus epidermidis (S273)* and is promising for antimicrobial application. More detail studies are currently underway.

Acknowledgements
This work was in financially supported by Putra IPS Grant (GP-IPS/2017/9520100) Universiti Putra Malaysia and STIRF-UTP Grant (Cost-Center 0153AA-F21), Universiti Teknologi Petronas.

References

[1] Gabriel, S., & Weiner, J. (1888). Ueber einige abkömmlinge des propylamins. Berichte der deutschen chemischen Gesellschaft, 21(2), 2669-2679.
[2] Seddon, K. R., Stark, A., & Torres, M. J. (2000). Influence of chloride, water, and organic solvents on the physical properties of ionic liquids. Pure and Applied Chemistry, 72(12), 2275-2287.
[3] Garcia, G., Atilhan, M., & Aparicio, S. (2015). Interaction Mechanism Insights on the Solvation of Fullerene B80with Choline-based Ionic Liquids. The Journal of Physical Chemistry B, 119(38), 12455-12463.
[4] Plechkova, N. V., & Seddon, K. R. (2008). Applications of ionic liquids in the chemical industry. Chemical Society Reviews, 37(1), 123-150.
[5] Sekar, S., Surianarayanan, M., Ranganathan, V., MacFarlane, D. R., & Mandal, A. B. (2012). Choline-based ionic liquids-enhanced biodegradation of azo dyes. Environmental science & technology, 46(9), 4902-4908.
[6] Clark, K. D., Nacham, O., Yu, H., Li, T., Yamsek, M. M., Ronning, D. R., & Anderson, J. L. (2015). Extraction of DNA by Magnetic Ionic Liquids: Tunable Solvents for Rapid and Selective DNA Analysis. Analytical chemistry, 87(3), 1552-1559.
[7] Moonen, K., Ulrichts, D., & Scheldeman, D. (2011). U.S. Patent Application No. 14/369,014.
[8] Reller, L. B., Weinstein, M., Jorgensen, J. H., & Ferraro, M. J. (2009). Antimicrobial susceptibility testing: a review of general principles and contemporary practices. Clinical infectious diseases, 49(11), 1749-1755.
[9] Kalmode, H. P., Vadagaonkar, K. S., Murugan, K., Prakash, S., & Chaskar, A. C. (2015). Deep eutectic solvent: a simple, environmentally benign reaction media for regioselective synthesis of 2, 3, 4-trisubstituted 1 H-pyrroles. RSC Advances, 5(44), 35166-35174.
[10] Yang, Z., & Pan, W. (2005). Ionic liquids: green solvents for nonaqueous biocatalysis. Enzyme and Microbial Technology, 37(1), 19-28.
[11] Taha, M., Almeida, M. R., Domingues, P., Ventura, S. P., Coutinho, J. A., & Freire, M. G. (2015). Novel Biocompatible and Self-buffering Ionic Liquids for Biopharmaceutical Applications. Chemistry–A European Journal, 21(12), 4781-4788.

2.5 FTIR Analysisand in-vitro radical scavenging capacity of *Boswellia papyrifera* (Del) stem bark extracts

Abstract

Boswellia papyrifera was extracted with different solvents (water, ethyl acetate, hexane and chloroform), using different protocols (cold-extraction and solvent partitioning) to evaluate the functional groups using Fourier transform infrared spectroscopy (FTIR) and antioxidant abilities of the extracts, four *in vitro* test systems were employed, such as (DPPH), Nitric oxide(NO), hydrogen peroxide (H_2O_2) radical scavenging assays and a ferric reducing antioxidant power (FRAP) assay. All the four solvents showed different functional groups related to the classes of bioactive compound presence. The four solvent extracts exhibited outstanding antioxidant activities that were similar to that of butylated hydroxyl toluene and Vitamin C. The ethyl acetate extracts exhibited the most significant scavenging capacities. Furthermore, the radical scavenging capacity and butylated hydroxyl toluene (BHT) and vitamin C of four solvent extracts followed the same order, *i.e*., there is a good correlation between antioxidant activities and BHT. The results showed that these extracts, especially the ethyl acetate extracts, could be considered as natural antioxidants and may be useful for curing diseases arising from oxidative deterioration.

Keywords: *Boswellia papyrifera*; Stem bark extract; FTIR; Radical scavenger

Introduction

Free radicals, which are generated in several biochemical reactions in the body, have been implicated as mediators of many diseases, including cancer atherosclerosis and heart diseases (Hayet *et al*.,2008). Synthetic antioxidants, such as butylated hydroxytoluene (BHT) and butylated hydroxyanisole (BHA), which are effective in their role as antioxidants, are commercially available and currently used in industrial processes. Free radicals are fundamental to any biochemical process and represent an essential part of aerobic life and metabolism (Tiwari, 2001). Reactive Oxygen Species (ROS) and Reactive Nitrogen Species (RNS) are products of normal cellular metabolism (Sudha *et al*., 2011). The most common ROS include superoxide anion, H_2O_2, peroxyl (ROO-) radicals and reactive hydroxyl (OH-) radicals and the nitrogen derived free radicals are nitric oxide and peroxynitrite anion (ONOO-) (Joyce, 1987)). These reactive species play an important role in pathogenesis of several oxidative stress related diseases like carcinogenesis, cardiovascular diseases, rheumatoid arthritis, ulcerative colitis and neurological degenerative diseases.(Halliwell and, Gutteridge, 2010). *Boswellia papyrifera* (Del.) *(Ararrabi)* Hochst belongs to a family of tropical plant called Bruceraceae (Fitchl and Admasu, 2004) which is distinguished by the presence of resin ducts in the bark (Groom, 2011). *B. papyrifera* is a deciduous tree which can be as tall as 12m, with a rounded crown and a straight regular bole. The bark is whitish to pale brown, peeling off in large flakes; slash red-brown and exuding a fragrant resin. The bark contains schizogenous olea-gum-resin pockets (Verghese,

2006). The *Boswellia* plants are known to contain several acidic triterpenes, some of which show analgesic, immunosuppressant, antileukemic, hepatoprotective, and anti-inflammatory activities. This paper is aimed at determining the functional groups and free Radical scavenging capacity of each of the four solvent extracts of *Boswellia papyrifera* stem bark.

Materials and methods

Sample collection and preparation of extract

The stem bark was collected and washed in clean water and dried at room temperature, after which it was pulverized to coarse powder using mechanical grinder. *Boswellia Papyrifera* aqueous stem bark extract were prepared according to Mittal *et al*; (1981) and Fernando *et al;* (1989) method.

Biochemical analysis

The free radical scavenging effects of the four solvent stem bark extracts of *Boswellia papyrifera* were evaluated against 2,2-diphenyl 1-picryl hydrazyl hydrate (DPPH), hydrogen peroxide, FRAPS and nitric oxide. The scavenging ability of the natural antioxidant of the four extract on DPPH were measured according to the method of Pan *et al.,*(2009), hydrogen peroxide was estimated according to the method of Jayaprakasha *et al*. (2004)., Nitric oxide was determined using Griess reagent (Marcocci *et al.,* 1994) and Ferric reducing-antioxidant power (FRAP) assay was conducted by the method developed by Benzie and Strain (1999).

Statistical analysis

The data was statistically analysed at P-value ($p<0.05$) significantly accepted and comparison between the groups were performed using one-way analysis of variance (ANOVA). The data are given as the mean ± standard deviation.

Results and discussion

Total and Percentage Yield of *Boswellia Papyrifera* Solvents Extracts

The total and percentage yield of *Boswellia Papyrifera* stem bark (1000g) of aqueous solvents extract were evaluated after 24 hours percolation. The total and the corresponding percentage yield of the Hexane, chloroform, ethyl acetate and aqueous extract were found to be 52.60g; 10.52%, 71.30g;14.26%, 170.24g;34.04% and 602.00g;60.20% respectively (table 1). Results obtained shows that the *Boswellia Papyrifera* stem bark extract percentage yield was found to be higher when water was used as the extracting solvent (Table 1). However, ethyl acetate extract yield was second when water was used as the extracting solvent. On the other hand, the results also indicated that hexane and chloroform extract showed low yield when compared with the ethyl acetate and aqueous extract. The differences in the extraction yields from the *Boswellia papyrifera* stem bark might be attributed to the difference in availability of extractable components, resulting from the varied chemical composition of plants (Eberhardt *et al*., 2007). And it could be due to better salvation of antioxidant compound(s) present in the *Boswellia papyrifera* stem bark as a result of interactions of

hydrogen bonds between the polar sites of the compound(s) present and the solvent (Eberhardt *et al*., 2007).

Table 1: Total yield and percent yield of Aqueous, Ethyl acetate, Hexane and Chloroform extracts of *Boswellia papyrifera* stem bark after 24 hours percolation.

Extract	Total yield (g)	Percent yield (%)
Hexane stem bark extract of *B.papyrifera*	52.60[c]	10.52
Chloroform stem bark extract of *B.papyrifera*	71.30[d]	14.26
Ethyl acetate stem bark extract of *B.papyrifera*	170.24[b]	34.04
Aqueous/residues of stem bark extract of *B.papyrifera*	194.40[a]	38.88
Aqueous stem bark extract of *B.papyrifera*	602.00	60.20

Each value is an average of three experimental samples and values are expressed as means ± SD

FT-IR Analysis of Aqueous, Ethyl acetate, Hexane and Chloroform Extracts of *Boswellia Papyrifera* Stem Bark

Boswellia Papyrifera aqueous stem bark extract shows a characteristic absorption band at 3332cm^{-1} which indicate the presence of OH band stretch this revealed the presence of phenols (Parag *et al.*,2013) while the peak band at 1641cm^{-1} is for N-C=O which is for quinone compounds, also the absorption band at 1466cm^{-1},1277cm^{-1} and 1171cm^{-1} are for CH_2(alkane), C-N stretch (primary and secondary amine) and C-O stretch (ethers) respectively (Ragavendran *et al*.,2011). Also the C-Br at 657cm^{-1} indicated the presence of aromatic halide (Ramamurthy and Kennan, 2007) in the aqueous stem bark extract of *Boswellia papyrifera* (Table 2, Figure 1).

The characteristic absorption bands exhibited by ethyl acetate were at 3337cm^{-1} are for functional group –O-H- and C=O was at 1961cm^{-1} which indicated the presence of polyphenols compound (Parag *et al.*,2013) in ethyl acetate extract of *Boswellia Papyrifera* stem bark. Also the band observed at 3337cm^{-1} and 1151cm^{-1} were for tannins due to presence of O-H and C-O stretch respectively. Terpenoids may also be present in ethyl acetate extract of *Boswellia Papyrifera* due functional groups C=O and C-O with characteristic absorption band at 1961cm^{-1} and 1151cm^{-1} respectively (Moses *et al*.,2013). The presence of N=O at 1961cm^{-1} revealed saponins (Muruganantham *et al*.,2009) while C-O stretch at 1151cm^{-1} was for anthraqiunones (Egwaikidi *et al*.,2009) . However, C=N stretch also showed at 2009cm^{-1} indicated flavonoids and cyanogenic glycosides (Moses *et al*.,2013). Unsaturated aromatic lactone which occurred either in the free or combined state with sugar glucose (caumaric glycosides) showed characteristic band at 1961cm^{-1} and 1151cm^{-1} for C-O and C=O stretch (Ashokkumar and Ramaswamy, 2014) (Table 3, figure 2).

Hexane extract of *Boswellia Papyrifera* stem bark showed a characteristic band at 2924cm^{-1} and 2855cm^{-1} which revealed the functional group C-H stretch this indicated the presence of alkane hydrocarbon in the hexane extract. Also at 1709 and 1743cm^{-1}

is for C=O which indicated aromatic ketones in the extract. While N-H bend at 1508cm^{-1} revealed primary and secondary amine (Egwaikidi *et al*.,2009). The band at 1460cm^{-1} was for CH_2 (Alkane) and the band at 1244 and 1308cm^{-1} indicated C-O stretch showed the presence of ethers in the extract (Ragavendran *et al*.,2011) (Table 2, Figure 3).

The FTIR spectroscopy analysis of chloroform stem bark extract of *Boswellia Papyrifera* (Table 2, Figure 4) revealed the presence of Tannins due to O-H and C-H stretch at the 3403 and 2928cm^{-1} respectively. While the characteristic band at 1709cm^{-1} indicated C=O band this revealed the presence of aromatic ketones in the extract (Parag *et al.*,2013). Primary and secondary amine was observed at 1516cm^{-1} due to N-H band. Also the extract exhibited a band at 1376cm^{-1} due to presence of S=O stretch this indicated sulphonamide (Ramamurthy and Kennan, 2007). The chloroform stem bark extract of *Boswellia Papyrifera* revealed the presence of alkaloids at 1268cm^{-1} due to C-N stretch (Ashokkumar and Ramaswamy, 2014).

In-vitro Evaluation of Free Radical Scavenging Capacity of Aqueous, Ethyl acetate, Hexane and Chloroform Extracts of *Boswellia Papyrifera* Stem Bark.

DPPH free radical scavenging activity

The 2,2-Diphenyl 1-Picryl Hydrazyl Hydrate (DPPH) radical scavenging activities of all the four solvents extract were shown on table 3. All the extracts showed different levels of DPPH radical scavenging activity over the range of 2-10 mg/ml concentration expressed in percentage. The highest DPPH radical scavenging activities ethyl acetate and aqueous extracts of *Boswellia papyrifera* extracts compared to hexane and chloroform extracts may be attributed to presence of some polyphenols such as flavonoids, terpenes, alkaloids etc (Abdulmumin *et al*.,2014) .

Hydrogen peroxide scavenging activity

Hydrogen Peroxide is highly important because of its ability to penetrate into biological membranes. H_2O_2 itself is not very reactive, but it can sometimes be toxic to cell because it may give rise to hydroxyl radicals in the cells (Gulcin *et al*., 2010). Scavenging of H_2O_2 by extracts may be attributed to their phenolics, which can donate electrons to H_2O_2, thus neutralizing it to water (Ebrahimzadeh *et al*., 2009). The results (Table3) showed that all the four solvent extracts scavenged H_2O_2 in a concentration dependant order.These antioxidant components present in the extracts are good electron donors, they may accelerate the conversion of H_2O_2 to H_2O (Ebrahimzadeh *et al*.,2009).

Ferric Reducing Antioxidant Power (FRAP)

The antioxidant potential of different extracts of *Boswellia papyrifera* stem bark was estimated for their ability to reduce ferric iron and 2,3,5-triphenyl-1,3,4-triaza-2-azoniacyclopenta-1,4-diene chloride(TPTZ) to the ferrous [TPTZ–Fe (III) complex to TPTZ–Fe (II)] (Table 2). The ferric reducing ability of the extracts revealed that all the four solvents have good ferric reducing antioxidant power (FRAP) activity (150.4–624.33 µM/g extract). The highest activity was noted for ethyl acetate extract. The low ferric reducing power of chloroform and hexane extracts may be attributed to low

content of monoterpenes hydrocarbons and oxygenated sesquiterpenes in hexane and chloroform extracts of *Boswellia papyrifera* stem bark (Pellegrini *et al*., 2003)

Table:1 FTIR Analysis of Aqueous, Ethyl acetate, Hexane and Chloroform extracts of *Boswellia papyrifera* stem bark.

		Absorption specrum ,Frequency (cm^{-1})			
Functional Group	Components (peaks)	Aqueous extract	Ethyl acetate extract	Hexane extract	chloroform extract
Phenols		-	-	-	3403
	-OH- Stretch and broad	3332	3337	-	-
Alkane	C-H Stretch	-	-	2924	2928
Isocyanide	C=N Stretch	-	2009	-	-
Alkane	C-H Stretch	-	-	2855	-
Ketones	C=O stretch	-	1961	-	-
Esters & Lactone	C=O Bend	-	-	1709	1709
Ketone	C=O Stretch	-	-	1743	-
Quinone, Aldehyde, Ketone	-N-C=O Stretch	1641	1620	-	-
1^0&2^0amine	N-H Bend	-	-	1508	1516
Alkane	CH_2 Bend	1466	1445	1460	1460
Ethers	C-O Stretch	-	-	1308	-
Sulphonamide	S=O Stretch	-	-	-	1376
Ethers	C-O Bend	-	-	1244	-
1^0&2^0amine	C-N Stretch	1277	-	-	1268
Ethers	C-O Stretch	1171	-	-	-
	C-O Stretch	-	1151	-	-
	C-O Stretch	-	-	1028	-
		-	-	-	1035
		-	1045	-	-
Halides	C-I Stretch	-	-	-	737
	C-Br or C-I Stretch	657	-	-	-

Nitric Oxide (NO)

All the four solvent extracts of *Boswellia papyrifera* may effectively reduce the generation of nitric oxide from sodium nitroprusside. The nitric oxide radical inhibition activity of the extracts in the order aqueous >ethyl acetate >hexane > chloroform (Table 2). The degree of inhibition of the NO free radicals was found to be increased in increasing concentration of the *Boswellia Papyrifera* stem bark extract in all the four solvent extract. The activity of the ethyl acetate extracts could be attributed to the bioactive components such as phenolic compounds (Abdulmumin *et al*., 2014)

Table: 2 Free Radical Scavenging Activity of Aqueous, Ethyl acetate, Hexane and Chloroform extract of *Boswellia papyrifera* stem bark

Extracts	DPPH (%)	Hydrogen Peroxide (%)	FRAP(µM/g dried sample)	Nitric Oxide(%)
Aqueous,	58.11±2.10	23.72±1.20	507.34±2.32	41.11±3.20
Ethyl acetate	63.23±0.32*	37.21±0.34*	624.33±10.27*	31.33±2.33*
Hexane	17.76±1.20	14.32±3.21	221.23±5.21	16.34±3.20
Chloroform	10.64±0.51	7.89±2.42	150.45±9.23	9.24±1.21

Each value is an average of five experimental samples and values are expressed as means ± SD

Value with asterisk are significantly ($p<0.05$) higher along the column

Conclusion

Today, antioxidative properties of the plants have become a great interest due to their possible uses as natural additives to replace synthetic ones. The results of the present study showed that all the extracts exhibited potent antioxidant activity. Among the four extracts ethyl acetate extract exhibited higher potency of free radical scavenging activity. The scavenging activity of *Boswellia papyrifera* stem extracts shows similar trend with the result of BHT and ascorbic acids, indicating that the free radical scavenging activity of *Boswellia papyrifera* stem extracts is highly related to the presence of functional groups in the compounds presence. Thus present data suggest that ethylacetate extract can be used as a good source of natural antioxidants for health benefits and further isolation of bioactive compounds are required for identifying the unknown compounds to establish their pharmacological properties.

Acknowledgement

We acknowledge the Tertiary Education Trust fund (TETFUND) and Hussaini Adamu Federal Polytechnics, Kazaure, Jigawa state. Nigeria for the financial support of this work.

References

Abdulmumin, Y, Matazu.K.I, Wudil.A.M, Alhassan.A.J, and Imam A.A .,(2014) Bioactive compound determination and curative Effects of Aqueous Stem Bark Extract of *Boswellia Papyrifera* (Del.) in carbon tetrachloride-Induced liver Damage In Rats. *Acta biological malaysiana.* vol. 3(3) Pp 91-101

Ashokkumar.R and Ramaswamy.M (2014).Phytochemical screening by FTIR spectroscopic analysis of leaf extracts of selected Indian Medicinal plants *Int.J.Curr.Microbiol.App.Sci* 3(1): 395-406

Eberhardt, T.L., X. Li, T.F. Shupe and C.Y. Hse, (2007) Chinese Tallow Tree (Sapium Sebiferum) utilization: Characterization of extractives and cell-wall chemistry. *Wood Fiber Sci*., 39: 319-324.

Ebrahimzadeh MA, Nabavi SF, Nabavi SM (2009) Antioxidant activities of methanol extract of *Sambucus ebulus L*. flower. *Pak J Biol Sci* 12:447-450.

Egwaikidi, P.A., S.O. Okeniyi and C.E. Gimba, (2009). Screening for antimicrobial activity and phytochemical constituents of some Nigerian medicinal plants. *J. Med. Plant. Res*., 3: 1088-109

Fitchl, R. and Admasu A.,(2004). Honeybee Flora of Ethiopia.MargrafVerlag, Weikersheim, Germany, Pp 510

Groom, N. (2011). Frankincense and myrrh: a study of the Arabian incense trade. Longman, London, 285 pp.

Gulcin I, Huyut Z, Elmastas M, Aboul-Enein HY (2010) Radical scavenging and antioxidant activity of tannic acid. *Arab J Chem* 43-53.

Halliwell B, Gutteridge JM (2010) Role of free radicals and catalytic metal ions in human disease: an overview. *Methods Enzymol* 186: 1-85.

Hayet E, Maha,M, Samia, A, Mata,M., Gros P, Raida, H., Ali,M.M.,Mohamed,A.S., Gutmann,L., Mighri,Z., Mahjoub A.(2008), *World J. Microbiol. Biotechnol.* **24;** 2933

Marcocci, I., Marguire, J.J., Droy-lefaiz, M.T., Packer, L., (1994). The nitric oxide scavenging properties of Ginkgo biloba extract. *Biochem. Biophys. Res. Commun*. 201, 748–755.

Mertens. M, Buettner, A. and Kirchhoff ,E (2009) . *Flavour Fragr. J*., Pp, 24, 279.

Moses A.G. Maobe and Robert M. Nyarango(2013) Fourier Transformer Infra-Red Spectrophotometer Analysis of *Urtica dioica* Medicinal Herb Used for the Treatment of Diabetes, Malaria and Pneumonia in Kisii Region, Southwest Kenya. *World Applied Sciences Journal* 21 (8): 1128-1135

Muruganantham, S., G. Anbalagan and N. Ramamurthy, (2009). FT-IR and sem-eds comparative analysis of medicinal plants,Eclipta alba hassk and Eclipta prostrata linn.Romanian *J. Biophys*., 19(4): 285-294.

Parag A. Pednekar, Bhanu Raman. (2013). Antimicrobial and Antioxidant Potential with FTIR analysis of *Ampelocissus latifolia (roxb.) Planch*. Leaves*. Asian Journal of Pharmaceutical and Clinical Research*. 6(1): 67-73

Ragavendran,P., Sophia,D., Arul Raj,C., and Gopalakrishnan V.K., (2011). Functional group analysis of various extracts of Aerva lanata (L.,) by *FTIR spectrum. Pharmacologyonline.* 1, 358-364.

Ramamurthy,N., and Kennan, S., (2007). Fourier transform infrared spectroscopic analysis of a plant (Calotropis gigantea Linn) from an Industrial Village, Cuddalore Dt, Tamilnadu, India. *Romanian Journal of Biophysics*. 17 (4): 269276.

Sudha G, Sangeetha priya M, Indhu shree R, Vadivukkarasi S (2011) In vitro free radical scavenging activity of raw pepino fruit (solanum muricatum aiton). Int J Curr Pharm Res: 137-140.

Tiwari A (2001) Imbalance in antioxidant defense and human diseases: Multiple approach of natural antioxidants therapy. *Curr Sci* 81: 1179-1187.

Zheng.W and Wang.S.Y (2009) “Antioxidant activity and phenolic compounds in selected herbs,”*Journal of Agricultural and Food Chemistry,* vol. 49, no. 11, pp. 5165–5175,

CHAPTER 3
FUNCTIONAL FOOD PRODUCTS

INTRODUCTION

Recently there is a high demand for functional food. Claims have been made that modified functional foods can improve health or general well-being of the consumer by providing benefits beyond basic nutrition. Chocolate is one functional food. The nutritional value, composition of minerals and vitamins contained in four different treatments of chocolate fortified with pumpkin and taro powders have been studied in detail.

3.1 Proximate, Vitamin, and Mineral Compositions in Chocolate Fortified with Pumpkin and Taro Powders

Abstract

Pumpkin and taro are categorized as underutilized crops as lack of study was conducted to investigate their ability as a source of mineral and vitamin supplement. The aim of this study was to observe the nutritional value, composition of minerals and vitamins contained in four different treatments of chocolate fortified with pumpkin and taro powders. Fine particles of pumpkin and taro powders with a thickness of 45 mm were prepared by drying and sieving process before the fortification process of chocolate with pumpkin and taro powders. Next, the chocolates were further analysed to determine their nutritional value through the proximate analysis of mineral content by using the Inductively Coupled Plasma-Optical Emission Spectrometry (ICP-OES) and vitamin content by using the Ultraviolet–Visible (UV–VIS) Spectrophotometry. The data were presented in the mean value of three replications. The result showed that the chocolate fortified with pumpkin and taro powders obtained the highest result in each chemical analysis. The results were as follows; moisture (1.80 $\pm$ 0.04%), protein (6.73 $\pm$ 0.13%), fat (36.07 $\pm$ 0.10%), fibre (8.00 $\pm$ 0.39%), vitamin A (2.37 $\pm$ 0.03mg/g), vitamin D (2.15 $\pm$ 0.05 mg/g), vitamin E (3.52 $\pm$ 0.18 mg/g), potassium (14.02 $\pm$ 0.11 mg/g), phosphorus (14.34 $\pm$ 0.10 mg/g), magnesium (9.23 $\pm$ 0.09 mg/g) and calcium (9.38 $\pm$ 0.15 mg/g). Thus, it was proven that pumpkin and taro powders can enhance the nutritional value instead of vitamin and minerals contained in the human diet.

Keywords: pumpkin; taro tuber; fortification; nutritional value, vitamins, minerals

Introduction

Chocolate bars are the most consumed cocoa-derived products by all age groups in all range of society over the world (Konar et al., 2015). Chocolate is made up of sugar and cocoa mass suspended in cocoa butter matrix (Andarea-Nightingale et al., 2009). The cocoa is derived from a cocoa plant (*Theobroma cocoa*). The primary chocolate is divided into three categories known as dark, milk, and white which have a different amount of cocoa solid, milk fat, and cocoa butter formulation (Konar et al., 2015). This kind of food is popular in giving sensory pleasure and positive emotions. Cocoa products and chocolate are also known as a rich source of flavonoids, which

are majorly flavanols; a potent antioxidant which provides anti-inflammatory agents which aid in giving benefits for cardiovascular health. Despite their positive health effects, the pleasant satisfactory of chocolate products is probably the main reason for their popularity. However, in order to improve the satisfactory of having chocolate, the nutritional value and clinical benefits of chocolate were altered negatively due to its dilution and addition of flavour modifiers as well as the extensive processing.

Pumpkin is a member of the Cucurbitaceae family origins to tropical and subtropical America. Pumpkin is mostly related to fruits of different species of the genus which are Cucurbita, such as C. *pepo L*., C. *maxima* Duchesne, C. *moschata* Duchesne, C. *argyrosperma* Huber, and C. *ficifolia* Bouché (Ferriol & Picó, 2008). A polysaccharide which is pectin broadly used in the food industry and can be extracted from pumpkin pulp. The latest study of the existent of polysaccharides containing biological activity is related to the capacity that can increase serum levels of insulin and reduce blood glucose and show the potential use in the control of diabetes addition (Caili et al., 2006). Some carotenoids such as β-carotene and α-carotene in pumpkins are the precursors of vitamin A, which is a fat-soluble vitamin and important for normal growth and development of the human body. In addition, the consumption of carotenoids has been proven to reduce the risk of atherosclerosis and other cardiovascular diseases, protect against macular degeneration, and prevent certain types of carcinomas of the skin and prostate because of their antioxidant activities (Rao & Rao, 2007). Pumpkins have a great potential for industrialisation considering the low production costs and nutritional value (Provesi & Amante, 2015).

There is a range of products that can be developed from pumpkins, which presents consumer foods that have long shelf-life and good nutritional value. Taro (*Colocasia esculenta*) is the main root crop in the humid tropics and also a great source of essential mineral nutrients. Taro cultivars are divided into two groups which are cultivars adapted to permanent irrigation (paddy cultivars) and upland conditions. Corms of typical upland varieties are usually round or slightly elongated, whereas the extremely elongated corms are paddy genotypes (Lebot, 2009). Corms vary in size, shape, and colour, depending on the age, genetic structure, and interactions between the genotype and environment. The corm of taro consists of three major parts which are the cortex, skin, and core (the central part) while there are four main parts of mineral composition in taro comb which are the upper, marginal central and lower (basal) parts (Mergedus et al., 2015). Calcium is concentrated in the lower and marginal parts. Instead of its nutritional content, it is traditionally used as a medicinal plant which provides a bioactive compound with important biological properties (Pereira et al., 2015). Both plants used in this study are underutilised crop and abundantly planted at the east coast of Malaysia. However, they are being neglected despite being a plant that can contribute many benefits to the human being. The use of the underutilised crop in Malaysia must be converted into the various needs of the community. As the demand for plant and crop attributes changes, neglected crops can overcome the constraints to the wider production and use.

Nowadays, people have begun to take care of their physical health. Functional food has become increasingly popular in recent years and lead to high demand. The modified functional food claims to improve health or well-being by providing benefits beyond basic nutrition. Chocolate can be categorised as one type of functional foods. Previous studies have been conducted on the effects of chocolate intake in

the cardiovascular system, cholesterol concentrations, and the release of neurotransmitters anandamide and serotonin, and health-related properties of high-quality dark chocolate containing the theobromine and caffeine stimulants (Lamuela-Raventós et al., 2005; Katz et al., 2011). Besides that, there are also studies of chocolate on the influence of theobromine and caffeine on mood and cognition (Smit & Rogers, 2000; Smit et al., 2004; Smit & Blackburn, 2005; Nehlig, 2010). The availability of underutilised crops like pumpkin and taro tuber is very broad and easy to find which is abundantly planted in Malaysia especially at the east coast. Most people use pumpkin and taro tuber for cooking only instead of converting them into various needs of the community. Pumpkin which is rich with carotenoid has been related to reduce the risk of atherosclerosis and other cardiovascular diseases, protect against macular degeneration, and prevent certain types of carcinomas such as those of skin and prostate (Rao & Rao, 2007). Meanwhile, some studies of the mineral compositions of taro corms suggested that potassium is the more abundant and essential mineral for many bodily functions while other abundant minerals include magnesium, phosphorus, calcium, vitamins C, E, and B (Huang et al., 2007; Lewu et al., 2010; Mwenye et al., 2011; Muhammad et al., 2014). However, there is lack of research on focusing their potential value as a functional food. Thus, this study was conducted to observe the nutritional value, composition of minerals, and vitamin content in four different treatments of chocolate fortified with pumpkin and taro powders.

Materials and Methods

Production of Chocolates

Extra dark and white chocolates were purchased at markets around Jerteh, Besut. 200 g of extra dark and white chocolates were chopped to reduce the size and melted in tempered machine at 35 ºC for white chocolate and 40 ºC to 45 ºC for dark chocolate. Next, both chocolates were moulded and coated with white chocolate. For fortified chocolate, 0.5% of taro and pumpkin powders were added after the melting process followed by the moulding and cooling processes. Four types of chocolate produced were chocolate fortified with taro and pumpkin powders (TP), chocolate fortified with pumpkin powder (P), chocolate fortified with taro powder (T), and non-fortified chocolate (C) as the controlled sample.

Proximate Analysis

The proximate analysis which consists of an analysis of moisture, ash, crude protein, fat, crude fibre, carbohydrate, and energy content was determined according to the method described by AOAC with slight modification (AOAC, 2000).

Vitamin Analysis

Vitamins A, D, and E of the chocolate samples were determined according to the method described by Ashok and Kumar (2011) with a slight modification.

Mineral analysis

Mineral analysis was conducted by using inductively coupled plasma optical emission spectrometry ICP-OES following a method described by AOAC 2000.

Statistical Analysis

All experiments were performed in triplicates. The results were analysed and tested by using independent T-test using the SPSS software. The mean value of the samples was subjected to the Turkey test to compare the properties and compositions of the samples. The statistical differences indicated 95% of confidence level.

Results and Discussions

Proximate Analysis Content

In the experiment, the data of four treatments of chocolates; TP, P, T, and C were recorded in Table 1. The proximate of four treatments of chocolates was analysed for their moisture, protein, fat, crude fibre, ash, carbohydrate, and energy to determine the differences in nutritional composition among the types of the chocolate samples. The chemical composition of the chocolates is shown in Table 1. For those types of chocolate, carbohydrate was the major nutrient (> 45%) and followed by fat (> 35% - 37%).

According to Torres-Moreno et al. (2014), the amount of carbohydrate content in chocolates is the major nutrients mainly represented as sugar with total content up to 45%. Meanwhile, the major nutrient in cocoa beans is the fat content. Thus, the amount of carbohydrate in chocolate is opposite to the amount of carbohydrate in cocoa beans. The value of carbohydrate percentage decreases with respect to an increase in the total fat content when the cocoa solid content of chocolate increases. The fibre content ranged between 3% and 8%, meanwhile protein content less than 7%, and ash and moisture were less than 2%. The types of chocolate composition varied depending on the types of the fortification. TP and C have significant differences in moisture, ash, protein, fibre, and carbohydrate. No significant difference between TP and C was observed in fat. TP and T have significant differences in protein, fat, fibre, and carbohydrate. There was no significant difference between TP and T in terms of moisture and ash. TP and P had significant differences in moisture, protein, fibre, and carbohydrate and no significant difference in ash and fat. T and P had significant differences in moisture and fat only and showed no significant difference in ash, protein, fibre, and carbohydrate.

TP showed the highest moisture (1.80%) followed by T (1.67%), P (1.30%), and C (1.29%). The range of moisture content obtained in those chocolates was relevant to the previous study reported by Torres-Moreno et al. (2014). The moisture content of the chocolates increased after they were being fortified with pumpkin and taro powders. When the amount of pumpkin flour increases, moisture content also increases (El-Demery, 2011; Ptitchkina et al., 1998). This may be due to the pumpkin powder which has a high tendency of water binding capacity to retain higher moisture in the food products.

The ash content obtained from different treatments of chocolates; C, T, P, and TP was found to be 1.51%, 1.60%, 1.61%, and 1.60%, respectively. From Table 1, the maximum ash content obtained by P was followed by TP, T, and C. Previous study on the evaluation of physico-chemical properties of toasted bread fortified with pumpkin (*Cucurbita moschata*) flour found that the pumpkin flour was rich with minerals such as sodium, potassium, calcium, iron, and phosphorus (El-Demery,

2011). Jun et al. (2006) reported that pumpkin is a good source of carotene, pectin, mineral salts, vitamins, and other substances that are beneficial to health. The ash content of taro reported by Mbofung et al. (2006) and Nijoku and Ohia (2007) ranged from 3.54 – 7.78%. The removal of moisture during drying also contributes to the increase of the amount of ash in taro. According to USDA (2010), chocolate also consists of minerals, especially potassium, magnesium, copper, and iron. These actually show the reasons of the fortified chocolates to have higher maximum ash content compared to the control sample.

Taro contains about 11% protein content which is high compared to the other root crops due to the presence of symbiotic soil bacteria in the root and rhizome parts of taro (Temesgen & Retta, 2015). The value of protein in pumpkin flour reported by Ptitchkina et al. (1998) was 9%, while See et al. (2007) found 9.65%. The value of protein content in the cookies after being fortified with pumpkin powder as reported by Kumar Pratyush et al. (2015) increased proportionally with the increase in pumpkin powder because of the good amount of protein content (6%). Some researchers also found out that the amount of protein in their food production increased after being fortified with pumpkin (El-Demery, 2011; Kumar Pratyush et al., 2015). Thus, the result obtained by the fortified chocolates, which was higher than the control, was in agreement with the previous study. However, the amount of protein content in the fortified chocolates and the control was quite close to each other in the range of 6%. This may be due to the small amount of ratio between pumpkin and taro to fortify the chocolates.

The fat content was the second highest component of those four treatments. The chocolate samples were made up from a dark chocolate compound that has high cocoa content and white chocolate compound high in cocoa butter (Beckett et al., 2008) in the same ratio. The high amount of cocoa in the dark chocolate contributes the high amount of fat in the chocolate (Torres-Moreno et al., 2014). There was no significant ($p>0.05$) difference among the chocolates except for T. The range of the fat content was close to the values reported by Torres-Moreno et al. (2014), where the fat content in the chocolate was > 32%. The result obtained was quite similar with the previous study by El-Demery (2011) which showed no significant difference between the control and toasted bread fortified with pumpkin flour. The evidence of the result was supported by See et al. (2007) who claimed that the lower fat content in pumpkin flour reduced the fat content in the food product compared to the control. The value of fat content in taro is very low as many other root and tuber crops because it is mainly composed of the lipids of the cell membrane (Temesgen & Retta, 2015).

The fibre result showed that the fortified chocolates were better than the control. Fruits and vegetables are the great sources of fibre even though the content is not as good as in cereals (De Escalada Pla et al., 2007: Kumar Pratyush et al., 2015). The fortification of taro and pumpkin in chocolates gives slightly improvement in fibre content. As TP has been fortified with both the pumpkin and taro powders, the sample has the highest result of fibre content (8.00%) and showed a significant difference with the control. Based on the previous study by Ptitchkina et al. (1998), pumpkin powder contains the main components of insoluble dietary fibre that are cellulose (40%), hemicellulose (4.3%), and lignin (4.3%), which are vital in buffering the pH in stomach due to the excess acid produced by the digestive system,

intestinal emptying, and also aiding faecal bulking (Vergara-Valencia et al., 2006). Therefore, consuming chocolate with the presence of fibre is beneficial for health.

The main component in chocolate is carbohydrate. The highest carbohydrate content was obtained in C (51.25%) followed by T (49.23%), P (48.90 %), and TP (45.80%). According to El-Demery (2011), in a study of toasted bread fortified with pumpkin flour, the value of carbohydrate and energy obtain decreased with the increased amount of pumpkin flour similar with the result obtained in the current study. On the other hand, the total carbohydrate in the toasted bread reduced in substitution of wheat with pumpkin flour (See et al., 2007). Starch is known as the main carbohydrate source needed in the human diet (Simsek & Nehir El, 2012) and the composition of starch in taro has been reported to be about 70-80% (Temesgen & Retta, 2015). The small size of starch granules which contain about 50% less amylose and amylopectin content has been claimed as highly digestible compared to other cereals (Temesgen & Retta, 2015). The trend of the fat content obtained in the chocolates is in agreement with the previous study.

The energy obtained in C (553.40%) was higher than P (534.81%), T (538.47%), and TP (534.79%). This may be due to the content of fibre in the fortified chocolates (T, P, and TP). Pratyush et al. (2015) reported that the energy content reduced with the increasing pumpkin flour in all products. The high fibre in food snack was vital to reduce healthier calories as it was associated with reduced risk of lifestyle diseases (Vergara-Valencia et al., 2006). However, the value obtained by the fortified chocolates cannot be claimed as a low-energy food as the maximum amount of energy for the low energy food is 58 KJ (14 kcal) per 100 g.

Table 1: Nutritional composition of four treatments of chocolates fortified with pumpkin and taro powders (per 100 g)

Nutrients	Composition (%)			
	Control (C)	Chocolate fortified with taro(T)	Chocolate fortified with pumpkin (P)	Chocolate fortified with pumpkin and taro powder (TP)
Moisture	$1.29^{a} \pm 0.22$	$1.67^{b} \pm 0.04$	$1.30^{a} \pm 0.05$	$1.80^{b} \pm 0.04$
Ash	$1.51^{a} \pm 0.05$	$1.60^{b} \pm 0.02$	$1.61^{b} \pm 0.05$	$1.60^{b} \pm 0.03$
Protein	$6.19^{a} \pm 0.21$	$6.30^{a} \pm 0.11$	$6.12^{a} \pm 0.14$	$6.73^{b} \pm 0.13$
Fat	$35.96^{b} \pm 0.13$	$35.15^{a} \pm 0.22$	$35.97^{b} \pm 0.11$	$36.07^{b} \pm 0.10$
Fiber	$3.80^{a} \pm 0.54$	$6.06^{b} \pm 0.44$	$6.12^{b} \pm 0.51$	$8.00^{c} \pm 0.39$
Carbohydrate	$51.25^{c} \pm 0.32$	$49.23^{b} \pm 0.60$	$48.90^{b} \pm 0.40$	$45.80^{a} \pm 0.44$
Energy	$553.4^{d} \pm 8.37$	$538.47^{a} \pm 7.04$	$543.81^{c} \pm 9.02$	$534.79^{b} \pm 6.43$

*Values in column followed by different superscript letter “a.b,c,d” are significantly different ($p<0.05$)

Vitamins Analysis

The presented data in Table 2 show the average vitamin contents of different treatments of C, T, P, and TP of chocolates fortified with pumpkin and taro powders. It shows that the vitamin content increased significantly with the content of pumpkin and taro powders in the chocolate. According to Jun et al. (2006), pumpkin is a good

source of carotene, vitamins, and mineral which give benefits to health. Other researchers also found that the high β-carotene in pumpkin gives a pleasant yellow-orange colour and is a major source of Vitamin A (Kumar Pratyush et al., 2015; Lee, 1983). This is in agreement with the increase in the concentration of vitamin A in the chocolate fortified with pumpkin powder. Lack of β-carotene in the human diet is considered a cost-effective approach to vitamin A related health problem (Berteram &Bortkiewica, 1995).

Vitamins / Treatments	A	D	E
Control(C)	$1.82^{a} \pm 0.12$	$1.32^{a} \pm 0.22$	$0.03^{a} \pm 0.01$
Chocolate fortified with taro powder (T)	$2.14^{b} \pm 0.01$	$1.88^{b} \pm 0.10$	$1.31^{b} \pm 0.18$
Chocolate fortified with pumpkin powder (P)	$2.22^{bc} \pm 0.01$	$1.91^{b} \pm 0.06$	$1.13^{b} \pm 0.19$
Chocolate fortified with pumpkin and taro powder (P)	$2.37^{c} \pm 0.03$	$2.15^{c} \pm 0.05$	$3.52^{c} \pm 0.18$

Table 2: Vitamin contents of chocolates fortified with pumpkin and taro powders

*Values in column followed by different superscript letter “a.b,c,d” are significantly different ($p<0.05$)

Minerals Analysis

Mineral contents in the chocolates of four different treatments fortified with pumpkin and taro powders are shown in Table 3. Mineral content was significantly observed between the control and all treatments which contained pumpkin and taro powders. However, there was no significant difference found between all treatments in their content of magnesium (Mg). The mineral content increased with both contents of pumpkin and taro powders in the chocolate which is in agreement with the previous study reported by El-Demery (2011) where the mineral content in the toasted bread increased as the pumpkin flour increased. The values obtained for Kalium, Phosphorus, Magnesium and Calcium were reasonably high in the fortification of both powders in chocolates compared to control that may satisfy the nutritional needs of consumers. In a previous study, Gomaa (2000) found that 5% of pumpkin pulp flour used in infant food formula gave improvements in its mineral content. The concentration of Ca and P in T is higher than C. This is because taro belongs to the family araceae which is known to be rich in oxalate calcium crystal due to the irritation of uncooked taro (Aboubakar et al., 2008; Sira, 2000). The covalent link between phosphorus and starch in the taro tuber was reported by Takeda et al. (1986). The higher amount of phosphorus content in starch granule resulted in lower resistant starch (Liu et al., 2007). On the hand, taro is a good source of iron, sodium, magnesium, zinc, and copper and an excellent source of potassium. The high concentration of potassium to sodium ratio food is recommended for patients with high blood pressure (Temesgen & Retta, 2015).

Table 3: Mineral content of chocolate fortified with pumpkin and taro powders

Minerals / Treatments	K	P	Mg	Ca
Control(C)	$12.16^{a} \pm 0.11$	$10.45^{a} \pm 0.49$	$9.00^{a} \pm 0.62$	$7.40^{a} \pm 0.34$
Chocolate fortified with taro	$12.17^{a} \pm 0.21$	$12.17^{b} \pm 0.18$	$9.15^{a} \pm 0.16$	$8.18^{b} \pm 0.19$

powder (T)				
Chocolate fortified with pumpkin powder (P)	$13.89^{b} \pm 0.19$	$13.25^{c} \pm 0.26$	$9.03^{a} \pm 0.17$	$8.92^{c} \pm 0.12$
Chocolate fortified with pumpkin and taro powder (P)	$14.02^{b} \pm 0.11$	$14.34^{d} \pm 0.10$	$9.23^{a} \pm 0.09$	$9.38^{c} \pm 0.15$

*Values in column followed by different superscript letter "a.b,c,d" are significantly different ($p<0.05$)

Conclusion

The present investigation was carried out with the development and preparation of chocolate fortified with pumpkin and taro powders. Chocolates containing both pumpkin and taro powders (TP) were found to be the most satisfactory after testing with chemical analyses like the proximate analysis (ash, moisture, protein, fat, fibre, carbohydrate and energy), vitamin analysis (vitamins A, D, and E) and mineral analysis (K, P, Mg, and Ca). C and TP were found to be significantly different in each chemical analysis. Meanwhile, chocolates containing pumpkin powder (P) and taro powder (T) were found to be significantly different in moisture, fat, energy, and minerals analyses. This study revealed that pumpkin and taro powder increased the nutritional value of the chocolates. Thus, chocolate can be one of the functional food varieties in the confectionary industry. The ideas and information gained from this research are useful to those who are interested in similar work in terms of increasing food nutritional value using underutilised local crops which are pumpkin and taro tuber.

Acknowledgements

We would like to thank the Food Analysis Laboratory, UniSZA for the facilities and the Pre-commercialisation grant R291 for the financial provided.

References

Aboubakar, Njintang Y.N., Scher J. and Mbofung C.M.F. (2008) Physiological, thermal properties and microstructure of six varities of taro (Calocasia esculenta L. Schott) flours and starches. Journal of Food Engineering 86, 294–305.

AOAC (2000). Official Methods of Analysis. 17th ed. Gaithersburg, Maryland, USA, AOAC International.

Andarea-Nightingale, L.M., Lee, S.Y., & Engeseth, N.J. (2009). Textural changes in chocolate characterized by instrumental and sensory techniques. Journal of Texture Studies, 40(4): 427-444.

Ashok, K., Gaurav, R.K. (2011). To Develop a Simple (UV-VIS Spectrometric) Method for the Estimation of Multivitamin with Special Reference to Capsules & Tablets. International Journal of Pharmagenesis, 2(1), pp. 43-48.

Berteram, J.S. and Bortkiewicz, H. (1995). Dietary carotenoid inhibit neoplastic transformation and modulate gene expression in mouse and human cell. Am. J. Clin. Nutr., 62: 132S-136S.

Caili, F., Huan, S., Quanhong, L. (2006). A review on pharmacological activities and utilization technologies of pumpkin. Plant Food Human Nutrition, 61(2): 73–80.

El-Demery ME, (2011). Evaluation of physico-chemical properties of toast bread fortified with pumpkin (Cucurbita moschata) flour, The 6th Arab and 3rd International Annual Scientific Conference on Development of Higher Specific Education Programs in Egypt and the Arab World in the Light of Knowledge Era Requirements, Faculty of Specific Education, Mansoura University, Mansoura, Egypt 13–14.

Ferriol, M., Picó, B. (2008). Pumpkin and Winter Squash. In Prohens, J., Nuez, F. (Eds.), Vegetables I (317–349). Springer, New York.

Huang, C. C., Chen, W. C., & Wang, C. C. (2007). Comparison of Taiwan paddy- and upland-cultivated taro (Colocasia esculenta L.) cultivars for nutritive values. Food Chemistry, 102(1): 250-256.

Jun, H., Lee, C., Song, G. and Kim, Y. (2006). Characterization of pectic and polysaccharides from pumpkin peel. Lebensmittel-Wissenchaft und-Technologie 39: 554-561

Lamuela-Raventos, R. M., Romero-Pérez, A. I., Andrés-Lacueva, C. & Tornero, A. (2005). Review: Health Effects of Cocoa Flavonoids. Food Science and Technology International, 11(3): 159-176.

Lebot, V. (2009). Tropical root and tuber crops: Cassava, sweet potato, yams and aroids. Wallingford, UK. CABI, Cambridge, MA.

Lee, K. W., Kim, Y. J., Lee, H. J. & Lee, C. Y. (2003). Cocoa has more phenolic phytochemicals and a higher antioxidant capacity than teas and red wine. Journal of agricultural and food chemistry, 51(25): 7292-7295.

Lewu, M. N., Adebola, P. O. & Afolayan, A. J. (2010). Effect of cooking on the mineral contents and anti-nutritional factors in seven accessions of Colocasia esculenta (L.) Schott growing in South Africa. Journal of Food Composition and Analysis, 23(5): 389-393.

Liu, Q., Tarn, R., Lynch, D., Skjodt, N.M., 2007. Physicochemical properties of dry matter and starch from potatoes grown in Canada. Food Chemistry 105, 897–907.

Katz, D. L., Doughty, K. & Ali, A. (2011). Cocoa and Chocolate in Human Health and Disease. Antioxidants & Redox Signaling, 15(10): 2779-2811.

Konar, N., Toker, O. S., Oba, S. & Sagdic, O. (2016). Improving functionality of chocolate:
A review on probiotic, prebiotic, and/or synbiotic characteristics. Trends in Food Science & Technology, 49: 35-44.

Mbofung, C.M.F., Aboubakar, Njintang, Y.N., Abdou Bouba, A., Balaam, F., 2006. Physicochemical and functional properties of six varieties of taro (Colocasia esculenta L. Schott) flour. Journal of Food Technology 4, 135–146.

Mergedus, A., Kristl, J., Ivancic, A., Sober, A., Sustar, V., Krizan, T., & Lebot, V. (2015). Variation of mineral composition in different parts of taro (Colocasia esculenta) corms. Food Chemistry, 170: 37-46.

Muhammad, L., Abbas, K., & Asa, N. (2014). Development and Proximate Properties of Acceptable Taro-Soybean Floue. International Journal for Research in Applied Science and Enggineering Technology (IJRASET), 2(4): 310-317.

Mwenye, O. J., Labuschagn, M. T., Herselman, L., & Benesi, I. R. M. (2011). Mineral Composition of Malawian Cocoyam (Colocasia esculenta and Xanthosoma sagittifolium) Genotypes. Journal of Biological Sciences, 11(4): 331-335.

Pereira, P. R., Winter, H. C., Vericimo, M. A., Meagher, J. L., Stuckey, J. A., Goldstein, I. J., Paschoalin, V. M., & Silva, J. T. (2015). Structural analysis and binding properties of isoforms of tarin, the GNA-related lectin from Colocasia esculenta. Biochimica et Biophysica Acta (BBA)- Protein and Proteomics, 1854(1): 20–30.

Provesi, J. G. & Amante, E. R. (2015). Carotenoids in Pumpkin and Impact of Processing
Treatments and Storage. Processing and Impact on Active Components in Food (71-80).

Ptitchkina N.M., Novokreschonova L.V., Piskunova G.V., Morris ER. (1998). Large enhancement in loaf volume and organoleptic acceptability of wheat bread by small additions of pumpkin powder: possible role of acetylated pectin in stabilizing gas-cell structure. Food Hydrocolloids 12:333–7.

Rao, A. V., & Rao, L. G. (2007). Carotenoids and human health. Pharmacological Research, 55(3): 207-216.

See E.F., Wan Nadiah W.A. and Noor Aziah A.A. (2007). Physico-chemical and sensory evaluation of breads supplemented with pumpkin flour. ASEAN Food J 14(2):123–30.

Simsek, S. & Nehir El, S. (2012). Production of resistant starch from taro (Calocasia Esculenta determination of its effect on health by in vitro methods. Carbohydrate Polymers, 90: 1204-1209.

Sira, P. E. E. (2000). Determination of the correlation between amylose and phosphorus content and gelatinization profile of starches and flours obtained from edible tropical tubers using differential scanning calorimetry and atomic absorption spectroscopy. Master Thesis, University of Wisconsin-Stout, 81 pp.

Smit, H. J., & Rogers, P. J. (2000). Effects of low doses of caffeine on cognitive performance,
mood and thirst in low and higher caffeine consumers. Psychopharmacology, 152(2): 167-173.

Smit, H. J., & Blackburn, R. J. (2005). Reinforcing effects of caffeine and theobromine as found in chocolate. Psychopharmacology, 181(1): 101-106.

Torres-Moreno, M., Torrescasana, E., Salas-Salvadó, J. and Blanch, C., (2014). Nutritional
composition and fatty acids profile in cocoa beans and chocolates with different Geographical origin and processing conditions. Food Chemistry.

Temesgen, M. & Retta, N., (2015). Nutritional Potential, Health and Food Security Benefits of Taro Colocasia Esculenta (L.). Food Science and Quality Management, 36: 23-30

USDA. Food Composition Databases Show Foods List. 15 April 2017. https://usdasearch.usda.gov/

Vergara-Valencia, N., Graados-Perez, E, Agama-Acevedo, E., Tovar, J., Ruales, J. and Bello- Perez, L.A. (2006) Fibre concentrate from mango fruit: Characterization, associated
antioxidant capacity and application as a bakery product ingredient. Lebensmittel-Wissenchaft und-Technologie 40(4): 722-729.

3.2 Physicochemical Properties of Cookies Incorporated with Breadfruit *(Artocarpus altilis)* Flour

Abstract

Production of cookies from breadfruit flour has potential to serve as vehicle for important nutrients. This is because breadfruit is reported to contain high amount of fibres, proteins, carbohydrates, minerals, fats and vitamins. The aims of this study is to determine the physicochemical properties of breadfruit flour (BF) cookies. These cookies were formulated in the ratio of 0:100, 20:80, 30:70, 40:60, 50:50, 100:0 (breadfruit flour: wheat flour:) (BF:WF),respectively. The results showed a significant difference ($p<0.05$) in terms of moisture, ash, protein, fibre and calorie among all tested cookies. An increasing level of breadfruit flour in the cookies formulation resulted in an increase in moisture, ash, fibre and hardness. Thus, the BF might have potential to be incorporated in cookies production and commercialised.

Keywords: Breadfruit flour, fiber, cookies, nutritional value

Introduction

Breadfruit has been identified as an alternate source of carbohydrate and the starch can be processed into many forms. Breadfruit is a rich source of carbohydrates, minerals and vitamins (Deivanai & Subhash, 2010). There are potentials in using wheat-breadfruit composite flour in bread, pancakes, pastries, muffin, cookies and other bakery products (Goburdhun et al., 2012). Cookies are considered to be a concentrated food due to high contents of carbohydrates, fats and low moisture. As such, they are a substantial source of energy. From the nutritional point of view, their quality can be enhanced by including a number of ingredients in the recipe. In this

way, cookies have a great potential to become a good medium for providing special dietary needs (Škrbić & Cvejanov, 2011). In Malaysia, the bakery industry has grown tremendously over recent years (Noor Aziah & Komathi, 2009). According to Sudha et al. (2007), bakery products are varied by the addition of value added ingredients. Thus, the increasing number of applications of composite flour in many bakery and pastry products has spurred a growing number of studies on the effects of different types of material used to produce flour, especially on their physicochemical and functional properties. Due to the growing market for confectioneries, local raw materials substitution for wheat flour is increasing (Noor Aziah & Komathi, 2009). Therefore, several developing countries have encouraged initiation in programmes to evaluate the feasibility of available alternative local flours as a replacement for wheat flour (Abdelghafor et al., 2011). Breadfruit flour may be commercialised in cookies production.It can also provide more nutritional value to the cookies. More information about breadfruit flour cookies and its nutrition that may be beneficial to humans is also be provided in this study. Thus, the main objective of this study was to determine the physicochemical properties of cookies produced by using different ratios of breadfruit and wheat flour.

Materials and Methods

Preparation of cookies

Cookies were prepared according to the formula suggested by Noor Aziah et al. (2012) with a slight modification. Formulas that were used for making cookies are shown in Table 3.1. The composition of the BF and WF were 0:100, 20:80, 30:70, 40:60, 50:50, 100:0 for formula WFC, BFC20, BFC30, BFC40, BFC50, BFC100,respectively. Cookies that were produced by using formula WFC, which does not contain BF, were used as a control. The dough was rolled and cut with a round cutter of diameter 32 mm and 5 mm thickness and baked on a greased pan for 20 minutes at 175ºC in an oven. The cookies were cooled at room temperature for 30 minutes before packed in an airtight plastic container prior to physical and chemical evaluations.

Table 3.1 Formulation of cookies

Ingredients (g)	WFC	BFC20	BFC30	BFC40	BFC50	BFC100
Wheat flour (WF)	42.5	34	29.75	25.5	21.5	0
Breadfruit flour (BF)	0	8.5	12.75	17	21.5	42.5
Sugar	20.5	20.5	20.5	20.5	20.5	20.5
Shortening	20.5	20.5	20.5	20.5	20.5	20.5
Egg	15.0	15.0	15.0	15.0	15.0	15.0
Baking Powder	0.7	1.0	1.0	1.0	1.0	1.0
Salt	0.4	0.4	0.4	0.4	0.4	0.4
Vanilla essence	0.4	0.1	0.1	0.1	0.1	0.1
Total	100	100	100	100	100	100

Colour analysis
The colour of sample was determined by using Konica Minolta Chroma Meter CR-400.

Weight Loss, diameter, thickness and spread ratio of the cookies
The cookies were randomly selected for analysis. To calculate weight loss, the before and after baking weight of cookies was taken. The height and diameter of cookies after baking were measured by using a calliper. To measure the diameter of cookies, four samples were placed next to one another and the total diameters were measured. Then, all cookies were rotated at 90^{o} and the new diameters were measured. This step was repeated for angles 180^{o}, 270^{o} and 360^{o},respectively. The average diameter was recorded. Cookies thicknesses were measured by stacking four cookies above another and then measuring the height. This step was repeated by restacking the cookies for four times. The average thickness was recorded. The spread ratio was calculated by dividing diameter of cookies with thickness of cookies (Zoulias et al., 2000).

Texture analysis
Texture properties of cookies was determined by using a texture analyzer TA-XT2i.

Determination of moisture
The moisture content of the sample was determined according to AOAC (2001).

Determination of ash, protein and fat
Ash, protein and fat content of the sample were determined according to AOAC (2004).

Determination of crude fiber
The crude fibre content of the sample was determined according to AOAC, (2000)

Determination of carbohydrate
The percentage of carbohydrate in the sample was determined by subtracting 100% with the percent of moisture, ash, crude protein and crude fat content (BeMiller 2010).

Determination of calorie
Determination of calorie was done by calculation. Carbohydrate and protein has four calories per gram and fat has nine calories per gram (US Food and Drug Administration, 2004).

Results and Discussion

Colour analysis of cookies
The colour result of cookies is shown in Figure 4.1. From the result, the lightness (L) of the cookies displayed a decreasing trend as the substitution level of breadfruit flour was increased. The L value of WFC100 (78.52) was significantly higher than BFC (69.87 – 57.89). Chaucan et al. (2016) reported that the reducing values of L meant that the composite cookies colour became darker when the substitution level of composite flour was at a higher level. The redness (a*) of the cookies had shown a reverse trend where the a* values increased as the breadfruit flour in the cookies

was increased. The yellowness (b*) of the cookies showed a decreasing trend as the level of breadfruit flour was increased. According to Chevallier et al. (2000), protein content was negatively correlated with lightness of cookies. It showed that Maillard reaction has played an important role in color formation, where because of Maillard browning and caramelisation of sugar brown pigments were produced during baking.

Table 4.1 Color analysis of cookies

	L	a*	b*
WFC100	78.52 ± 0.27f	-0.19 ± 0.10[a]	24.98 ± 0.49[c]
BFC20	69.87 ± 0.09e	3.82 ± 0.41[c]	23.74 ± 0.50[b]
BFC30	66.45 ± 0.04[d]	3.00 ± 0.20[b]	21.65 ± 0.66[a]
BFC40	64.78 ± 0.08[c]	6.18 ± 0.36[d]	24.72 ± 0.29[c]
BFC50	62.70 ± 0.19[b]	6.72 ± 0.09[d]	24.70 ± 0.08[c]
BFC100	57.89 ± 0.05[a]	8.34 ± 0.60[e]	24.31 ± 0.63[bc]

Values in the same column with different alphabet are statistically significant from each other ($p<0.05$). Presented data are mean value of triplicate ± standard deviation.

Diameter, thickness, spread ratio and weight loss of cookies

Diameter (mm), thickness (mm), spread ratio (mm) and weight loss (g) of the cookies are presented in Table 4.2. Protein content influences the viscosity of dough cookies because the protein gluten expansion is not resumed in cookies making. Diameter of cookies was inversely correlated between protein content. However, from the result WFC100 has a significantly higher diameter as compared to BFC, even though it has the highest protein content (7.03, Table 4.4). This trend was the same as a study by Noor Aziah et al. (2012) where chickpea cookies have the highest diameter even though the protein content was high. The thickness of the cookies decreases significantly as the BF level was increased. According to Noor Aziah et al. (2012) reduction of dough viscosity will increase the spread rate of cookies. From the result, WFC has a significantly higher ($p<0.05$) spread ratio as compared to BFC20, 30, 40 and 50 because WFC has lower dough viscosity as compared to the other dough. The result showed that breadfruit flour substitution had significantly affected ($p<0.05$) the cookies weight loss, where it was decreased as the BF increased. WFC100 (0.82) weight loss was highest as compared to BFC30, BFC40, BFC50 and BFC100,respectively. This means that the WFC100 has the lowest water holding capacity as compared to the other cookies because it has the highest protein content (7.03, Table 4.4). This finding was support by the study from Noor Aziah et al. (2012) where they found that chickpea cookies has the lowest weight and a higher weight loss as compared to mug bean and control cookies due to its high protein content. It is said that water holding capacity for non-wheat protein is higher than in wheat flour.

Therefore, the cookies with BF weight loss was lower ascompared to WFC100 because BF was a non-wheat protein thus it had a higher water holding capacity.

Table 4.2 Diameter, thickness, spread ratio and weight loss of cookies

	Diameter (mm)	Thickness (mm)	Spread Ratio (mm)	Weight Loss (g)
WFC100	17.20 ± 0.00^{f}	2.23 ± 0.04^{c}	7.82 ± 0.00^{d}	0.82 ± 0.01^{c}
BFC20	16.40 ± 0.00^{e}	2.11 ± 0.01^{b}	7.73 ± 0.02^{c}	0.78 ± 0.03^{bc}
BFC30	16.20 ± 0.00^{d}	2.11 ± 0.02^{b}	7.71 ± 0.00^{c}	0.74 ± 0.05^{ab}
BFC40	16.12 ± 0.04^{c}	2.13 ± 0.01^{b}	7.59 ± 0.00^{b}	0.72 ± 0.01^{a}
BFC50	15.84 ± 0.03^{b}	2.10 ± 0.01^{b}	7.51 ± 0.02^{a}	0.72 ± 0.05^{a}
BFC100	15.72 ± 0.04^{a}	1.93 ± 0.04^{a}	8.21 ± 0.02^{e}	0.69 ± 0.00^{a}

Values in the same column with different alphabet are statistically significant from each other ($p<0.05$). Presented data are mean value of triplicate ± standard deviation.

The hardness of cookies (Table 4.3) increased significantly as the BF level increased. BFC100 recorded the highest hardness (4.20) while WFC100 recorded the lowest hardness (2.47). According to Axel et al. (2017), breadfruit is a gluten-free fruit. A typical wheat-based cookie is made from soft flour which means it has a lower protein (gluten) content than hard wheat flour that is used to make wheat breads. Protein content in the flour helps to hold the dough and final cookies or bread together making the cookie soft and easy to chew but strong enough to keep from crumbling. However, using a gluten-free flour will cause the dough to no longer have the majority protein structure because gluten-free flour do not have the same type of proteins that can hold other contents together (Ryberg, 2010). Thus, the dough cannot efficiently hold water and other ingredients, thus making the dough crumble and harden as the level of BF was increased.

Table 4.3 Texture analysis of cookies

Cookies	Hardness
WFC100	2.47 ± 0.06^{a}
BFC20	3.17 ± 0.15^{b}
BFC30	3.21 ± 0.19^{b}
BFC40	3.37 ± 0.31^{bc}
BFC50	3.69 ± 0.17^{c}
BFC100	4.20 ± 0.29^{d}

Values in the same column with different alphabet are statistically significant from each other ($p<0.05$).Presented data are mean value of triplicate ± standard deviation.

Chemical analysis of cookies

The moisture content of cookies increased significantly ($p<0.05$) with increasing levels of added BF (Table 4.4). The highest moisture content was 4.29% which was in BFC100. Ebere and Kiin-Kabari (2015) reported that the moisture content of cookies increased as the levels of cashew-apple fibre increased. According to Monitoba Agriculture (2017), the moisture content of cookies should not exceed 6% and from the result; the moisture content of produced cookies still falls within the range. The ash content of cookies was found to be significantly increased as the BF was increased from 1.25 % in WFC100 to 2.20 % in BFC100. Ragone, (2003) reported that breadfruit contains a higher ash content than wheat and this could be the reason for the higher ash content in cookies that contain BF. According to Adekunle and Mary (2014), the high ash content indicated high levels of minerals in samples. Olaoye et al. (2007); biscuit, Ajani et al. (2012); snacks and Agu et al. (2007); biscuit also discovered that ash content of their products increased with increase in the proportion of breadfruit flour. There were significant difference ($p<0.05$) in the protein content of the produced cookies. The protein content significantly decreased as BF level increased. WFC100 indicated a higher protein content (7.03%) as compared to cookies substituted with breadfruit flour with range (6.62% – 4.60%). The fibre content of cookies ranged between 0.33% and 3.99%, where it showed a corresponding increase with increasing levels of BF. The fibre content in BFC100 was significantly higher ($p<0.05$) as compared to other cookies. This showed that breadfruit has a relatively higher crude fibre than wheat and this could justify the result obtained for the different cookies samples. This observation was supported with the finding of Olaoye et al. (2007) for biscuits and Ajani et al. (2012) for snacks where they found that fibre content of the products increased as the BF increased.

Table 4.4 Moisture, ash, protein and fibre content of cookies

	Moisture **(%)**	Ash **(%)**	Protein **(%)**	Fiber **(%)**
WFC100	1.99 ± 0.03^{a}	1.25 ± 0.02^{a}	7.03 ± 0.05^{e}	0.33 ± 0.06^{a}
BFC20	2.51 ± 0.05^{b}	1.44 ± 0.00^{b}	6.62 ± 0.06^{d}	1.48 ± 0.27^{b}
BFC30	3.05 ± 0.03^{c}	1.65 ± 0.03^{c}	6.20 ± 0.00^{c}	1.95 ± 0.37^{c}
BFC40	3.24 ± 0.04^{d}	1.67 ± 0.04^{c}	5.95 ± 0.07^{b}	2.07 ± 0.19^{c}
BFC50	3.02 ± 0.04^{c}	1.81 ± 0.01^{d}	5.91 ± 0.06^{b}	2.53 ± 0.06^{d}
BFC100	4.29 ± 0.11^{e}	2.20 ± 0.04^{e}	4.60 ± 0.01^{a}	3.99 ± 0.18^{e}

Values in the same column with different alphabet are statistically significant from each other ($p<0.05$). Presented data are mean value of triplicate ± standard deviation.

Based on Table 4.5, there was no significant difference ($p>0.05$) of fats and carbohydrate content between the six cookies formulation. The result for the calorie content showed that WFC100 (514.93) was significantly higher ($p<0.05$) from the

BFC (509.58 - 507.78). This might be due to the high percentage of fats, protein and carbohydrate content in WFC100.

Table 4.5 Fat, carbohydrate and calorie content of cookies

	Fat (%)	Carbohydrate (%)	Calorie (kcal)
WFC100	25.64 ± 0.09[a]	63.76 ± 0.46[a]	514.93 ± 0.78[b]
BFC20	25.57 ± 0.37[a]	63.52 ± 0.61[a]	509.58 ± 0.96[a]
BFC30	25.49 ± 0.06[a]	63.49 ± 0.19[a]	508.46 ± 0.38[a]
BFC40	25.65 ± 0.68[a]	63.43 ± 0.50[a]	508.56 ± 1.91[a]
BFC50	25.51 ± 0.23[a]	63.37 ± 0.49[a]	508.29 ± 1.12[a]
BFC100	25.20 ± 0.18[a]	63.24 ± 0.56[a]	507.78 ± 0.34[a]

Values in the same column with different alphabet are statistically significant from each other ($p<0.05$).Presented data are mean value of triplicate ± standard deviation.

Conclusion

The results in this study showed that the BF has potential to be commercialised in cookies production and provides more nutritional values. The BF that has high fibre can be used as an ingredient for producing high fibre products. An increasing level of breadfruit flour in the cookies had resulted in increasing moisture, ash and fibre content but decreased in protein content. However, the addition of breadfruit flour gave no significant effect ($p>0.05$) on the fats and carbohydrate content.

Acknowledgements

This research was funded by Research Acculturation Grants Scheme (RAGS/1/ 2015-RR172), Ministry of Higher Education Malaysia. Authors also would like to thank the Research Management, Innovation & Commercialization Centre, RMIC UniSZA.

References

Abdelghafor, R. F., Mustafa, A. I., Ibrahim, A. M. H. & Krishnan, P. G. (2011). Quality of bread from composite flour of sorghum and hard white winter wheat. *Advance Journal of Food Science and Technology,* 3: 9-15.

Adekunle, O., A. & Mary, A., A. (2014). Evaluation of cookies produced from blends of wheat, cassava and cowpea flour. *International Journal of food Studies, 3:* 175-185.

Agu, H. O., Ayo, J. A., Paul, A. M. & Folorunsho, F. (2007). Quality characteristics of biscuits made from wheat and African breadfruit (*Treculia africana*). *Nigerian Food Journal,* 25(2): 19-27.

Ajani, A. O., Oshundahunsi, O. F., Akinoso, R., Arowora, K. A., Abiodun, A. A. & Pessu, P. O. (2012). Proximate Composition and Sensory Qualities of Snacks Produced from Breadfruit Flour. *Global Journal of Science Frontier Research*, 12(7): 1-8.

AOAC. (2000). Official Method of Analysis 15th Edition. Association of Official Analysitical Chemists Washington, D. U.S.A.

AOAC. (2001). Official Method of Analysis. Association of Official Analytical Chemist, Washington, DC.

AOAC. (2004). Official Method of Analysis 5th Edition. Association of Official Analytical Chemist, Washington, DC.

Axel, F., Garry, G., Josh, S., Murch, S., Lampert, B., Zink, P. & Ragone, D. (2017). Global breadfruit, food security for a growing world: why breadfruit? Retrieved from: http://globalbreadfruit.com/about/why-breadfruit/

BeMiller, J. N. (2010). Carbohydrate Analysis. Indiana.

Chaucan, A., Saxena, D., C. & Singh, S. (2016). Physical, textural, and sensory characteristics of wheat and amaranth flour blend cookies. *Cogent Food & Agriculture,* 2: 1-8.

Chevallier, S., Colonna, P., & Della V., G. (2000). Contribution of major ingredients during baking of biscuit dough systems. *Journal of Cereal Science, 31*, 241–252.

Deivanai, S. & Subhash, J. B. (2010). Breadfruit (*Artocarpus altilis* Fosb.) – An Underutilized and Neglected Fruit Plant Species. *Middle-East Journal of Scientific Research,* 6(5): 418-428.

Ebere, C., O., & Kiin-Kabari, D., B. (2015). Pysico-chemical and Sensory Properties of Cookies Prepared from Wheat Flour and Cashew-Apple Residue as a Source of Fibre. *Asian Journal of Agriculture and Food Sciences,* 3(2): 213- 218.

Goburdhun, D., Ruggo, A. & Boodia, N. (2012). Prosiding Potential of Breadfruit from a Food Security Perspective in Mauritius. *Study of Composite Wheat-Breadfruit Flour.* 16-17 Nov 2012, Faculty of Agriculture, University of Mauritius.

Monitoba Agriculture (2017). Water Content of Common Food Products.

Noor Aziah, A. A. & Komathi, C. A. (2009). Acceptability attributes of crackers made from different types of composite flour. *International Food Research Journal,* 16: 479-482.

Noor Aziah, A. A., Mohamad Noor, A. Y. & Ho, L. H. (2012). Physicochemical and organoleptic properties of cookies incorporated with legume flour. *International Food Research Journal,* 19(4): 1539-1543.

Olaoye, O. A., Onilude, A. A. & Oladoye, C., O. (2007). Breadfruit flour in biscuit making. *African Journal of Food Science*, 20-23.

Ragone, D. (2003). National Tropical Botanical Garden. Elsevier Science Ltd, Kalaheo, Hi, USA.

Ryberg, R. (2010). The ultimate gluten-free cookie book: 125 favorite recipe. Da Capo Press, Cambridge.

Škrbić, B. & Cvejanov, J. (2011): The enrichment of wheat cookies with high-oleic sunflower seed and hull-less barley flour: Impact on nutritional composition, content of heavy elements and physical properties. *Food Chemistry*, 124: 1416– 1422.

Sudha, M. L., Vetrimani, R. & Leelavathi, K. (2007). Influence of fibre from different cereals on the rheological characteristics of wheat flour dough and on biscuit quality. *Food Chemistry,* 100: 1365-1370.

US Food and Drug Administration. (2004). Calories count: report of the working group on obesity. *Rockville, MD.*

Zoulias, E. & Oreopoulou, V. T. C. (2002). Textural properties of low-fat cookies containing carbohydrate- or protein-based fat replacers. *Journal of Food Engineering*, 55: 337-342.

3.3 Nutritional Value and Physicochemical Characteristics of Yogurt Containing Breadfruit Resistant Starch

Abstract

Breadfruit or Artocarpus altilis contains a high nutritional value but has not been widely commercialised. The aim of this study was to determine the physicochemical properties such as colour, titratable acidity, viscosity, pH, and nutritional value as well as the sensory evaluation of three yogurts produced by different concentrations of breadfruit resistant starch (BFRS) (1%, 3%, and 5%) as a prebiotic source. Lactobacillus bulgaricus and Streptococcus thermophiles were used as the starter cultures. Yogurt BFRS 1% showed a significant difference ($p<0.05$) in the value of titratable acidity from other formulations. However, the pH values for BFRS 1% was comparable to the commercial yogurt ($p>0.05$). There was a significant difference ($p<0.05$) in the value of lightness, redness, and yellowness between BFRS 1%, BFRS 3%, and BFRS 5% yogurt. The proximate composition showed that the ash, fat, fibre, and carbohydrate contents of the yogurt produced also differed significantly ($p<0.05$). In conclusion, the sensory evaluation results showed that yogurt containing 1% of BFRS was the best formulation with quite similar properties to the commercial yogurt.

Keywords: Breadfruit resistant starch; prebiotic source; starter cultures; yogurt; nutritional value.

Introduction

Many underutilised raw materials have been found useful in the food and non-food

industries. Conversion of underutilised fruit into flour or starch will provide a more stable form and increase its versatility and tendency towards finding alternative sources of starch from underutilised starch sources rather than relying on known starch sources (Adebowle et al., 2005). Starch can be divided into three categories based on its nutritional classifications, which are rapidly digestible starch, slowly digestible starch, and resistant starch. Resistant starch is not digested in the small intestine and enters the colon for fermentation (Chung et al., 2011). Resistant starch is the sum of starch and products of its degradation that are not absorbed in the small human intestine. Resistant starch is one of the portions of starch which can resist digestion by human pancreatic amylase in small intestines and thus reach the colon (Yao et al., 2009). The popularity of yogurt has increased due to its health benefits which are attributed by consuming yogurts containing live and active cultures.

The beneficial effects in numerous studies include the prevention of cancer, improvement of gastrointestinal health, amelioration of lactose intolerance symptoms, and protection from infections caused by food-borne microorganisms (Chandran et al., 2008). The rise in yogurt consumption by the community is related to the choices available in the marketplace which include a variety of flavours, good texture, convenience, and packaging innovations to fulfill consumer expectations of health food trends. Due to the high carbohydrate content (76.7%), breadfruit starch has been used as important sources of energy over the years (Adebowle et al., 2005). In developing countries, the current usage of breadfruit is limited caused by poor storage properties of fresh fruits. According to Adebowale et al. (2005), it is reasonable to maximise the potentials of this valuable fruit by processing it into different food products with a better shelf life. Thus, the focus of this research was to determine the potential of breadfruit yogurt to be commercialised in the market produced by different concentrations of breadfruit resistant starch. Therefore, the main objectives of this work were to produce yogurt with different concentrations of breadfruit resistant starch and determine its nutritional value and physicochemical characteristics, as well as the sensory evaluation.

Materials and Methods

Preparation of Yogurt containing Breadfruit Resistant Starch

Different formulation of breadfruit resistant starch, BFRS (1%, 3% and 5%) was incorporated in the yogurt as shown in Table 3.1. The BFRS yogurt mixture was heated at 60˚C for 5 minutes and then cooled until reached 40˚C. Then, 5% of yogurt starter culture was inoculated into breadfruit yogurt mixture, incubated at 37˚C for 24 hours and stored at 4˚C in the chiller. Two sample yogurts, CWS and CWTS were also prepared as control.

Table 3.1: Formulation of BFRS Yogurt

Ingredients	Formulation of yogurt				
	CWS	CWTS	BFRS 1%	BFRS 3%	BFRS 5%
Milk (g)	450	475	470	460	450
Sugar (g)	25	-	-	-	-

Resistant starch (g)	-	-	5	15	25
Starter culture (g)	25	25	25	25	25
Total (g)	500	500	500	500	500

CWS: Control with sugar; CWTS: Control without sugar; BFRS: Breadfruit resistant starch

Proximate Analysis

Proximate analysis of yogurt breadfruit resistant starch was conducted according to AOAC (2000).

Physicochemical analysis

The analysis to determine the physicochemical properties of yogurt samples were pH value, titratable acidity, colour measurement and viscosity.

Sensory Evaluation

The parameter used in sensory analysis was colour, flavour, aroma, texture, and overall acceptability of yogurt by following the 7- point of hedonic scale.

Statistical analysis

In this study, the significance was analyzed and tested by using one-way analysis of variance (ANOVA) from SPSS version 14.0 software.

Result and Discussions

Colour of Yogurt

Table 4.1 shows the colour characteristics of yogurt produced and there was a significant difference ($p<0.05$) between BFRS 1%, 3%, and 5%. The BFRS 5% yogurt had lower L* values (61.76) compared to the commercial one (71.91). The value of lightness in BFRS yogurt was lower than the control as the percentage of breadfruit resistant starch increased in the yogurt formulation. This was due to the red pigments of BRS which gave a darker colour compared to the control yogurt. However, the result shows that there was no significant difference ($p>0.05$) on lightness (L) of colour between commercial and BFRS 3% yogurts.

Table 4.1 The colour of commercial yogurt and Breadfruit Resistant Starch yogurt.

Sample	Parameter		
	Lighness (L)	Redness (a)	Yellowness (b)
Commercial	$71.91^{b} \pm 3.96$	$-2.67^{b} \pm 0.55$	$8.91^{a} \pm 0.94$
CWTS	$79.13^{c} \pm 2.71$	$-3.77^{a} \pm 0.46$	$8.00^{a} \pm 0.38$
CWS	$78.43^{c} \pm 4.68$	$-3.91^{a} \pm 0.49$	$7.99^{a} \pm 0.42$
BFRS 1%	$77.46^{c} \pm 3.58$	$-1.53^{c} \pm 0.92$	$13.05^{b} \pm 0.68$
BFRS 3%	$68.42^{b} \pm 6.07$	$-0.27^{d} \pm 1.23$	$15.88^{c} \pm 1.64$
BFRS 5%	$61.76^{a} \pm 7.57$	$0.95^{e} \pm 1.43$	$17.80^{d} \pm 1.71$

The data was expressed as mean value of triplicate ± SD. Values in the same column with different alphabet are significant difference ($p<0.05$).

Titratable acidity

Based on Table 4.2, there was a significant difference ($p<0.05$) of acidity value between commercial yogurt and other formulations (CWTS, CWS, BFRS 1%, and BFRS 5%). The acidification was responsible for the process of coagulation and formation of milk gels (Sert et al., 2017). The acidity of yogurt increased as pH decreased. The rate of acidification is important in achieving a balance between the strength of gel as well as commercially feasible fermentation time (Sah et al., 2016). This result indicates that CWTS and CWS formulations had the most stable structure compared to other formulations due to their lowest acidity values.

Viscosity of yogurt

There was no significant difference ($p>0.05$) among all formulations for the viscosity values (Table 4.2). However, according to Sahan et al., (2008), viscosity can increase over time due to the rearrangement of protein-protein contacts.

pH of yogurt

Based on Table 4.2, the range value of pH among BFRS yogurt produced was 4.10 - 4.40. These values were similar to the yogurt added with fibre and calcium ranging from 4.5 to 4.5 (Aportela et al., 2005). There was a significant difference ($p<0.05$) between BFRS 1% and other BFRS (3%, 5%) formulations. It can be concluded that BFRS 1% yogurt was more acidic than that of BFRS 3% and BFRS 5%. According to Lucey (2004), the pH was reduced by lactic acid during fermentation. The pH of commercial yogurt (4.16) was significantly lower than other formulations (CWTS, CWS, BFRS 3%, and BFRS 5%). The pH values of yogurt increased as the concentration of breadfruit resistant starch increased. According to Sah et al. (2016), the semi-solid texture of yogurt gel was a consequence of the development of a three-dimensional network of milk proteins caused by the pH reduction.

Table 4.2 Titratable acidity, Viscosity and pH values of Yogurt

Samples	Parameter		
	Titratable acidity (%)	Viscosity (cP)	pH
Commercial	1.91^{c} ± 0.09	47.33^{a} ± 26.56	4.16^{a} ± 0.14
CWTS	1.37^{a} ± 0.16	32.00^{a} ± 6.93	4.47^{b} ± 0.08
CWS	1.37^{a} ± 0.13	24.00^{a} ± 6.00	4.43^{b} ± 0.05
BFRS 1%	1.70^{b} ± 0.17	29.33^{a} ± 4.04	4.10^{a} ± 0.29
BFRS 3%	2.01^{cd} ± 0.13	29.33^{a} ± 2.30	4.38^{b} ± 0.19
BFRS 5%	2.07^{d} ± 0.20	35.67^{a} ± 13.28	4.40^{b} ± 0.15

The data was expressed as mean value of triplicate ± SD. Values in the same column with different alphabet are significant difference ($p<0.05$).

Proximate Composition

The results in Table 4.3 show the proximate composition of all tested yogurts. There was no significant difference ($p>0.05$) for attributes of moisture between commercial and BFRS yogurt. The ash content of yogurt was ranged from 0.55-1.18g/100g. There was a significant difference ($p<0.05$) between commercial yogurt and BFRS yogurt which showed that BFRS 5% yogurt had the highest value compared to

others. According to Trachoo and Mistry (1998), ash value is an index of mineral content which is needed for bone development, body functions and teeth formation. This indicates that BFRS 5% yogurt is the better source of minerals among the samples. There was a significant difference ($p<0.05$) of fat content between different formulations of BFRS yogurt. Fat plays an important role in improving the consistency of yogurt and also provides twice the energy as the same quantity of carbohydrate and protein (Ehirim & Onyeneke, 2013). Therefore, this indicates that BFRS 5% yogurt was a better source of energy compared to other yogurt formulations.

It has also been reported in previous studies that a high-fat content of yogurt is related to lower syneresis amounts (Isanga & Zhang, 2009). There is a significant difference ($p>0.05$) between commercial and BFRS yogurts where BFRS 1% yogurt had the lowest value of protein content. From this data, the protein values increased as the substitution of breadfruit resistant starch increased. The higher protein and lower fat contents increased the nutritional quality of food and could also prevent the rancidity of fermented products. The crude fibre contributes to the health of the gastrointestinal system and metabolic system in humans (Schneeman, 2002). There was a significant difference ($p<0.05$) between commercial and CWTS yogurt with BFRS yogurt formulations. The CWTS formula had the lowest mean value (0.09) while BFRS 5% had the highest value (3.23). This result shows that as the substitution of BRS concentration increased, the fibre content increased. The consequences of a fibre addition need to be established since it may induce changes in the textural and structural properties of yogurt (Espirito et al., 2012; Vasiljevic et al., 2007). There was a significant difference ($p<0.05$) of carbohydrate content between commercial yogurt with BFRS yogurt formulations. According to Ehirim and Ndimantang (2004), low carbohydrate value is attributed to the process of fermentation which converts lactose to lactic acid and makes this yogurt an ideal food for lactose intolerant individuals. BFRS 5% had a low carbohydrate content compared to BFRS 1% and BFRS 3%. The calories of tested yogurts were ranging from 362.48 to 411.46 kcal/100g as shown in Table 4.3. The calories of BFRS 5% yogurt were higher than the commercial yogurt ($p<0.05$) which might be due to the higher fat (9.09%) and protein (19.02%) contents compared to other formulations.

Table 4.3 Proximate composition of Control and Breadfruit resistant

Parameter	Formulation of Yogurt					
	Commercial	CWTS	CWS	BFRS 1%	BFRS 3%	BFRS 5%
Moisture (%)	7.92 ± 0.19^{ab}	8.68 ± 0.59^{b}	7.25 ± 0.21^{a}	7.65 ± 0.51^{a}	8.11 ± 0.30^{ab}	7.46 ± 0.89^{a}
Ash (%)	0.64 ± 0.03^{a}	0.55 ± 0.02^{a}	0.80 ± 0.02^{b}	0.79 ± 0.15^{b}	1.08 ± 0.09^{c}	1.18 ± 0.08^{c}
Protein	17.08 ± 0.07^{b}	18.24 ± 0.36^{c}	32.58 ± 0.45^{d}	12.98 ± 1.09^{a}	13.32 ± 0.78^{a}	19.02 ± 0.43^{c}
Fat	0.29 ± 0.11^{a}	0.15 ± 0.13^{a}	0.14 ± 0.02^{a}	0.10 ± 0.07^{a}	6.86 ± 1.09^{b}	9.09 ± 0.94^{c}
Fibre	0.17 ± 0.33^{a}	0.09 ± 0.51^{a}	1.27 ± 0.58^{b}	0.92 ± 0.11^{b}	1.87 ± 0.17^{c}	3.23 ± 0.36^{d}
Carbohydrate	74.08 ± 0.21^{d}	72.20 ± 0.40^{c}	59.32 ± 0.76^{a}	78.48 ± 0.90^{e}	71.93 ± 1.69^{c}	63.25 ± 1.09^{b}
Energy (kcal)	367.22 ± 0.23^{a}	362.48 ± 1.63^{a}	367.40 ± 2.30^{a}	372.76 ± 6.57^{a}	402.71 ± 12.42^{b}	411.46 ± 7.44^{b}

The data was expressed as mean value of triplicate ± SD.
Values in the same row with different alphabet are significant difference ($p<0.05$).

Sensory Evaluation of Yogurt

The sensory analysis results of the tested yogurt are shown in Table 4.4. The range score for the colour attribute in BFRS yogurt was 2.93-4.40, which was significantly lower than the commercial yogurt (5.90). The panelists preferred the lighter colour of commercial yogurt rather than BFRS yogurt. The range score for the aroma attribute of BFRS yogurt was ranging from 3.00-3.97, which was significantly lower than the commercial yogurt (5.77). The texture was one of the major criteria that consumers use to judge the quality of foods. The mean texture attribute of yogurt ranged from 3.47-5.77, in which the score of BFRS yogurt was significantly lower than the commercial, CWTS, and CWS yogurt. This was likely due to the different values of viscosity that showed the BFRS yogurt had low viscosity compared to others. Desired textural properties of set-style yogurt are a firm gel, smooth homogeneous consistency, and no expelled whey at the surface (Tamimme & Robinson, 2007). The attribute taste mean showed that there was no significant difference ($p>0.05$) between BFRS yogurts. The flavour in yogurt consists mostly of lactic acid, acetaldehyde, and diacetyl (Pinto et al., 2009; Gallardo-Escamilla et al., 2005). The fermentation products such as acetaldehyde, diacetyl, lactic acid, and other organic components importantly contribute to the characteristic flavour of yogurt. The range score for the taste attribute of BFRS yogurts was from 2.57 to 3.07. The taste value mean of BFRS yogurts decreased as the BFRS substitution increased. From the data, BFRS 1% yogurt showed the highest mean score (3.07). The substitution of BFRS in this study showed that there was an effect on the taste of yogurt. According to Pinto et al. (2005), the strain variability affects the production intensity of flavour compounds during the production of yogurts and finally determines consumer acceptability. For the overall acceptability attribute, the acceptance of yogurts was affected by the substitution of BFRS ($p<0.05$) between commercial and BFRS yogurts. However, BFRS 1% yogurt achieved the highest score for overall acceptability among BFRS yogurts.

Table 4.4 Sensory evaluation of yogurt

Attribute	Yogurts					
	Commercial	CWTS	CWS	BFRS 1%	BFRS 3%	BFRS 5%
Colour	5.90±1.1^{c}	6.03±0.96^{c}	5.90±0.96^{c}	4.40±1.57^{b}	3.47± 1.59^{a}	2.93±1.64^{a}
Aroma	5.77±1.07^{c}	5.43±1.19^{c}	5.50±1.20^{c}	3.97 ±1.43^{b}	3.27± 1.55^{a}	3.00±1.46^{a}
Texture	5.77±1.14^{b}	5.73 ±0.94^{b}	5.67 ±1.15^{b}	3.83 ±1.56^{a}	3.47±1.61^{a}	3.77±2.03^{a}
Taste	4.60±1.73^{bc}	4.03±1.67^{b}	5.03±1.43^{c}	3.07±1.34^{a}	2.83±1.49^{a}	2.57± 1.48^{a}
Overall Acceptability	5.20±1.35^{c}	4.73 ±1.31^{c}	5.33±1.15^{c}	3.43±1.45^{b}	2.90±1.32^{ab}	2.70±1.47^{a}

Values in the same row with different alphabet are significant difference ($p<0.05$).

Conclusion

The substitutions of breadfruit resistant starch (1%, 3%, and 5%) significantly affected the nutritional and physicochemical properties of yogurt. The yogurt was rich in ash content, an indication of minerals and also contained other nutrients in adequate quantities. These results might prove that the consumption of probiotic bacteria and prebiotic within food products is the most popular way to re-establish

the gastrointestinal microflora balance and synbiotic functional food, which offer additional health benefits to the consumer. Thus, breadfruit might have a potential to be commercialised as resistant starch.

Acknowledgements
This research was funded by Research Acculturation Grants Scheme (RAGS/1/ 2015-RR172), Ministry of Higher Education Malaysia. Authors also would like to thank the Research Management, Innovation & Commercialization Centre, RMIC UniSZA.

References

Adebowale, K.O., Olu-Owolabi, B. I., Olawumi, E. K. & Lawal, O. S. (2005). Functional properties of native, physically and chemically modified breadfruit (Artocarpus altilis) starch. *International Crops and Products*, 21: 343-351.

AOAC International. (2000). Official Methods of Analysis of the Association of Official Analytical Chemist, 17th Ed (edited by Horowitz W). Gaithersburg, MD: AOAC International.

Aportela-Palacios, A., Sosa-Morales, M. E., & Vélez-Ruiz, J. F. (2005). Rheological and physicochemical behavior of fortified yogurt, with fiber and calcium. *Journal of Texture Studies*, 36: 333-349.

Chandran, R. C., White, C. H., Kilara, A. & Hui, Y. H. (2008). Manufacturing yogurt and fermented milks, Blackwell Publishing, Australia.

Chung, H.J., Donner, E., & Liu, Q. (2011). Resistant starch in foods. *Comprehensive Biotechnology* (Second Edition), M. Moo-Young(Ed), Academic Press, Burlington.

Ehirim FN, Ndimantang BE(2004). Production and evaluation of yoghurt from cow- soy milk blends. *Journal of Agriculture and Food Science.*

Ehirim FN, Onyeneke EN (2013). Physicochemical and organoleptic properties of yoghurt manufactured with Cow milk and Goat milk. *Natural and Applied Science.*

Espírito Santo, A. P., Perego, P., Converti, A., & Oliveira, M. N. (2012). Influence of milk type and addition of passion fruit peel powder on fermentation kinetics, texture profile and bacterial viability in probiotic yoghurts. *Food Science and Technology*, 47(2): 393-399.

Gallardo-Escamilla, F., Kelly, A., & Delahunty, C. (2005). Influence of starter culture on flavor and headspace volatile profiles of fermented whey and whey produced from fermented milk. *Journal Of Dairy Science*, 88(11): 3745-3753.

Isanga, J., & G. Zhang. (2009). Production and evaluation of some physicochemical parameters of peanut milk yoghurt. *Food Science Technology*, 42:1132–1138.

Lucey, J.A. (2004). Cultured dairy products: An overview of their gelation and

texture properties. *International Journal Dairy Technology,* 57: 77-84.

Pinto, S., Clemente, M. D. G., & De Abreu, L. R. (2009). Behaviour of volatile compounds during the shelf life of yoghurt. *International Journal Of Dairy Technology*, 62(2): 215- 223.

Sah, B. N. P., Vasiljevic, T., McKechnie, S. & Donkor, O. N. (2016). Physicochemical, textural and rheological properties of probiotic yogurt fortified with fibre-rich pineapple peel powder during refrigerated storage. *Journal of Food Science and Technology*, 65: 978-986.

Sahan N., Yasar, K & Hayaloglu, AA. (2008). Physical, chemical and flavour quality of non-fat yogurt as affected by a b-glucan hydrocolloidal composite during storage. *Food Hydrocolloids*, 22(7): 1291–1297.

Schneeman, BO. (2002) Gastrointestinal physiology and functions. British Journal Nutrition, 88 (2): 159-163.

Sert, D., Mercan, E., & Dertli, E. (2017). Characterisation of lactic acid bacteria from yogurt-like product fermented with pine cone and determination of their role on physicochemical, textural and microbiological properties of product, *LWT - Food Science and Technology.*

Tamime, A.Y., Robinson, R.K., 2007. Yoghurt- Science and Technology, 3 ed. (pg:40), Woodhead Publishing in Food Science, Technology and Nutrition, Woodhead, Cambridge.

Trachoo. N & Mistry.VV (1998). Application of ultra filtered sweet butter milk and sweet butter milk powder in manufacture of non- fat and low fat yoghurt. *Journal Dairy Science*, 81: 774-788.

Vasiljevic, T., & Shah, N.P. (2008). Probiotics-from Metchnikoff to bioactives. *International Dairy Journal*, 18(7): 714-728.

Yao, N.,Paez, A.V. & White, P.J. (2009). Structure and Function of Starch and Resistant Starch from Corn with Different Doses of Mutant Amylose-Extender and Floury-1 Alleles. *Journal of Agricultural and Food Chemistry.*, *57* (5): 2040–2048.

CHAPTER 4
ENVIRONMENTAL STUDIES OF A GOLD MINE

INTRODUCTION

Greenhouse gases in the atmosphere can cause climate change. Carbon dioxide emitted by the mining industry is the major gas contributing to increase of anthropogenic greenhouse gases in the atmosphere. Mining operation discard wastes particularly at mine tailings. These wastes at the waste dumps and stockpiles are potential solid buffers in storing atmospheric carbon dioxide in a stable carbonate form by mineral carbonation processes. Mining activities can also be a source of water pollution affecting water quality and physico-chemical characteristics of water. Heavy metals can remain for long periods in water and affect the aquatic ecosystem. Mine impacted water releases contaminants into the environment and assimilates into the food chain of living things, transferring from aquatic species to other consumers such as human beings. This has become a major health concern.

4.1 Mineralogy of Waste Dump and Stockpile from Selinsing Gold Mine for Carbon Sequestration

Abstract

Wastes that are discarded from mining operation particularly at mine tailings, waste dumps, and stockpiles have a potential as a solid buffer in storing atmospheric carbon dioxide in a stable carbonate form by mineral carbonation processes. This study was conducted to identify major minerals from different types of gold mining wastes which are waste dump and stockpile at Selinsing Gold Mine and to determine the potential of carbonate and silicate minerals from gold mining wastes for mineral carbonation process. Field sampling were done where rock samples were collected at waste dump and stockpile and its mineralogy of both mining wastes were analyzed using x-ray diffraction analysis. Findings indicated that quartz, mica, dolomite, and calcite are major minerals found at waste dump and stockpile because parent rocks from rock samples are derived from volcanic, sedimentary, and metamorphic rocks. Results also demonstrated that carbonate-rich minerals such as dolomite, calcite, and siderite are in stable carbonates form that are considered a reservoir for carbon storage due to its high availability in gold mining wastes for mineral carbonation process. Silicates minerals (chlorite, pyroxene, mica, amphiboles) that are present at both waste dump and stockpile contain magnesium and calcium silicates ions which can form carbonate minerals when react with carbon dioxide by mineral carbonation process. Therefore, the presence of potential minerals from gold mining wastes provides a great possibility for carbon sequestration which can also encourage evaluation of carbon footprint in mining industry.

Keywords: Gold Mine Waste; Rock Mineralogy; Metal-bearing Silicates; Mineral Carbonation Process; Passive Carbon Sequestration

Introduction

Anthropogenic carbon dioxide (CO_2) emission mainly from mining industry is the major gas that contributes to increase of anthropogenic greenhouse gases (GHG) in the atmosphere and can cause climate change. In Malaysia, CO_2 emissions is at a current level of 257.69 million tonnes (Mt) in 2014 and is expected to increase in 12.1 tonnes of CO_2 emission per capita by 2020 (Zaid et al., 2015). According to International Energy Agency (IEA) modelling, 13% of cumulative CO_2 emissions reductions is needed which signify 6 billion tonnes (Bt) of CO_2 emissions per year in 2050 to decrease temperature rises to 2°C that cause global climate change. Besides, Malaysia has committed to decrease GHG emissions up to 40% by the year 2020 as declared in policy commitment (MNRE, 2011). In order to stabilize CO_2 in the atmosphere, carbon capture and storage (CCS) by mineralization is an environmentally reliable approach in storing CO_2 permanently in stable carbonates form (Lackner et al., 1995; Renforth, 2011; Arce et al., 2017). Thus, there is a need to evaluate the potential of carbon sequestration of mining wastes to reduce CO_2 emissions to the atmosphere.

CCS involves trapping of CO_2 from the gas streams into geological formations such as soils and rocks in carbonate form by natural carbonation reaction (Harrison et al., 2013; Wilson et al., 2009). Carbonate minerals that are formed in the soil include formation of stable carbonate or bicarbonate to capture carbon from weathering of primary minerals that release ion such as hydrogen (H^+), magnesium (Mg^{2+}), and calcium (Ca^{2+}), reacting with CO_2 (Assima et al., 2014; Lechat et al., 2016; Power et al., 2013; Wilson et al., 2009). This natural process of carbonation provides a great potential for carbon storing of mining residue in reducing CO_2 production in long term.

Various types of mining wastes are favourable for passive carbon sequestration. Potential feedstock of carbon sequestration from mining waste consists of alkaline earth metal-bearing silicates (1), hydroxide minerals (2) and silicate waste rocks (3) that are rich in divalent cations such as magnesium, calcium and iron oxide (Manning and Renforth, 2012; Power et al., 2013). Mine waste rocks from ultramafic-hosted ore deposits are commonly preferred for carbonation mineralization due to abundance of magnesium silicates (Mg-silicates) from final product of mining process and also contains primary ultramafic minerals such as olivine (Mg_2SiO_4) and lizardite ($Mg_3Si_2O_5(OH)_4$ (Hitch et al., 2010). For instance, olivine will react with CO_2 and water to form lizardite and magnesium carbonates ($MgCO_3$) as shown in reaction *(1)*, while lizardite later reacts with CO_2 to form magnesite ($MgCO_3$) in reaction *(2)* (Manning and Renforth, 2012; Renforth, 2011). These carbonation reactions of Mg-silicates produce a stable carbonate form.

$$2Mg_2SiO_4\ (olivine) + CO_2 + 2H_2O \rightarrow Mg_3Si_2O_5(OH)_4\ (lizardite) + MgCO_3 \qquad (1)$$

$$Mg_3Si_2O_5(OH)_4\ (lizardite) + 3CO_2 \rightarrow 3MgCO_3\ (magnesite) + 2SiO_2 + 2H_2O \qquad (2)$$

During rock weathering, carbonation reaction of calcium silicates (Ca-silicates) in metamorphic rocks produces wollastonite ($CaSiO_3$) minerals, which can increase carbon uptake (Manning and Renforth, 2012; Renforth, 2011) that are shown in

reaction *(3).* As a result of rock weathering, it accelerates carbonation of Ca-silicates that occur naturally and promote carbon sequestration.

$$CaSiO_3 \text{ (wollastonite)} + CO_2 + 2H_2O = CaCO_3 \text{ (calcium carbonate)} + H_4SiO_4 \qquad (3)$$

This process occurs under ambient environmental conditions in mine wastes and tailings. From weathering process, CO_2 is being stored as solid carbonate minerals. Increase of both Ca or Mg-silicates weathering and pedogenic carbonates are highly required for carbon sequestration to remove CO_2 from the atmosphere (Manning and Renforth, 2012). Therefore, the presence of carbonates cations and silicates minerals will enhanced carbonation reaction for CO_2 capture in mining waste. The objectives of this study are to identify major minerals from different type of gold mining wastes which are waste dump and stockpile at Selinsing Gold Mine and to determine the potential of carbonate and silicate minerals from gold mine wastes for mineral carbonation process.

Methods

Study Area

An active open pit gold mine site, Selinsing Gold Mine which was located at Raub in the state of Pahang (coordinate: N 4°15'0", E 101°47'10") (Figure 1) was chosen to represent gold mine industry in Malaysia because it is known as the Malaysian's Central Gold Belt District of Peninsular Malaysia (Makoundi et al., 2014). The gold mine is hosted within a sequence of felsic tuff (tuffaceous origin), very fine clastic argillite with calcareous material (carbonaceous shale), grey-black limestone, quartz-rich, and quartzite conglomerate, host by sedimentary rocks included phyllite, siltstone, cataclasite, mylonite, and serpentinized of mafic to ultramafic rocks (Makoundi et al., 2014; Pour et al., 2016). The major mineral found at the Selinsing Gold Mine are pyrite (FeS_2), quartz (SiO_2), and dolomite [$CaMg(CO_3)_2$] (Makoundi et al., 2014).

Figure 1. Location map of Selinsing Gold Mine at Raub, Pahang (Makoundi et al., 2014)

Field Sampling

Field sampling was done at Selinsing Gold Mine, where two types of mine waste such as waste dump, and stockpile were collected. Waste rock samples were collected at waste dump and at stockpile of super lower grade gold. The sampling technique used was stratified strategy sampling, which is based on previous geological information of mineralization at different sampling points. The rock samples were collected using a rock pit and each sample was kept in a separated polythene bags upon collection.

X-Ray Diffraction Analysis

Rock samples were crushed and were grounded into fine particles using agate mortar and pestle. The fine samples were sieved to one mm size fraction using particle sieves because grain size of samples is a critical consideration that can affect results of x-ray diffraction (XRD) analysis (Saat et al., 2009). Then, sieved samples were grounded into a very finely powder form using a special mortar and about 1 ± 0.5 g of fine powder samples were placed on special sample holder before being attached on x-ray machine (Arce et al., 2017). Powder samples were analyzed using Philips PW3440/60 X'Pert Pro model of XRD instrument (Cu-Kα radiation) at 1°/min rate (0.02° step size) over the 2–65° scattering angle range (Harrison et al., 2013; Lechat et al., 2016), where the range of detection limit are between 1 to 2% (Kandji et al., 2017). The instrument was used to classify mineral characterization at waste dump and stockpile (Harrison et al., 2013; Kandji et al., 2017).

Results and Discussion

Mineralogy of Waste Rock

Overall, 15 types of minerals were identified from XRD in waste rock samples at waste dump and stockpile of the Selinsing Gold Mine. There were four major minerals found in both types of gold mining wastes which are quartz, mica, dolomite, and calcite, followed by other minerals such as kaolinite, pyroxene, goethite, anatase, chlorite, illite, larosite, rutile, siderite, amphiboles, and opal. Major minerals were discovered widespread at both mining wastes due to parent rocks from waste rock samples were originated from volcanic, sedimentary (eg: limestone, carbonaceous shale, conglomerate), and metamorphic rocks (eg: phylite) (Makoundi et al., 2014; Pour et al., 2016). Figure 2 and 3 indicated that the highest peak of quartz and mica were present in both types of mining wastes because these minerals were resistant to weathering (Shamshuddin, 2011). Thus, quartz and mica minerals were considered as the common minerals found in all types of rocks.

Carbonate Minerals for Carbon Sequestration

In general, the presence of dolomite and calcite minerals from gold mining wastes are carbonate minerals which have potential for carbon sequestration. This is because carbonates are produced by natural carbonation reaction (Harrison et al., 2013; Lackner et al., 1995; Wilson et al., 2009), where Ca and/or Mg oxides reacted with CO_2 to produce stable carbonate such as calcite as shown in reaction (4) and dolomite in reaction (5) (Lackner et al., 1995; Lechat et al., 2016; Power et al., 2013; Renforth, 2011; Wilson et al., 2009):

$$CaO + CO_2 \rightarrow CaCO_3 \text{ (calcite)} \quad (4)$$

$$CaO + MgO + 2CO_2 \rightarrow CaMg(CO_3)_2 \text{ (dolomite)} \quad (5)$$

Mineral carbonation process is another weathering process where the rock minerals are reacting with additive such as carbonic acid (H_2CO_3) to form stable carbonate (Hitch et al., 2010). Further reaction of calcite with carbonic acid will form calcium ion and bicarbonate as shown in reaction below:

$$CaCO_3 + H_2CO_3 \rightarrow Ca^{2+} + 2HCO_3^- \text{ (bicarbonate)} \quad (6)$$

Findings also indicated that carbonate minerals were found at both mining wastes because the host rocks of waste dump and stockpile of Selinsing Gold Mine are from sedimentary rocks (Makoundi et al., 2014). Furthermore, these minerals were favourable in all type of rocks including metamorphic and sedimentary rocks, except for dolomite that exist only in sedimentary rocks (Hitch et al., 2010). Therefore, dolomite and calcite-rich minerals that are naturally present at Selinsing Gold Mine are considered a reservoir for carbon storage due to its high availability in gold mining wastes.

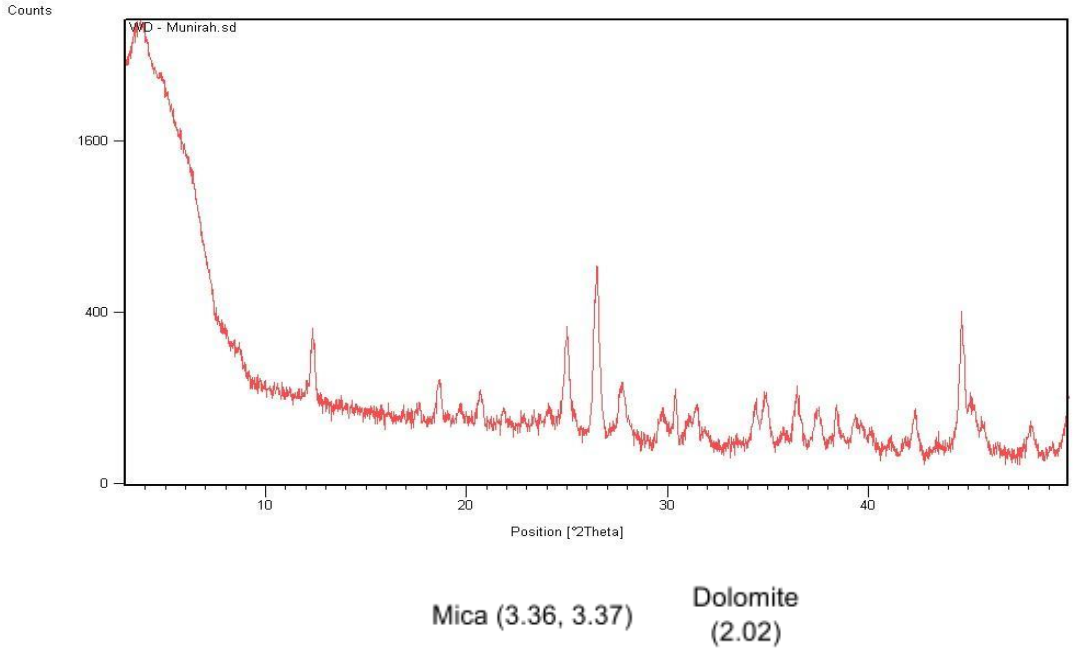

Figure 2. Major minerals with d-spacing from XRD diffractogram of rock at waste dump

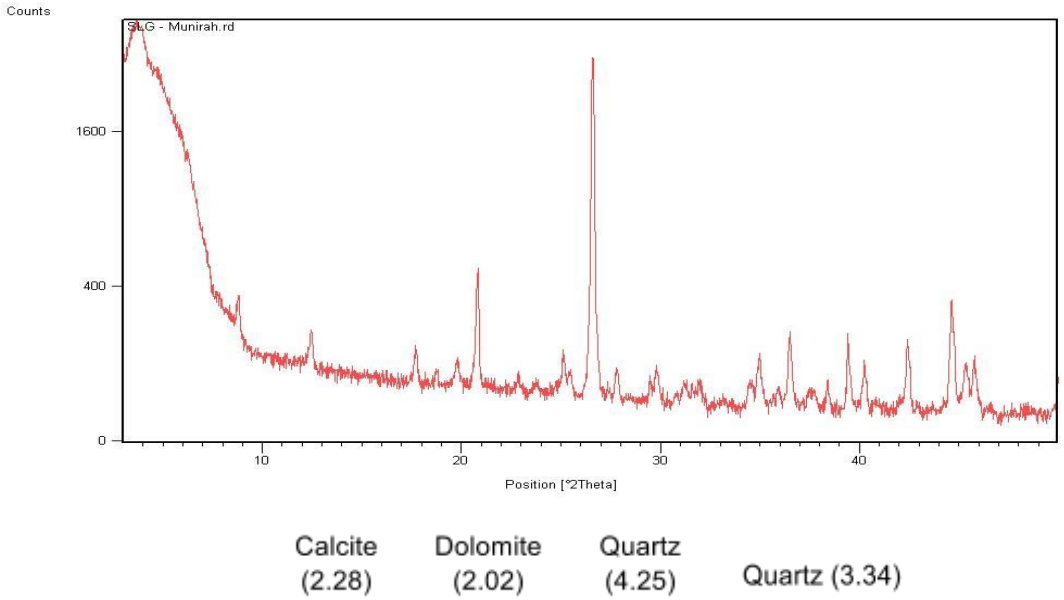

Figure 3. Major minerals with d-spacing from XRD diffractogram of rock at stockpile

From the XRD results, majority of minerals were present in waste dump and stockpile except for minerals such as siderite, amphiboles, and rutile which were found at stockpile, whereas opal mineral was present only at waste dump (Table 1). Stockpile seems to have numerous mineral composition compared to waste dump because waste rock samples at stockpile are categorized as super lower grade of gold from open pit mining operation, where parent rocks are from metamorphic and sedimentary rocks (Makoundi et al., 2014; Pour et al., 2016).

Siderite mineral is one of carbonate minerals that have potential for mineral carbonation process, other than calcite and dolomite minerals. This is because siderite mineral consists of iron oxide (FeO) that can react with CO_2 to form marginally stable carbonate minerals as shown in reaction (*7*) (Lackner et al., 1995; Power et al., 2013; Wilson et al., 2009):

$$FeO + CO_2 \rightarrow FeCO_3 \text{ (siderite)} \quad (7)$$

In mineral carbonation process, CO_2 was deposited as siderite which is one of the key mineral targets of sequestration of anthropogenic carbon (Hitch et al., 2010; Novhe et al., 2014). Besides that, ore minerals at the Selinsing gold residue are rich in iron component such as pyrite, galena, arsenopyrite and gold (Makoundi et al., 2014). Thus, siderite was highly found at gold mining waste especially at stockpile through mineral carbonation process.

Silicate minerals for carbon sequestration

Minerals are divided into primary and secondary minerals, which were derived from metamorphic and sedimentary rocks respectively. Primary minerals such as quartz, mica, pyroxenes and amphiboles were formed from mineralization process, while secondary minerals were produced during weathering of primary minerals that release clay minerals such as quartz, kaolinite, illite, carbonate minerals (calcite, dolomite, siderite), iron hydroxide minerals (goethite) and sulphide minerals (Shamshuddin, 2011; Novhe et al., 2014). Table 1 shows that silicates minerals such

as chlorite, pyroxene, mica, and amphiboles that were present at waste dump and stockpile are the sources for mineral carbonation. These silicate minerals contain magnesium and/or calcium silicates ions which can react with CO_2 to form stable carbonate mineral (Hitch et al., 2010; Manning and Renforth, 2012; Power et al., 2013). For instance, reaction of chlorite mineral with CO_2 will produce magnesite as shown in *reaction (8):*

$$Mg_6Si_4O_{10}(OH)_8 \text{ (chlorite)} + 6CO_2 \rightarrow 6MgCO_3 \text{ (magnesite)} + 4SiO_2 + 4H_2O \qquad (8)$$

The presence of Mg and Ca-silicates from chlorite, pyroxene, mica, and amphiboles minerals at mining wastes are favourable for mineral carbonation process. Therefore, silicate minerals such as chlorite, pyroxene, mica, and amphiboles from waste dump and stockpile of Selinsing Gold Mine have potential for mineral carbonation process.

Table 1 Composition of minerals found from rock sample at different type of mining wastes

Minerals	Chemical formula	Waste dump	Stockpile
Primary minerals			
1. Quartz [a]	SiO_2	√	√
2. Mica [a]	$K(Mg,Fe)_3(AlSi_3O_{10})(OH)_2$	√	√
3. Pyroxene [a]	$(Ca,Na)(Mg,Fe,Al)(Al,Si)_2O_6$	√	√
4. Amphiboles [a]	$NaCa_2(Mg,Fe,Al)_5(Al,Si)_8O_{22}(OH)_2$		√
Secondary minerals			
5. Dolomite [b,c]	$CaMg(CO_3)_2$	√	√
6. Calcite [b,c]	$CaCO_3$	√	√
7. Siderite [b,c]	$FeCO_3$		√
8. Kaolinite [a]	$Al_2Si_2O_5(OH)_4$	√	√
9. Chlorite [a]	$Mg_6Si_4O_{10}(OH)_8$	√	√
10. Goethite [c]	$HFeO_2$	√	√
11. Illite	$(K,H_3O)(Al,Mg,Fe)_2(Si,Al)_4O_{10}[(OH)_2,(H_2O)$	√	√
12. Anatase	TiO_2	√	√
13. Larosite	$(Cu,Ag)_{21}(Pb,Bi)_2S_{13}$	√	√
14. Rutile	TiO_2		√
15. Opal	$SiO_2.nH_2O$	√	

[a] Silicates minerals
[b] Carbonate minerals
[c] Non-silicates minerals

Conclusion

Gold mining wastes have a great potential for carbon sequestration in reducing CO_2 in the atmosphere. Quartz, mica, dolomite, and calcite are the major minerals that are mainly discovered at waste dump and stockpile of Selinsing Gold Mine. However, dolomite and calcite-rich minerals are considered a reservoir for carbon capture and storage because both minerals were in a stable carbonate form. The presence of silicates minerals such as chlorite, pyroxene, mica, and amphiboles at both mining wastes are the potential feedstock of carbon sequestration because these minerals are rich in calcium and magnesium divalent cation for mineral carbonation process. The potential minerals from gold mining wastes can encourage evaluation of carbon footprint in mining industry.

Acknowledgements
This research was funded by Universiti Putra Malaysia and Ministry of Higher Education Malaysia through the IPM 9453700 and FRGS 5524757 research grants. The authors would like to thank laboratory staffs at Department of Land Management, Faculty of Agriculture, Universiti Putra Malaysia for provided XRD instrument for mineralogical analysis throughout this study.

References

Arce, G.L.A.F., Neto, T.G.S., Ávila, I., Luna, C.M.R., José C.S., João A.C.J. (2017). Influence of physicochemical properties of Brazilian serpentinites on the leaching process for indirect CO_2 mineral carbonation. *Hydrometallurgy*. 169: 142–151.

Assima, G.P., Larachi, F., Molson, J., Beaudoin, G. (2014). Comparative study of five Québec ultramafic mining residues for use in direct ambient carbon dioxide mineral sequestration. *Chemical Engineering Journal*. 245: 56–64.

Harrison, A.L., Power, I.M., Dipple, G.M. (2013). Accelerated carbonation of brucite in mine tailings for carbon sequestration. *Environmental Science & Technol*ogy. 47: 126−134.

Hitch, M., Ballantyne, S.M., Hindle, S.R. (2010). Revaluing mine waste rock for carbon capture and storage. *International Journal of Mining, Reclamation and Environment*. 24(1): 64–79.

Kandji, E.H.B., Plante, B., Bussière. B., Beaudoin, G., Dupont, P.P. (2017). Geochemical behavior of ultramafic waste rocks with carbon sequestration potential: a case study of the Dumont Nickel Project, Amos, Québec. *Environmental Science and Pollution Research*. 24(12): 11734–11751.

Lackner K.S., Wendt, C.H., Butt, D.P., Joyce, E.L., Sharp, D.H. (1995). Carbon dioxide disposal in carbonate minerals. *Energy*. 20(11): 1153–1170.

Lechat, K., Jean-Michel L., Molson, J., Beaudoin, G., Hébert R. (2016). Field evidence of CO_2 sequestration by mineral carbonation in ultramafic milling wastes, Thetford Mines, Canada. *International Journal of Greenhouse Gas Control*. 47: 110–121.

Makoundi, C., Zawa, K., Large, R.R., Meffre, S., Chun-Kit, L., Hoe, T.G. (2014). Geology, geochemistry and metallogenesis of the Selinsing gold deposit, central Malaysia. *Gondwana Research*. 26: 241–261.

Manning, D.A.C., Renforth, P. (2012). Passive sequestration of atmospheric CO_2 through coupled plant-mineral reactions in urban soils. *Environmental Science & Technol*ogy. 1–7 pp.

Mineral and Geoscience Department Malaysia, Ministry of Natural Resources and Environment Malaysia (MNRE). *Industri Perlombongan Malaysia* (2013).

Novhe, N.O., Yibas, B., Netshitungulwana, R., Lusunzi, R. (2014). Geochemical and minerological characterization of mine residue deposits in the komati/crocodile catchment, South Africa: an assessment for acid / alkaline mine drainage. *An Interdisciplinary Response to Mine Water Challenges. Proceedings of the 12th Congress of International mine Water Association (IMWA).* 359–365.

Power, I.M., Harrison, A.L., Dipple, G.M. (2013). Carbon mineralization: from natural analogues to engineered systems. *Reviews in Mineralogy & Geochemistry*. 77: 305–360.

Pour, A.B., Hashim, M., Makoundi, C., Zaw, K. (2016). Structural mapping of the Bentong-Raub Suture Zone using PALSAR remote sensing data, Peninsular Malaysia: Implications for sediment-hosted/orogenic gold mineral systems. *Resource Geology*. 66(4): 368–385.

Renforth, P. (2011). Mineral carbonation in soils: engineering the soil carbon sink. PhD thesis. Newcastle University for the degree of Doctor of Philosophy.

Saat, A., Hamzah, Z., Bakar, Z.A. (2009). XRF determination of major elemental contents of clay samples from north-west Peninsular Malaysia. *Journal of Nuclear and Related Technologies*. 6(1): 230–236.

Shamshuddin, J. (2011). Methods in Soil Mineralogy, Universiti Putra Malaysia Press, Selangor, Malaysia.

Wilson, S.A., Dipple, G.M., Power, I.M., Thom, J.M., Anderson, R.G., Raudsepp, M., Gabites, J.E., Southam, G. (2009). Carbon dioxide fixation within mine wastes of ultramafic-hosted ore deposits: examples from the Clinton Creek and Cassiar Chrysotile deposits, Canada. *Economic Geology.* 104: 95–112.

Zaid, S.M., Myeda, N.E., Mahyuddin, N., Sulaiman, R. (2015). Malaysia's rising GHG emissions and carbon 'lock-in' risk: a review of Malaysian building sector legislation and policy. *Journal of Surveying, Construction and Property*. 6(1): 1-13.

4.2 Water Quality of Gold Mine-Impacted Water at Selinsing Gold Mine, Pahang

Abstract

Mining activities is one of the sources of the water pollution in the world. Extraction of raw earth material inhibits the release of pollution into the water sources. Water quality and physico-chemical characteristic of water should be checked regularly to ensure the safety of the consumer. Parameters such as biological oxygen demand (BOD), pH, turbidity, chemical oxygen demand (COD), conductivity, dissolved oxygen, total dissolved solid (TDS), total suspended solid (TSS) and ammonia nitrogen (AN) is determined to identify water quality of mine-impacted water at Gold Mine Selinsing Pahang before being release to Sungai Kermoi, following Water Quality Index formula. Three sampling locations were chosen within the areas for analysis. The samples were analyzed for their parameters and identify their WQI. The results shows that tailing storage facility (TSF) (S1), categorize under class II, which is slightly polluted, process tank (S2), is polluted, under class III and retention pond (S3) is categorized under class I, which is the water is clean to be discharge to environment.

Keywords: Gold mine; water pollution; WQI; water quality; physico-chemical characteristic

Introduction

Mining activities had become one of the country's sources of income and also to obtain raw material of the earth resources. Mining product such as tin, copper, bauxite, iron, kaolin, raw gold, barite, silica, coal, illuminate, mica, limestone (Ashraf et al., 2015) are used as primary products or secondary products from these industries. During extraction of raw earth resources, such as extraction of gold, use of cyanide and mercury gave potential harm to the ecosystem which affects the health of humans and livestock, besides activities of open pit mining causes degradation of natural landscape (Porgo&Gokyay, 2016).

Also, heavy metals i.e.; arsenic, copper, cadmium, lead, chromium, lead, mercury and zinc can remain in water for long term and biologically effect the aquatic ecosystem. Mine impacted water has become a concern as it will release contaminants into the environment and assimilate into the food chain of living things. As its features of indestructible, it will be transferred from the aquatic species to the other consumer like human. Thus, as it will be released into watercourses, it needs to be treated and evaluate first so that it complies with the standard National Water Quality Standard (NWQS) requirements.

Water quality also had become a concern due to the growth of industries, use of variety of fertilizers and human activities causing the water sources to be affected and can cause water-borne disease. In order to minimise the pollution of the water from the mining activities, each mining industries must put some initiatives to mitigate the issue. Most of each mining industries have their own tailing storage facility and water treatment plant before releasing the mine-impacted water into the river. Evaluation of the effectiveness of tailing storage facilities is needed to ensure the quality of water discharge from this facility. Water quality assessment is a must to determine the extent of the contaminated water. Therefore, this study aims to determine the quality of mine-impacted water of Selinsing Gold Mine, Raub in order to evaluate their suitability as a raw water resource.

Materials and Method

Sampling was conducted at Selinsing Gold Mine, Raub Pahang, where performed at three different locations (S1= Process tank, S2= Tailing Storage Facility, S3= Retention pond); that represent each steps during treatment process of the gold mine-impacted water. Some parameters were analyse to determine the water quality which depends on the types of water (Patil et.al, 2012). Each analysis was carried out with respective methods and suitably apparatus were used for different analysis. Some in-situ measurements were determined for pH, temperature, dissolved oxygen, turbidity, salinity, conductivity and dissolved oxygen; while some samples were brought back to the laboratory for analysis of biological oxygen demand (BOD), chemical oxygen demand (COD), ammonia nitrogen (AN) and total suspended solid (TDS).

Besides, the selected bottles were chosen suitably according to the analysis to be carried out on the water samples. Also, sampling preservation was undertaken to preserve the water sample before further analysis. For example, few drops of sulphuric acid (H_2SO_4) were added for chemical oxygen demand (COD) analysis. Besides, BOD bottle that contains water sample for analysis of biological oxygen

demand (BOD) was wrap by aluminium foil to make sure there is no penetration of sunlight into the bottle and all the samples were stored in Coleman or cold box at 4ºC during the transportation and kept in the chiller once reached the laboratory.

Water analysis

Appropriate techniques were applied while sampling as for each water sources, there is different in depth, accessibility and topography. All in-situ parameters were taken using different instrument, corresponding to the analysis. Turbidity was measured using HACH portable turbidimeter. Conductivity and temperature were taken using YSI pro30 meter. Dissolved oxygen (DO) was measured using DO meter. Total dissolved solid (TDS) and pH were measured using Myron L Ultimeter III.

In laboratory, Chemical Oxygen Demand (COD) and ammonia nitrogen (NH_3-N) was determined using UV-visible detector (DR900 HACH) with respective reagent. Meanwhile, biological oxygen demand (BOD) was tested by using DO probe for initial DO and DO after 5 days incubated at 25ºC. Total suspended solid (TSS) was measured by weighting of solute of the filtered sample before and after ignition at 105ºC in oven. The laboratory analysis of BOD, COD, TSS and NH_3-N were carried out according to APHA Standard Methods (APHA, 2012). The data obtained were then compared to the National Water Quality Standards for Malaysia (Table 1) and calculated for the Water Quality Index based on the formula below;

WQI = (0.22* SlDO) + (0.19*SIBOD) + (0.16*SICOD) + (0.15*SIAN) + (0.16 * SISS) + (0.12 * SipH)

Table 1: Selected parameters of water quality classification according to National Water Quality Standards (NWQS) for Malaysia (DOE, 2008)

Parameter	Unit	Class I	IIA	IIB	III	IV	V
pH		6.5-8.5	6-9	6-9	5-9	5-9	-
DO	mg/L	7	5-7	5-7	3-5	<3	<1
BOD	mg/L	1	3	3	6	12	>12
COD	mg/L	10	25	25	50	100	>100
TSS	mg/L	25	50	50	150	300	300
AN	mg/L	0.1	0.3	0.3	0.9	2.7	>2.7

Class I	Conservation of natural environment Water supply I – Practically no treatment necessary Fishery I – Very sensitive aquatic species
Class IIA	Water supply II – Conventional treatment Fishery II – Sensitive aquatic species
Class IIB	Recreational use with body contact Water supply III – Extensive treatment required
Class III	Fishery III – Common of economic value and tolerant species; livestock drinking
Class IV	Irrigation
Class V	None of the above

Results and Discussion

Physico-chemical parameter determination in water

Assessment of water physico-chemical characteristics reports that the parameters vary across the locations as shown in Table 1. Tailing Storage Facility (TSF) (S1) is the first station to receive the mine-impacted water after the process of extraction of gold, followed by process tank and retention pond. Tailing Storage Facility is an embankment builds by the mine waste rock to store tailing from the mining operation ("Tailing Storage Facilities", 2015). Tailings are materials that have been discarded or extraction by-product of gold ore. Then, process tank (S2) is the next stage of water treatment where, the water is piped to the S2 for further treatment before going through the retention pond and released into Sungai Kermoi. Based on the data obtained, tailing storage facility is categorised under class I based on NWQS as it has undergone treatment at the facility.

Table 2: Mean physico-chemical parameters of the water samples

Location	pH	Temp	TDS	Cond.	Turbid.	DO	TSS	BOD	COD	AN
Selinsing Gold Mine, Raub		(°c)	(ppm)	(µS/cm)	(NTU)	(mg/L)				
S1-Tailing Storage Facility (TSF)	8.27	31.2	1569	2188	21.9	2.1	4.4	3.70	52	0.27
S2-Process tank	7.97	31.6	2259	2232	22.8	11.12	68.49	5.27	218	12.7
S3-Retention pond	8.11	32.4	355	542	3.78	12.85	3.58	1.70	5	0.09
MOH (2009) (untreated raw water)	5.5-9.0	**	1500	**	1000	**	**	6	10	1.5
MOH (2009) (treated water)	6.5-9.0	**	100	**	5	**	**	**	**	1.5
WHO (2009) & USEPA (2009)	6.8-9.2	**	500	**	5	**	**	**	**	**

Water Quality Index

Table 3: Status of water quality of each sampling point

Location	WQI	Class	Status
S1-Tailing Storage Facility (TSF)	81.45	Class II	Slightly Polluted
S2- Process tank	57.32	Class III	Polluted
S3-Retention pond	94.14	Class I	Clean

Class I

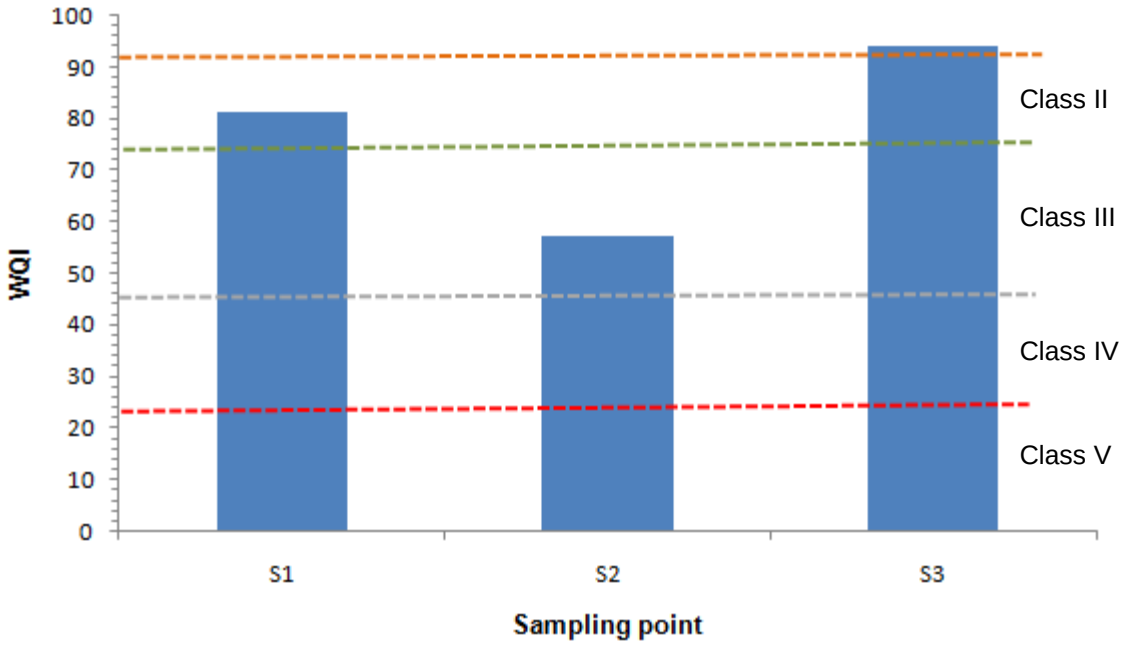

Figure 1: Status of water quality of each sampling point

Assessment of water quality index over three sampling points (S1, S2, S3) has shown that the water quality is different at different stages of water treatment as shown in Table 2 and illustrated in Figure 1. From the table and figure, it shows that S2 has the lowest WQI (57.32) which is categorised in class III (polluted), while S1 (81.45) and S3 (94.14) are categorised slightly polluted and clean respectively. S3 which is retention pond is the last stage before it is discharge to the river, thus the quality of mine- impacted water is believed to be at satisfactory level when it is released into the environment. As seen in figure 1, although the water at S3 is under clean category by the Department of Environment (DOE), further treatment is still needed for use as drinking resources as it is nearly to become slightly polluted.

Conclusion

Generally, water quality status of the mine-impacted water in the studied area has been investigated. Physico-chemical characteristic of the samples were compared to National Water Quality Standards and the water quality of the S3 was categorised under class I and the WQI is 94.14. Water treatment process at the treatment plant is likely to have achieve the target; where to reach permissible concentration of parameters of the water before releases to Sungai Kermoi.

Acknowledgement

This research was funded by Universiti Putra Malaysia and Ministry of Higher Education Malaysia through the IPM 9453700 and FRGS 5524757 research grants. The authors would like to acknowledge laboratory staff of Faculty of Environmental Studies, Universiti Putra Malaysia and officer of Selinsing Gold Mine for the technical support throughout this study.

References

1. Bakar, A.F.B., Yusoff, I., Fatt, N.T., Othman, F., & Ashraf, M.A. (2013). *Arsenic, Zinc, and Aluminium Removal from Gold Mine Wastewater Effluents and Accumulation by Submerged Aquatic Plants (Cabombapiauhyensis, Egeria densa, and Hydrillaverticillata).*Hindawi Publishing Corporation.

2. Yayintas, O.T., Yilmaz, S., Turkoglu, M. &Dilgin, Y. (2007*). Determination of heavy metal pollution with environmental physicochemical parameters in waste water of Kocabas Stream (Biga, Canakkale, Turkey) by ICP-MS.* Environ Monit Assess, 127, 389-397.

3. "Tailing Storage Facilities." Waihi Gold-Oceana Gold. N.p., 2015.

4. Kamar Shah Ariffin (2012). *Mesothermal Lode Gold Deposit Central Belt Peninsular Malaysia*. Earth Sciences, InTech.

5. Ashraf, M.A., Sarfraz, M., Naureen, R., Gharibreza, M. (2015). *Environmental Impacts of Metallic Elements: Speciation, Bioavailability and Remediation.* Springer.

6. "Management of Tailings and Waste Rock in Mining Activities" (2009). European Commission.

7. Porgo, M., &Gokyay, O. (2016). *Environmental Impacts on gold mining in Essakane site of Burkina Faso.* Human and Ecological Risk Assessment: An International Journal, 23(3), 641-654.

8. Ayantobo, O.O., J.A. Awomeso, G.O. Oluwasanya, B.S. Bada& A.M. Taiwo. (2014). *Gold Mining in Igun-Ijesha, Southwest Nigeria: Impacts and Implications for Water*

9. Patil. P.N, Sawant. D.V, Deshmukh. R.N. (2012), Physico-chemical parameters for testing of water – A review, International Journal of Environmental Sciences 3(3)

10. Sharma V, Walia Y. K., (2015). Water Quality Assessment Using Physico-Chemical Parameters and Heavy Metals of Gobind Sagar Lake, Himachal Pradesh (India). Curr World Environ ,DOI: http://dx.doi.org/10.12944/CWE.10.3.28

11. Kusin F.M., Muhammad S.N., Madzin Z., Zahar M.S.M., (2016). Integrated River Basin Management: incorporating the use of abandoned mining pool and implication on water quality status, Desalination and Water Treatment, DOI: 10.1080/19443994.2016.1168132

12. Gaikwad R.W., Sapkal V.S., Sapkal R.S. (2011). Acid Mine Drainage: A Water Pollution Issue In Mining Industry. 2(4).

13. Acheampong, M. A. (2013). Sustainable Gold Mining Wastewater Treatment by Sorption Using Low-Cost Materials. CRC/Balkema.

14. Acheampong, M.A., Paksirajan, K., Lens, P.N.L., 2013. Assessment of the effluent quality from a gold mining industry in Ghana. Environmental Science and Pollution Research 20, 3799-3811.

15. Bank, D., Younger P.L., Amesen R.T., Eversen E.R. & Banks, S.B. (1997). Mine Water Chemistry: The Good, The Bad And The Ugly. 32, 157-174.

4.3 Assessment of the Compositions of Major and Trace Elements in Soil of a Gold Mining Area in Selinsing, Pahang

Abstract

Distribution of major and trace elements in mine-impacted soil may be different according to the different mining activities. Therefore, this study focuses on the composition of major and trace elements in soils from gold mining area in Selinsing, Pahang. The main objective of this study is to determine the composition of major and trace elements in soil of a gold mine impacted area. Five samples of soils were collected from three different sampling points which are borrow pit, waste dump and stockpile that consists of lower grade, super lower grade and high grade. The samples were digested using aqua regia mixture with ratio 3HCL:1HNO_3 and analyzed by using ICP-MS. The results showed that composition of potassium (K) was the highest among the major elements (Ca, Mg, Na and K) which was 148.982 mg/kg from waste dump sample. Meanwhile, for trace elements, all five samples had the highest composition of iron (Fe) and the lowest was cadmium (Cd). Results of trace elements demonstrated that all concentrations of those elements except As were found below the recommended guideline values. By comparing between sampling points, distribution of elements was higher at stockpile areas, followed by waste dump area and the lowest was at borrow pit. Disturbance and process involved in natural process of geochemical cycle through gold mining has led to the release of heavy metals.

Keywords: gold mining; major; trace elements; soil

Introduction

In the development of any country, natural resources are necessary and the resources include metallic, non-metallic minerals and fossil fuels. Furthermore, from the earth surface or beneath the surface, the extraction of deposits of mineral can be done and this process is known as mining. In addition, this process only undergoes wherever the minerals are present and when there is economically viable (Ako et al., 2014). In Malaysia, 90% of gold mining are located in Pahang state which are at Penjom, Bukit Selinsing Koyan and Raub while Selinsing gold mining that is located in Bukit Selinsing Koyan is known as the lead of gold producer which produced 1,648 kg (52,982 troy ounces) in 2013, an increase of about 19% from that of 2012 (Pui, 2013).

The development of industrialization increases the release and production of toxic contaminants into the environment. Those toxic contaminants would come from

exposure of heavy metals or trace elements produced from two sources which are natural and anthropogenic or human activity. Mining is one of the human activities and classified as the main factor that significantly increases those contaminants into the environment aside from contributing to the social and economic benefits to the nations. Traditional gold mining develops because of the demand for gold even though this activity can cause serious contaminant exposure (Ako et al., 2014).

Release of toxic elements from the wastes of mine and tailings can be related to the environmental pollution (Fashola, 2016). According to D'Amore (2005) the exceed of recommended level of heavy metals accumulation in soils is caused by the disturbance and process that involved in natural processes of geochemical cycle through gold mining which is known as anthropogenic activities (Fashola, 2016).

Materials and methods

Study area

Selinsing Gold Mine which is at Bukit Selinsing Koyan, is located about 51 km north of Raub in northwest Pahang, Peninsular Malaysia. Selinsing Gold Mine is known as the largest gold producing area in Malaysia. Historically, it has produced only slightly in excess of a tonne of gold, mainly under foreign management.

Field sampling

The samples were collected at Selinsing gold mining site in Pahang, Malaysia. The type of samples collected was soil, at three sampling points which were borrow pit, waste dump, and stockpile areas that consist of super lower grade (SLG), lower grade (LG), and high grade (HG). The samples were collected by using scoop and all the samples were kept into different zip plastic bags with correctly labelled.

Laboratory analysis

All the samples were taken to laboratory to undergo the process of preparation and laboratory analysis. First of all, the soil samples were crushed by using mortar to make the samples into small particles. Grinding was done to ensure the samples were in form of powder or smaller particles to be able to undergo the digestion before being analyzed. Acid digestion of aqua regia mixture with ratio 3HCL:1HNO_3 was done to extract the trace elements contained in the samples. Digested samples were filtered, diluted and analyzed by using an Inductively Coupled Plasma Mass Spectrometry or ICP-MS to determine the concentration of major and trace elements in the samples.

Results and discussion

Table 1 below shows the composition of major and trace elements in soil from Selinsing gold mining. The references of recommended guideline values for some trace elements in soil have been included.

Table 1 Composition of Major and Trace Elements in Soil from Selinsing Gold Mining

Location	Ca	Mg	Na	K	Fe	Mn	Zn	Sr	As	Cr	Cd	Ni	Cu	Co	Pb
	(mg/kg)														
S1 -Stockpile LG	167.376	146.031	13.71	122.523	3766.548	75.951	19.833	1.111	262.35	0.9	0.025	1.688	4.156	1.365	1.646
S2 -Stockpile SLG	40.699	41.673	14.922	67.576	2992.271	11.579	4.715	0.846	65.298	1.388	0.009	0.741	0.034	0.003	2.361
S3 -Stockpile HG	21.441	5.261	15.222	38.239	1003.815	5.502	3.26	0.135	63.471	1.465	0.023	2.325	3.276	2.176	0.901
S4 -Borrow pit	19.341	7.116	14.591	74.262	318.217	0.249	2.173	0.067	1.842	1.829	0.002	0.649	0.849	0.024	0.249
S5 –Waste dump	21.431	93.826	15.988	148.982	336.833	71.388	12.904	0.872	29.967	1.249	0.035	1.387	8.692	1.098	6.376
Mean	54.038	58.781	14.887	90.316	1683.537	32.934	8.577	0.606	84.586	1.366	0.0188	1.358	3.401	0.933	2.311
Standard Deviation	63.945	60.554	0.836	44.628	1596.203	37.437	7.577	0.473	102.771	0.337	0.013	0.694	3.407	0.929	0.409
Canadian Ministry of Environment (2009)Standard Deviation	**	**	**	**	**	**	290	**	11	64	1.4	37	63	40	45
UK Environment Agency (2009)	**	**	**	**	**	**	**	**	43	**	1.8	230	**	**	**
Australian Department of Environment and Conservation (2010)	**	**	**	**	**	500	200	**	20	400	3	60	100	50	600

** not specified

The results obtained are presented in Table 1 by comparing the values of the data according to the recommended guideline values adapted from Canadian Ministry of Environment (2009), UK Environment Agency (2009) and Australian Department of Environment and Conservation (2010). From the results of the concentration of major elements (K, Na, Mg, and Ca), all samples except from stockpile LG had the highest concentration of K. Tailings and waste produced from gold mining activities can cause the release of harmful elements, thus leading to environmental pollution. There are some elements that play roles in growth of living things such as, plants, human and microorganisms. For example, chromium is an element that stimulates growth for agricultural crops if it is in small amount but it also can contribute to diseases if present in excess (Fashola et al., 2016). According to Babalola (2016), elements like Zn, Cu, Ni, Co and Cr play their role as micronutrients and they also are needed for redox process. Meanwhile other elements like Pb, Cd and As are known as non-essential elements for living organisms. In fact, those metals are found to be very toxic and cause environmental pollution. The results obtained indicated that As was found to be above the recommended guideline values and future mitigation measures should be proposed to control the distribution of this toxic element. The results also indicated that Fe was one of the toxic elements that high in concentration for all samples from all sampling points. The range of concentration of Fe was between 318.217 to 3766.548 mg/kg. The sequence of the most high concentration to the lowest concentration was Fe> As> Mn> Zn> Cu> Pb> Cr> Ni> Co> Sr> Cd. Overall, by comparing between sampling points, distribution of all elements was higher at stockpile areas, followed by waste dump area and the lowest was at borrow pit.

Conclusion

The process of mining activities can affect the environment due to deposition of trace elements into the soil in that area. If the results found to be above from recommended guideline values, there would be undesirable impacts on human health and other living organisms and future mitigation measures should be proposed to control the distribution of the toxic elements.

Acknowledgements

This research was funded by Universiti Putra Malaysia and Ministry of Higher Education Malaysia through the IPM 9453700 and FRGS 5524757 research grants. The authors would like to thank laboratory staffs at Department of Science, Faculty of Environmental Studies, Universiti Putra Malaysia for providing ICP-MS instrument for heavy metals analysis throughout this study.

References

1. Abuduwaili, J., yong Zhang, Z., & qing Jiang, F. (2015). Assessment of the distribution, sources and potential ecological risk of heavy metals in the dry surface sediment of Aibi Lake in Northwest China. *PloS one*, *10*(3), e0120001.

2. Ako, T. A., Onoduku, U. S., Oke, S. A., Adamu, I. A., Ali, S. E., Mamodu, A., & Ibrahim, A. T. (2014). Environmental impact of artisanal gold mining in Luku, Minna, Niger State, North Central Nigeria. *Journal of Geosciences and Geomatics*, *2*(1), 28-37.

3. Ariffin, K. S., & Hewson, N. J. (2007). Gold-Related Sulfide Mineralization and Ore Genesis of the Penjom Gold Deposit, Pahang, Malaysia. *Resource geology*, *57*(2), 149-169.

4. Castilhos, Z., Rodrigues-Filho, S., Cesar, R., Rodrigues, A. P., Villas-Bôas, R., de Jesus, I., & Beinhoff, C. (2015). Human exposure and risk assessment associated with mercury contamination in artisanal gold mining areas in the Brazilian Amazon. *Environmental Science and Pollution Research*, *22*(15), 11255-11264.

5. Chakraborti, D., Rahman, M. M., Murrill, M., Das, R., Patil, S. G., Sarkar, A., & Das, K. K. (2013). Environmental arsenic contamination and its health effects in a historic gold mining area of the Mangalur greenstone belt of Northeastern Karnataka, India. *Journal of hazardous materials*, *262*, 1048-1055.

6. Fashola, M. U., Ngole-Jeme, V. M. & Babalola, O. O. (2016). Heavy Metal Pollution from Gold Mines: Environmental E ffects and Bacterial Strategies for Resistance. Journal of Environmental Reasearch and Public Health. 1-20.

7. Gibb, H., & O'Leary, K. G. (2014). Mercury exposure and health impacts among individuals in the artisanal and small-scale gold mining community: a comprehensive review. *Environmental Health Perspectives (Online)*, *122*(7), 667.

8. Ikemefuna, P. (2012). Evaluating the influence of open cast mining of solid minerals on soil, landuse and livelihood systems in selected areas of Nasarawa State, North-Central Nigeria. *Journal of Ecology and the Natural Environment*, *4*(3), 62-70.

9. Kpan, J. D., Opoku, B. K., & Gloria, A. (2014). Heavy metal pollution in soil and water in some selected towns in Dunkwa-on-Offin District in the Central Region of Ghana as a result of small scale gold mining. *Journal of Agricultural Chemistry and Environment*, *3*(02), 40.

10. Li, Q., Ji, H., Qin, F., Tang, L., Guo, X., & Feng, J. (2014). Sources and the distribution of heavy metals in the particle size of soil polluted by gold mining upstream of Miyun Reservoir, Beijing: implications for assessing the potential risks. *Environmental monitoring and assessment*, *186*(10), 6605-6626.

11. Naicker, K., Cukrowska, E., & McCarthy, T. S. (2003). Acid mine drainage arising from gold mining activity in Johannesburg, South Africa and environs. *Environmental pollution*, *122*(1), 29-40.

12. Ogola, J. S., Mitullah, W. V., & Omulo, M. A. (2002). Impact of gold mining on the environment and human health: a case study in the Migori gold belt, Kenya. *Environmental geochemistry and health*, *24*(2), 141-157.

13. Pui, K. T. (2013). The Mineral Industry of Malaysia. *Minerals Yearbook USGS Malaysia [Advance Release].*

14. Rikhtegar, N., Mansouri, N., Ahadi Oroumieh, A., Yazdani-Chamzini, A., Kazimieras Zavadskas, E., & Kildienė, S. (2014). Environmental impact assessment based on group decision-making methods in mining projects. *Economic Research-Ekonomska Istraživanja*, *27*(1), 378-392.

15. Vodyanitskii, Y. N. (2016). Standards for the contents of heavy metals in soils of some states. *Annals of Agrarian Science*, *14*(3), 257-263.

CHAPTER 5

METAL COMPLEXES REACTIONS

INTRODUCTION

Cancer therapeutics comprising transition metal-based complexes anticancer agents are widely used in the treatment of cancer. One good example is cisplatin an established antitumor platinum-based drugs, routinely used in the clinic. However, patients administered these chemotherapeutic drugs suffer from severe side effects and the drug itself develop drug resistance. Hence, a search for less toxic non platinum-based antitumor agents is necessary.

5.1 Synthesis and Biophysical Characterization of Interaction between a Novel Ruthenium(II) Complex and DNA Molecule

Abstract

Transition metal-based complexes constitute a vast range of cancer therapeutics, widely used in the clinic as anticancer agents. Cisplatin is one example of established antitumor platinum-based drugs, routinely used in the clinic. Despite their excellent anticancer properties, these chemotherapeutic drugs suffer from severe side effects and drug resistance. These limitations have prompted a search for more effective and less toxic non platinum-based antitumor agents. Among various metal-based drugs, ruthenium complexes have aroused as alternative drugs to cisplatin in chemotherapy owing to similar ligand exchange kinetics to those of platinum(II)-based drugs while displaying only low toxicity. In this study, a novel ruthenium(II) polypyridyl complex, $[Ru(dppn)_2PIP]^{2+}$ (dppn = benzo[i]dipyrido-[3,2-a;2',3'-c]phenazine, PIP= phenylimidazo[4,5-f][1,10]phenanthroline) has been synthesized and characterized by ^1H NMR spectroscopy, mass spectrometry, FT-IR, UV-Visible spectroscopy. The DNA binding interaction of this complex with Calf Thymus DNA (CT-DNA) was investigated using UV-Visible titration and viscosity studies. The absorption band observed at 463 nm corresponded to the metal-to-ligand charge transfer (MLCT) while bands at 278 and 369 nm corresponded to intra-ligand (IL) π-π* transitions of the PIP and dppn ligands. The binding affinity, K_b for this complex was 2.0×10^7 M^{-1} and this high binding affinity suggested that $[Ru(dppn)_2PIP]^{2+}$ bound to DNA via intercalation. The strong binding affinity might be due to the extended π system of the intercalative ligand, PIP or dppn which increase the affinity of complex to the DNA.

Keywords: ruthenium; polypyridyl; DNA binding; intercalation

Introduction

Research centered on binding of metal complexes with nucleic acid has been extensively studied since the last two decades. Among many metals, ruthenium(II) complexes consisting polypyridyl ligands have attracted great attention, due to easy combination of rigid chiral structures spanning all three spatial dimensions and a rich

photophysical properties suitable as DNA binding agents. Thus, research on DNA binding of Ru(II) complexes has initiated vigorous attention. Mostly, these complexes can bind to DNA by non-covalent interactions, such as intercalation, electrostatic, groove binding [1].

Three novel Ru(II) polypyridyl complexes, $[Ru(phen)_2(dppn)]^{2+}$, $[Ru(bpy)_2(dppn)]^{2+}$ and $[Ru(dmb)_2(dppn)]^{2+}$ were reported previously and their DNA interaction and photocleavage properties were also investigated via spectroscopic and viscosity studies. It was found that the dppn ligand was able to intercalate into DNA base pairs with high binding affinity, $K_b \sim 10^5\ M^{-1}$ [2].

Tan et al reported the effects of the ancillary ligands on the DNA binding of novel polypyridyl ligand MIP [MIP = 2-(2,3-methylenedioxyphenyl)imidazo[4,5-f]1,10-phenanthroline] and its Ru(II) complexes, $[Ru(phen)_2(MIP)]^{2+}$ (1) (phen = 1,10-phenanthroline) and $[Ru(dmp)_2(MIP)]^{2+}$ (2) (dmp = 2,9-dimethyl-1,10-phenanthroline) [3]. The DNA binding interaction of these two compounds towards CT-DNA was investigated by spectroscopic methods and viscosity studies. The results suggested that phen-based complex (1) binds to CT-DNA via intercalation, while dmp-based complex (2) binds to CT-DNA via a partial intercalative mode. Considering the similarity in term of the main ligand, the difference in binding mode is probably due to the different size of the ancillary ligands.

The DNA binding mode can be tailored by careful design of intercalative ligand. This might result in the changes in the DNA binding behavior, photophysical properties, excited state reactivity and biological activities of the complexes. Extensive studies are usually required to fully delineate the DNA binding mode and strength of Ru(II) complexes. These complexes binding to DNA will be useful as new DNA probes, photodynamic therapy agents and to perform other biological functions such as phot cleavage activities. Herein, a novel ruthenium(II) polypyridyl complex is reported and the biophysical interaction of this novel Ru(II) polypyridyl complex with CT-DNA was investigated.

Results and Discussion

The reaction of $[Ru(dppn)_2Cl_2.2H_2O]$ with PIP in a ratio 1:1 treated with potassium fluorophosphate resulted in formation of $[Ru(dppn)_2PIP]^{2+}$ in PF_6 salt. The purified complex was collected as a red-orange solid with 52.0 % yield. The ^1H NMR spectrum of $[Ru(dppn)_2PIP]^{2+}$ in deuterated acetonitrile were properly defined and integrated. There are twelve signals which corresponded to the protons of dppn and PIP ligands. The signal at 9.70 ppm corresponded to the proton attached to the carbon adjacent to a nitrogen atom in the aromatic ring of pip ligand. The signal that corresponded to the proton directly attached to nitrogen atom in PIP was not observed in the spectrum. This might be due to fast exchange chemistry of the active proton in the imidazole ring or it was obscured by the nitrogen quadrapole broadening property [6]. However, FTIR was used in this case to confirm the presence of NH. The IR spectrum of the Ru(II) complex was recorded in the region of 4000-280 cm^{-1} and the data is summarized in Table 1. A broad and strong peak at 3392 cm^{-1} was assigned as secondary amine group of imidazole v(N-H). The carbon-nitrogen bonds absorptions v(C=N) and v(C-N) were observed at 1616 and 1412 cm^{-1}, respectively. The accumulated MS, NMR and IR data was in agreement with the proposed structure and confirm the formation of the complex.

Table 1. IR data of $[Ru(dppn)_2PIP]^{2+}$

Wave number (cm^{-1})	Functional group	Intensity
3392	N-H	strong, broad
3072	C-H	strong, sharp
1616	C=N	medium, sharp
1412	C=C	strong, sharp
1077	C-N	strong, sharp

The UV-Visible absorption spectrum for $[Ru(dppn)_2PIP]^{2+}$ was recorded in acetonitrile, with a concentration of 15 µM at room temperature. Through comparison to related molecules [7, 8], the bands centered at around 278 nm (ε = 60600 M^{-1} cm^{-1}) and 369 nm (ε = 17500 M^{-1} cm^{-1}) were assigned to intra-ligand π→π* transitions in the complex. The metal-to-ligand charge transfer (MLCT) transition was observed at higher wavelength,463 nm (ε = 12200 M^{-1} cm^{-1}) and this is due to the transition of $Ru(d_\pi)$ →ligand.

DNA-binding studies

The DNA binding interaction between a ruthenium(II) complex, $[Ru(dppn)_2PIP]^{2+}$ and CT-DNA has been studied and discussed. The UV-Vis titration of the complex in a buffer was performed at room temperature using a fixed concentration of the complex with increasing concentration of DNA.

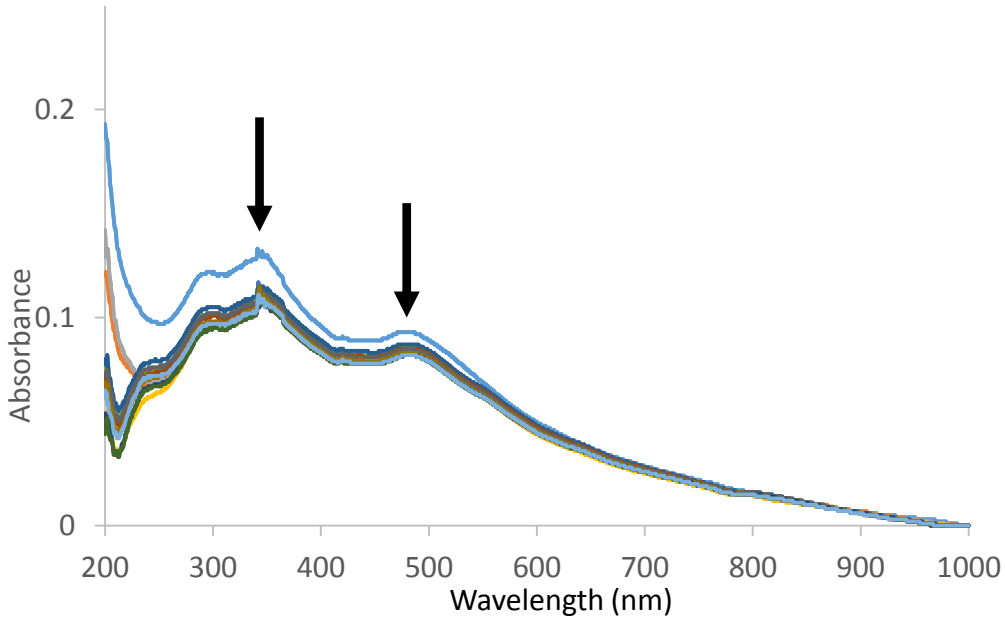

Figure 1: UV-Visible spectra of ruthenium(II) complex in Tris-HCl buffer upon addition of CT-DNA. [Complex] = 15µM, [DNA]= 0-90 µM.

It can be seen in Figure 1, the absorbance was decreased upon the increase of the concentration of DNA. It is usually observed that the absorption of an intercalators results in hypochromism and bathchroism. This is due to strong stacking interaction between the DNA base pairs and aromatic chromophore of the ligands. Generally, the extent of hypochromism commonly parallel to the intercalative binding strength. In this case, no obvious red shift was observed, however it was found that about 23 % of hypochromicities upon DNA binding interaction. It is commonly known that hypochromism effect is related to synergic non-covalent interactions: electrostatic, groove or intercalation and is often the in parallel to the binding strength [9]. The binding constant, K_b of this compound with CT-DNA was determined in order to qualitatively describe the binding strength. Absorbance at 284 nm was monitored while increasing the concentration of DNA and K_b was obtained according to the following equation [10]:

$$[DNA]/(\varepsilon_a - \varepsilon_f) = [DNA]/(\varepsilon_b - \varepsilon_f) + 1/K_b(\varepsilon_b - \varepsilon_f)$$

Where [DNA] is the concentration of CT-DNA in base pairs, the apparent absorption coefficient, ε_a, ε_f and ε_b correspond to $A_{observed}$/[Ru], the extinction coefficient for the free ruthenium complex and the extinction coefficient for the free ruthenium complex in the fully bound form, respectively .

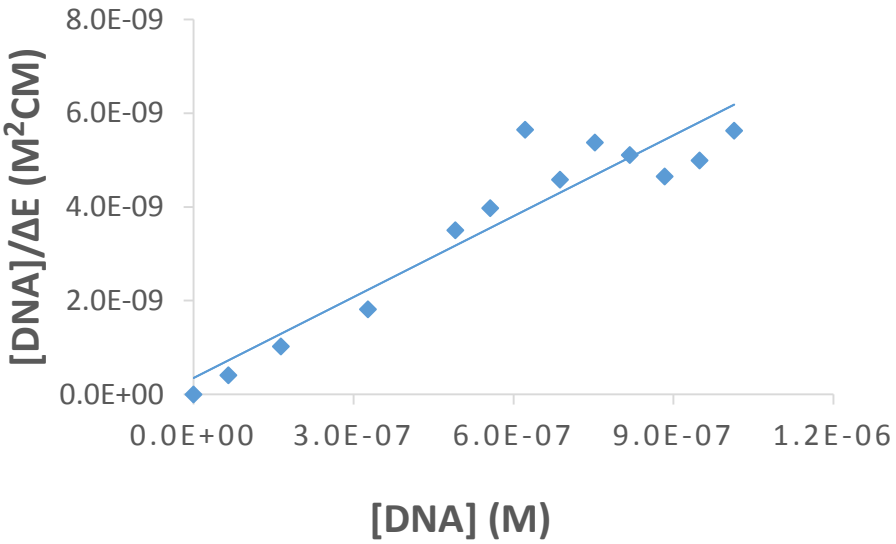

Figure 2: [DNA]/(Δε) vs [DNA] for the Ru(II)-DNA interaction.

In plots of [DNA]/(ε_a- ε_f) *versus* [DNA] in Figure 2, K_b is given by the ratio of slope to the intercept. The K_b of $[Ru(dppn)_2PIP]^{2+}$ complex obtained was 2.0 x 10^7 M^{-1}. $[Ru(dppn)_2PIP]^{2+}$ complex has a higher binding affinity towards DNA compared to other ruthenium(II) complex, for example $[Ru(Melm)_4(p\text{-}cPIP)]^{2+}$ and $[Ru(Melm)_4(PIP)]^{2+}$ which the K_b value approximately 10^5 [11]. This is because of the extended π system of the intercalative ligand which is PIP or dppn, result in the increased interaction of this dppn complex with the DNA.

In order to determine the binding mode of the ruthenium complex, viscosity studies of CT-DNA were carried out by varying the concentration of this ruthenium complex. The viscosity of DNA studies are regarded as the most conclusive of a DNA binding model in solution in the absence of crystallographic structural data. Usually, a

classical intercalators result in lengthening of DNA helix as base pairs are separated to accommodate the binding ligand, which, in turn, leads to increment of the viscosity of DNA [12]. In contrast, a partial intercalators could bend (or kink) the DNA helix and reduce its effective length and, concomitantly, its viscosity [1].

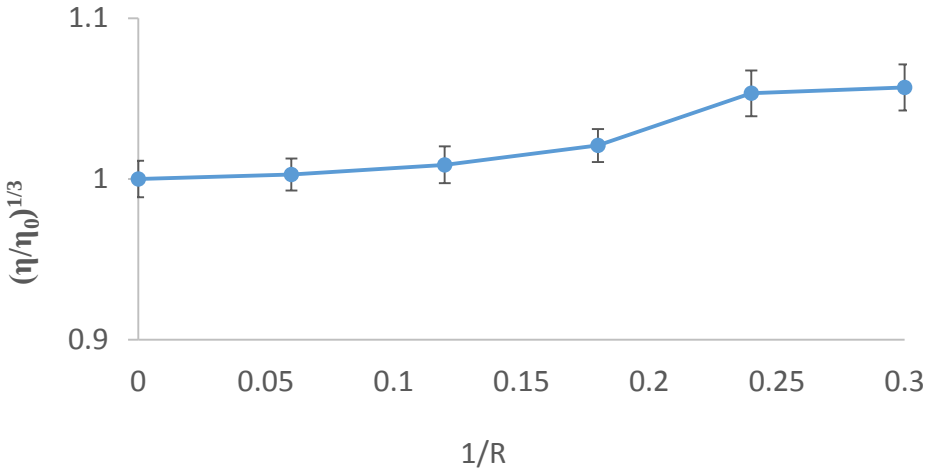

Figure 3: Viscosity of CT-DNA in the presence of increasing ratio of $[Ru(dppn)_2(PIP)]^{2+}$.

Based on Figure 3, $[Ru(dppn)_2PIP]^{2+}$ slightly increased the relative viscosity of DNA solution. Therefore, it can be concluded that $[Ru(dppn)_2PIP]^{2+}$ interacts with DNA *via* intercalation. This preliminary result suggests that this novel complex may be suitable as DNA probes or anticancer agent.

Conclusion

In this study, a novel ruthenium(II) complex, $[Ru(dppn)_2PIP]^{2+}$ was synthesized and characterized *via* ^{1}H-NMR, mass spectrometry, FT-IR, and UV-Vis spectroscopy. The DNA binding study of the complex was carried out by using absorption spectral study and viscosity measurements. From the results obtained, it showed that interaction of the complex, $[Ru(dppn)_2PIP]^{2+}$ with the CT-DNA was *via* intercalation binding mode. The K_b of $[Ru(dppn)_2PIP]^{2+}$ has been determined as 2.0 x 10^7 M^{-1}. This high K_b might be due to the extended π system of the intercalative ligand which is PIP or dppn which increase the interaction of complex with the DNA. The results obtained suggest that this complex shows a potential as DNA probe or anticancer agent. However, further studies are needed to fully delineate the binding mechanism of this complex to DNA.

Acknowledgements

This work was in financially supported by Putra IPS Grant (GP-IPS/2017/9520100) Universiti Putra Malaysia. The authors would like to extend our thanks to those directly and indirectly involved in this project.

References

[1] Zeng, L., Xiao, Y., Liu, J., & Tan, L. (2012). Synthesis, characterization, DNA-binding and cytotoxic properties of Ru(II) complexes: [Ru(MeIm)4L]2+ (MeIm=1-methylimidazole, L=phen, ip and pip). Journal of Molecular Structure, 1019, 183–190.

[2] Vidhisha, S., Reddy, K. L., Kumar, Y. P., Srijana, M., & Satyanarayana, S. (2014). Synthesis, characterization, antibacterial activity and investigation of DNA binding for Ru(II) molecular “light switch” complexes. International Journal of Pharmaceutical Sciences Review and Research, 25(1), 197–205.

[3] Tan, L. F., Chao, H., Zhen, K. C., Fei, J. J., Wang, F., Zhou, Y. F., & Ji, L. N. (2007). Effects of the ancillary ligands of polypyridyl ruthenium(II) complexes on the DNA-binding and photocleavage behaviors. Polyhedron, 26(18), 5458–5468.

[4] Liu, J., Zheng W., Shi, S., Tan, C., Chen, J., Zheng, K. and Ji, L. (2008). Synthesis, antitumor activity and structure-activity relationships of a series of Ru(II) complexes. Journal of Inorganic Biochemistry, 102 (2): 193–202.

[5] Sullivan, B. P., Meyer, T. J. and Salmon, D. J. (1978). Mixed phosphine 2,2’-bipyridine complexes of ruthenium. Inorganic Chemistry, 17 (12): 3334–3341.

[6] Devi, C. S., Kumar, D. A., Singh, S. S., Gabra, N., Deepika, N., Kumar, Y. P. and Satyanarayana, S. (2013). Synthesis , interaction with DNA , cytotoxicity , cell cycle arrest and apoptotic inducing properties of ruthenium(II) molecular ‘ light switch ’ complexes. European Journal of Medicinal Chemistry 64: 410–421.

[7] Zhong, V., Huang, H., He, A. and Zhang, H. (2008) Synthesis and luminescent properties of novel polymeric metal complexes with bis(1,10-phenanthroline) group. Dye Pigment, 77 (3): 578–583.

[8] Hiort, C., Lincoln, P. and Norden, B. (1993) DNA binding of .DELTA.- and .LAMBDA.-[Ru(phen)2dppz]2+. Journal of The American Chemical Society, 115 (9): 3448–3454.

[9] Shi, S., Yao, T., Geng, X., Jiang, L. and Liu, J. (2009) Synthesis , characterization , and DNA binding of chiral complexes D - and L - [Ru(bpy)2(pyip)]2+. Chirality, 283: 276–283.

[10] Srishailam, A., Kumar, Y. P., Venkat Reddy, P., Nambigari, N., Vuruputuri, U., Singh, S. S. and Satyanarayana, S. (2014). Cellular uptake, cytotoxicity, apoptosis, DNA binding, photocleavage and molecular docking studies of ruthenium(II) polypyridyl complexes. Journal of Photochemistry and Photobiology B: Biology, 132: 111–23.

[11] Chen L. M., Peng F., Li G. D., Jie X. M., Cai K. R., Cai C., Zhong Y., Zeng H., Li W., Zhang Z., Chen J. C. (2016). The studies on the cytotoxicity in vitro, cellular uptake, cell cycle arrest and apoptosis-inducing properties of ruthenium methylimidazole complex [Ru(MeIm)4(p-cpip)]2+. Journal of Inorganic Biochemistry, 156, 64–74.

[12] Kumar, K. A., Reddy, K. L., & Satyanarayana, S. (2010). Synthesis, DNA interaction and photocleavage studies of ruthenium(II) complexes with 2-(pyrrole) imidazo-[4,5-f]-1,10-phenanthroline as an intercalative ligand. Transition Metal Chemistry, 35(6), 713–720.

CHAPTER 6

SENSOR APPLICATIONS

INTRODUCTION

Two great approaches applied in surface chemistry are self-assembled monolayers and click reaction. Analytical and bioscience have applied the idea of merging these techniques based on their ability to provide an excellent platform to investigate kinetics of electron transfer. Immobilization of functionality complex on different surfaces can serve as a good platform to construct redox-active interface for various purposes especially in sensing application.

6.1 Derivatization of ferrocene on indium tin oxide (ITO) by CLICK reaction

Abstract

Self-assembled monolayers (SAMs) and click reaction are among two great approaches applied in surface chemistry. The idea of merging these attractive techniques were abundantly found in high-impact fields such as analytical and bioscience application based on their ability in providing an excellent platform to investigate kinetics of electron transfer. Thus, in this study, SAMs and greener concept of click reaction namely Copper(I)-catalyzed azide-alkyne cycloaddition (CuAAC) were introduced to bind two molecular building block by tailoring a terminal reactive group onto a diferent funtionality of modified surfaces in torable, facile and selective experimental design with zero by-product. Initially, a modification onto solid surfaces bare indium tin oxide (ITO) were performed by silanization using 6-azidosulfonylhexyltriethoxysilane (ASTES) through a simple dipping technique of SAMs. The readily azide terminated-ITO surfaces were then subjected to CuAAC reaction to “click” terminal active alkyne group called ethynyl feroccene. The selection of ferrocene is driven by fact of its uniqueness in having low potential and excellent reversible redox behaviour. Contact angle goniometer (CA), cyclic voltammetry (CV), atomic force spectroscopy (AFM) and x-ray photoelectron spectroscopy (XPS) were used to characterize these modified surfaces. From the findings, successful silanization was proved by increased in root mean square roughness (rms) value of ordered island-like structure of azide-terminated monolayer compared to bare ITO surface. Furthermore, the difference in surface wettability of azide and ferrocene-azide monolayer (click monolayer) obtained from CA also became one of indicator. The cyclic voltammogram that illustrated high reversibility of click monolayer which contradict with shown blocking behaviour of azide monolayer then support the results. Thus, it can be concluded the chosen route that succeeded in immobilization of functionality complex on different surfaces can serve as a good platform to construct redox-active interface for various purposes especially in sensing application.

Keywords : SAMs; Click reaction; indium-tin oxide; azide

Introduction

Click chemistry was discovered to be one of interesting approach in designing functional SAMs due to their high efficiency and compatibility with a wide range of solvents and SAMs functionalities. Among those functionalities, great works were found on alkylsiloxane [CH_3-CH_2-Sio_x] as it has greater physical and chemical stability compared to other functionality like thiol as it desorbs at higher temperatures and sensitive towards pH conditions and solvents [1][2]. However, due to limitation which is difficulty in functionalizing the opposite end of the monolayer as they having a high reactivity, azide-containing siloxane was created by Lummerstorfer and Hoffmann. Early studies demonstrated azide functional alkanes could be assembled onto gold surface and modified successfully with alkyne ferrocene for analytical application through click rection which later became an attractive features useful in bioscience field [3].

Generally, azides and alkynes are chosed as they are convenient to introduce, inert to molecular oxygen and can tolerate for other functionality. It results in formation of irreversible and quantitative triazole [4]. This reaction which leads to ferrocene-derived triazole systems had an ability to perform reaction efficiently under robust conditions as it behaved well in aqueous medium and can be used to modify highly functional biomolecules such as nucleic acid as it was extremely chemoselective [5]. It also can be a helpful tool in drug delivery and gene therapy that included under bioapplications ans sensing applications [6]. Based on the same idea, in this study by mean to tailor ethynyl ferrocene onto azide monolayer, experimental design on formation of ferrocene-terminated self-assembled monolayers (Fc-SAMs) was designed through copper(I)-catalyzed azide-alkyne cycloaddition (CuAAC). This approach was chose as it is one of the most studied molecular aggregates on metal electrodes, easy to fabricate and able to provide a stable and reproducible system to investigate the effect of electron transfer [7]. In addition, the versatility of the reaction route was improved by presence of ferrocene that able to behave as an electron mediator due to their fairly high stability in aqueous media, solubility in various solvent, having great redox properties which has low potential and high reversibility in terms of oxidation/reduction. The electron-donating groups on its Cp ring also facilitate the oxidation of the ferrocene moiety, which reflected by increase of redox potential [8]. Thus, by considering the excellent properties offered by chose tenchniques and functionalities,the designed ferrocene-azide monolayer on ITO surface is believed able to portray as a great platform in exploring sensing area for various purposes.

Experimental design

Materials and Chemicals

6-azidosulfonylhexyltriethoxysilane (ASTES) 95% was purchased from Gelest Inc. while dichloromethane (DCM) obtained from Sigma-Aldrich. For ethanol, copper(II) sulphate pentahydrate, sulphuric acid, sodium ascorbate, all of these chemicals were purchased from R&M chemicals. Ethynyl Ferrocene that used for click reaction was obtained from Ark Pharm Inc. ITO substrate was purchased from Sigma-Aldrich for the purpose of silanization.

Sample Preparation

Silanization of Azide Monolayer

Cleaning of Indium-Tin Oxide (ITO) was performed before the self-assembly process. The substrate was cleaned using piranha solution which made up by mixing hydrogen peroxide (H_2O_2) with concentrated Sulphuric Acid (H_2SO_4) in ratio of 1:3. Copious amount of deionised water was used to rinse the ITO glass to remove any residue before dried using N_2 gas stream. The silanization of azide derivative 6-azidosulfonylhexyltriethoxysilane (ASTES) on cleaned ITO surface was then performed through simple technique of self-assembled monolayers in glove bag due to high sensitivity of the silane with air as it can trigger polymerization process. Generally, the working substrate was immersed in 1 mM ASTES which diluted in dichloromethane solvent and left for 48 hours. The samples were then removed from the glove bag and dried by purging of nitrogen gas.

Surface Modification Azide Monolayer by Click Reaction

The azide monolayer was further modified with 1 mM solution of ethynyl ferrocene. During the immersion, 1 mol % of catalyst copper(II) sulphate pentahydrate and 15 mol% sodium ascorbate were added into the vial. In order to prevent photo-oxidation of the surface SAM, exposure of light was kept to a minimum [4]. The general procedure for the derivatization process was shown in Figure 1.

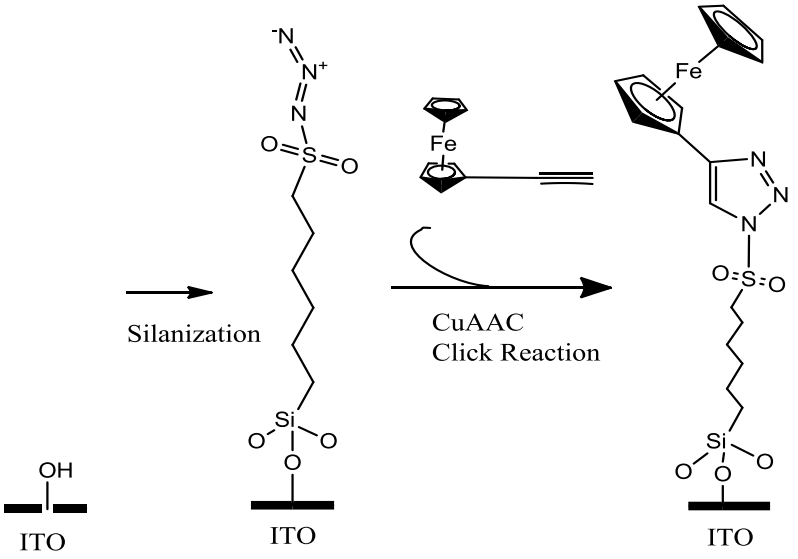

Figure1. Schematic representation of modification of azide derivative 6-azidosulfonylhexyltriethoxysilane (ASTES) by ethynyl ferrocene on ITO

Surface Analysis

The size of ITO substrate sent for characterization was small with dimension of (22mm x 10mm) and thickness of 0.013 mm. The wetting properties of modified surfaces were determined using dynamic contact angle instrument with a model Thermo Cahn DCS 300 Analyzers at three different spots for each surfaces. The measurement on surface roughness and topography were performed using an

atomic force microscope (*Quesant Instrument Corporation, Q-Scope 250*) in contact mode with a Si_3N_4 cantilever. The root mean square (RMS) value for modified surfaces was determined by Scan Atomic software. The electrochemical characterization using cyclic voltammetry (CV) was carried out measured using AUTOLAB instrument Model uAutolab Type III (Eco Chemie B. V., Netherlands). Reference Ag/AgCl (3.0 M KCl) and counter platinum electrode were required to run the three-electrode system analysis at room temperature in 0.1 M Perchloric Acid solution. The data analysis of CV was run through *General-Purpose-Electrochemical-System*-Software (GPES).The XPS analysis was conducted by X-ray Microprobe Phi Quantera II with a spectrometer fitted with a monochromated Al Kα scanning X-ray source in range energy of 1486.6 eV. The wide and high resolution scans were done by using beam size of 300 microns with 50 watts power and pass energy of 280 eV and 112 eV, respectively. Prior to elemental analysis, all the binding energies (BEs) were referenced to carbon C-C component at 285 eV while the background subtraction was performed using linear and shirley type depending on the suitability of the peak shape formed by using Casa XPS software. The defined peaks obtained through fitting with Gauss-Lorentz profile, the elemental composition data of electrode surface was displayed.

Results and discussion

Surface Characterization of bare ITO, Azide Monolayer and Click Monolayer

Contact Angle

The wetting properties of modified surfaces were investigated using contact angle goniometer. The value of contact angle produced depends on the interaction of water with the outer most atom stack on the monolayer. Upon silanization on cleaned ITO, based on the reviews, measured contact angle value for azide-functionalized surface which is 6-azidosulfonylhexyltriethoxysilane (ASTES) must be around 75 °– 77° [2] [11] [12] [13]. Figure 2 shows the wetting properties of the azide monolayer as the time of immersion varied from 0 which presented bare ITO and extended up to 72 hours. It clearly shows that the hydrophobicity of surface monolayer increased proportionally with time. According to the graph, at 48 to 72 hours of immersion, a stable and uniform monolayer started to form as only small difference of contact angles were recorded between that times which about 75° to 77° respectively. It proved that the ASTES head group was successfully tailored at optimum condition of 48 h as the average value of contact angle recorded was about 77.3° after three different spots were measured on the surface. The low error bar calculated indicates that a uniform monolayer has been formed under this favourable condition. Next, the click reaction in this study was performed under optimum condition of silanization which was 48 H in N_2 atmosphere. The silane monolayer which was modified on hydrophilic ITO surface (<10°), losing its hydrophobicity (75-77°) due to attached ferrocene group. The average value of contact angle measured for click monolayer was 72.6° which indicated that ferrocene possess hydrophilicity behaviour. The reduced contact angle value from hydrophobic azide to hydrophilic ferrocene monolayer was expected as reported in the literature [13] [14].

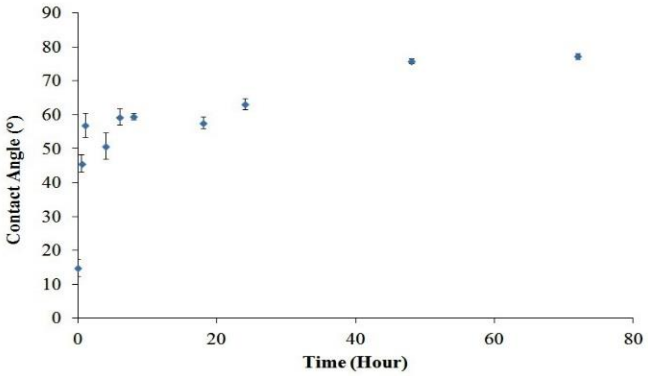

Figure 2 Graph on variation of contact angle (°) against time of immersion (h) under N_2 atmosphere of azide monolayer

Atomic Force Spectroscopy (AFM)

Modified surfaces topography and its root mean square roughness (rms) were observed by AFM analysis. From the morphology as ilustrated in Figure 3(a), it can be concluded that the bare ITO having a clean and flat surface. However, the bright/dark colour contrast in the figures indicates that the ITO possess a non-uniform surface which is likely due to the minor contamination. The value of rms measured was about 0.515 nm, showing that the cleaned ITO having relatively a smooth surface. The clean and smooth surface formed on the substrate was a good precursor for silanization to occur successfully. Figure 3(b) displayed a topography image of azide monolayer with rms value of 14.899 nm. The measured rugosity value of the monolayer was higher than the bare ITO (0.515 nm) indicating that silanization process was occurred.

The topography difference between these surfaces (ITO and ASTES) can be seen clearly on the 3D images. Instead of forming a flat surface, after the modification process, the aizde monolayer formed a dense, complete and homogenous morphology monolayer with ordered island-like structure. The differences in the topographies suggest that formation of monolayer has been occurred on the top of monolayer. Based on reviews, nucleation and growth of condensed phase islands will occur as a results of monolayer formation. As the time of immersion increasing, the number and size of islands also increased. The growth of islands was likely to happen due to collision between adsorbate molecules that move randomly on the surface [15, 16]. The homogeneity of formed monolayer is possible as the silanization process was performed using a freshly prepared solution in an optimum condition. The homogeneity and uniformity of this monolayer allowed ferrocene moiety to be click on the silane in a similarly, uniform and homogenous pattern [17].

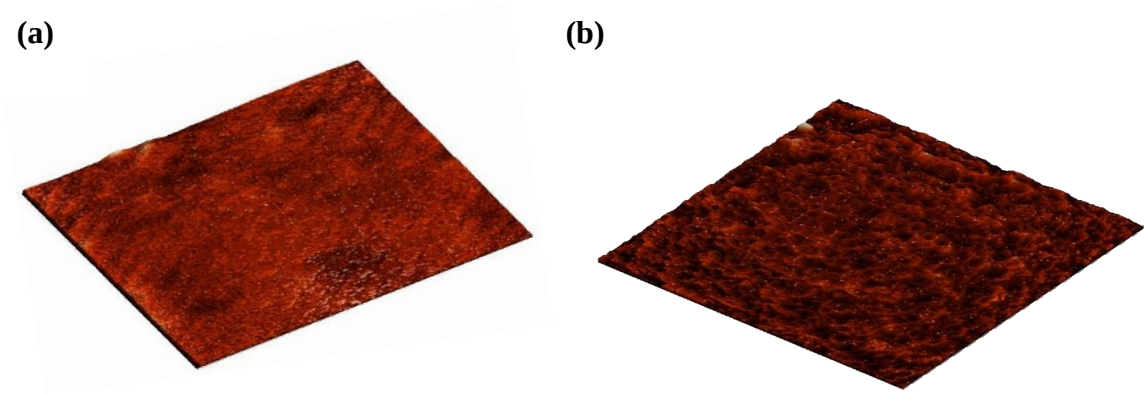

Figure 3(a) 3-D AFM Topography of Clean ITO with Z-range of 0-8 nm and (b) 3-D AFM Topography of azide monolayer with Z-range of 0-170 nm of size 10 x 10 μm^2

X-Ray Photoelectron Spectroscopy (XPS)

Further confirmation of azide monolayer was characterized using x-ray photoelectron spectroscopy (XPS). Figure 4(a) displays high resolution XPS of C1s signal which was fitted with three components. The major peak which presented at 285.0 eV was assigned to aliphatic carbon bound atom C-C. The broader peak detected at ~285 eV were attributed by C-S bond (285.3 eV) and peaks at 284.2 eV and 286.2 eV were originated from hydrocarbon contamination which possibly a C-H group which happened during sample handling for XPS analysis [18] [19]. In addition, the peak at around 287.7 eV produced from the C1s spectrum was associated with electron deficient carbon atom in the carbonyl group which might resulted from unavoidable oxidation on monolayer sample [20]. Apart from that, the C=O bond resulted from the contamination of sample that happened during film preparation in the vacuum chamber where the oxygen contaminant originates from the residual gases such as CO and CO_2 and water [18]. The bounded contaminant also might come from the air as the sample was exposed and stored in atmospheric environment. Theoretically, an azide monolayer should produced three distinct peaks at around 400 eV, 401 eV and 405 eV in narrow scan of N1s [1] [12]. From the N1s spectrum shown in Figure 4(b), there are three characteristic peaks were detected. The peak at 400 eV binding energy represents electron rich nitrogen atom while detection of peak at 401.8 eV attributed by neutral nitrogen atom from the azide group [21] [11]. While the small peak present around 405 eV binding energy is corresponding to electron-deficient nitrogen atom located in the middle of the azide group. However, the peak of that type of nitrogen was not so intensed due to azide functional group of ASTES was slowly decomposed photochemically and potentially due to X-ray damage.

From the peak fitting analysis, a small portion of peak around 400 eV was also contributed by amine-like nitrogen which arises from degradation of ASTES that happened during deposition and sample handling using XPS tool [[22]. Meanwhile, peak at 402.8 eV which represents N-O was detected in the spectrum as there might be oxygen trapped due to surface contamination or N_2 trapped within the deposition of azide monolayer [23].

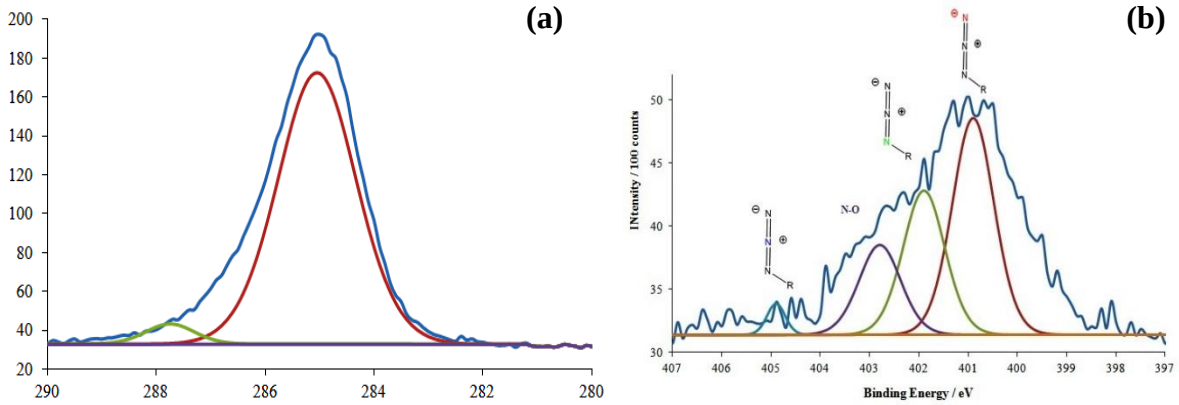

Figure 4 (a) C1s high resolution scan of for azide monolayer and (b) high resolution scan of N1s for azide monolayer

Next, the attachement of alkyne group ethynyl ferrocene on azide monolayer was also monitored based on the chemical composition obtained through XPS analysis. Figure 5(a) shows the C1s spectrum of click monolayer. The peak of C1s spectrum at 285.0 eV for click monolayer was majorly contributed by aliphatic carbon bound atoms of ASTES and carbon atom from cyclopentadienyl ring of ethnylferrocene [24]. In term of quantitative analysis of XPS result, the peak intensity of C1s for both spectra can be used to distinguish the monolayers. Based on the quantification data, it shows that the clicked monolayer produced higher C-C intensity at 285.0 eV about 54.87% compared to 45.34% for azide monolayer. This is consistent with the increasing carbon number on the monolayer that came from ferrocene species. Meanwhile, the broad peak formed at around ~285 eV was contributed by C-C carbon contamination and C-S bond [23]. The spectrum also shows another important characteristic peak at 286.7 eV which was assigned to carbon bonded nitrogen atom due to formation of triazole ring [19][24]. This data became one of the indications to prove the successful conversion of azide group. To note, a successful CuAAC reaction is can be determined based on conversion of 1,2,3- trizole ring from azide group. The formation of 1,2,3-triazole group by click reaction can be revealed through the loss of peak around 405 eV followed by broadening of peak at 400.0 eV in N1s spectrum shown by Figure 5(b) [11] [13] [22]. The broad peak was correspond to nitrogen atom from immobilized triazole ring while peak at 402.3 eV indicates the formation of C-N bond between azide clicked ethynylferrocene [21]. Besides that, triazole ring formation can be analyzed quantitatively by comparing the peak ratios area between N-N and C-N (2:1 ratio) [19] [24]. However, from the analysis, the ratio calculated was 5:1 which deviated from the review. This might be happened due to some of the carbon forming a bond with oxygen contaminant, thus lead to a lower intensity of C-N bond formation. The incomplete conversion of azide to triazole ring also might contribute to this problem. Apart from formation of triazole ring, another indication to show successful CuAAC reaction is presence of ferrocene moiety which correlates with disappearance of azide derivative. The Fe2p spectrum of click monolayer was displayed in Figure 5(c). A splitting of components at two peaks which represent spin orbit for $Fe2p_{3/2}$ and $Fe2p_{1/2}$ at 708.6 eV and 721.4 eV

respectively were observed [13] [24] [25]. In addition, the absence of Fe(III) species on the monolayer was confirmed as no high-binding energy signal which correspond to this species was detected. This proved that no oxidation of ferrocene units to ferricenium species occurred under the reaction condition used [24]. This became the evidence to show that the experimental condition used was suitable for derivatization of ferrocene species as it can maintain the oxidation state of active species toward the end of reaction.

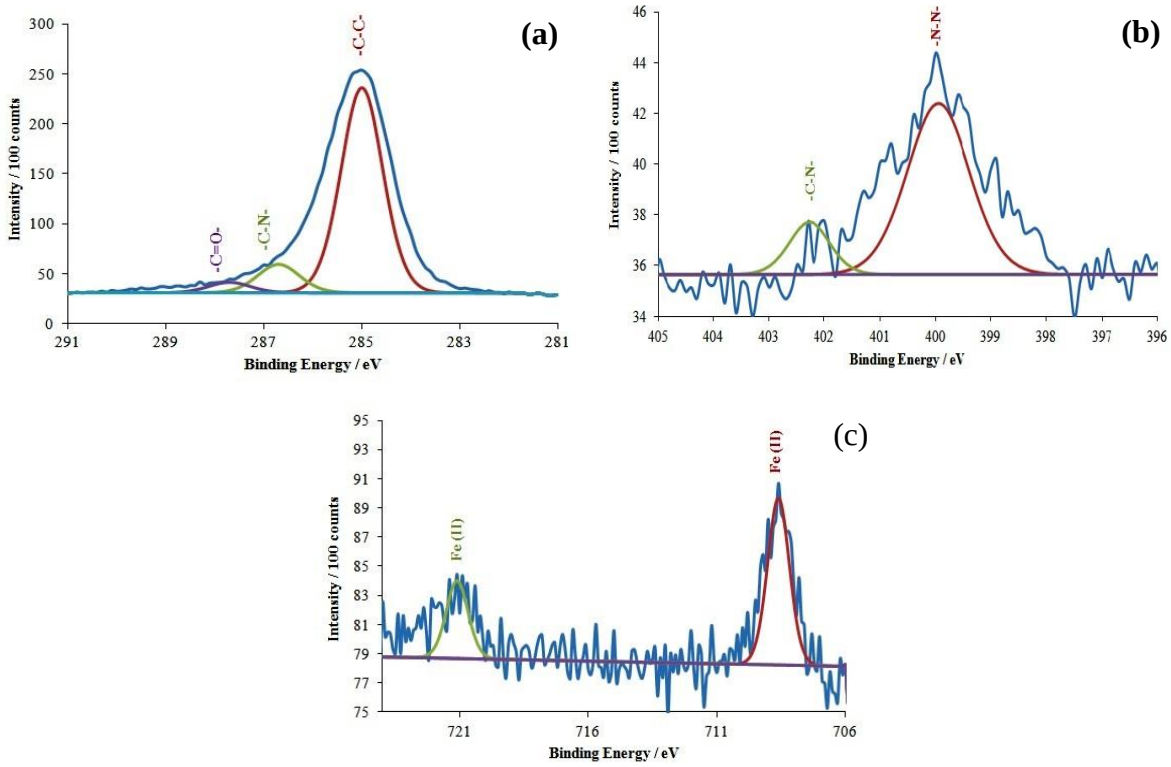

Figure 5 High resolution scan of click monolayer based on (a) C1s spectrum and (b) N1s spectrum and (c) Fe2p spectrum

Electrochemical Behaviour of Click Monolayer by Cyclic Voltammetry (CV)

The electrochemical behaviours of modified electrodes were investigated in neutral solution containing 0.1 M Perchloric Acid solution as supporting electrolyte at scan rate of 100 mV/s. From graph illustrated in Figure 6, it clearly shows that the voltammogram of azide monolayer produce no characteristic peaks which indicates that the redox reaction is inhibited. Even so, this inhibition proved that a highly ordered and compacted azide monolayer was formed on the ITO substrate, thus possess a good blocking current behaviour. In contrast, when looking at the click monolayer voltammogram, it shows a reversible redox reaction indicating that the electron transfer reaction was occured. The ability of the monolayer to show reversible electrochemical properties under scan rate as low as 0.1 V/s concluded that formation of a well-defined SAMs and efficient charge transfer reaction on ferrocene redox group was happened. In addition, the great behaviour was contributed by interaction of extended conjugation of cyclopentadiene group on ferrocene with the 1,2,3-triazole ring [14]. The redox signal also can be directly addressed to indicate occurrence of the catalytic reaction as ethynyl ferrocene could not be able to react spontaneously with the surface azide without presence of catalyst such as Copper (II) that introduced in the reaction [11].

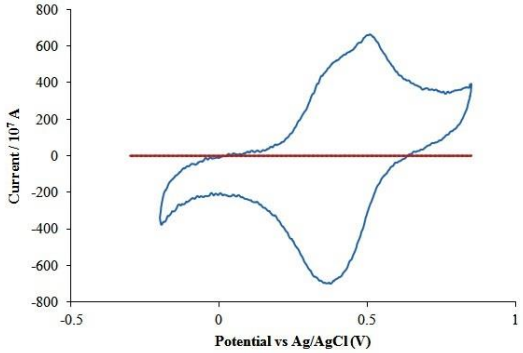

Figure 6 Cyclic Voltammogram of azide monolayer(red line) and click monolayer monolayer(blue line) in 0.1M Perchloric Acid

Conclusion

In summary, an attempt for derivatization of ethynyl ferrocene on modified indium-tin oxide (ITO) by azide derivative 6-azidosulfonylhexyltriethoxysilane (ASTES) was successfully performed. The nucleophilic CuACC reaction was used to "click" ferrocene moiety onto the monolayer to enhance its versatility particularly in sensing application. The results reveal that a uniform and homogenous azide monolayer was formed with higher rms value compared to rougher topography of bare ITO through AFM analysis. Furthermore, a quick confirmation was done from contact angle goniometer tool where the wetting properties of hydrophobic azide monolayer under optimum condition was measured at 75.9° which coincides with literature value. The identification on click monolayer formation was also done by measured wettability 72.6° that indicates a hydrophilic character of ferrocene. Another indication to distighuish the chemical composition between azide and click monolayer was shown by XPS analysis. Based on the narrow scan of C1s, the formation of C-N bond at ~286 eV followed by loss of peak at 405 eV which indicated the conversion of azide to triazole ring followed by detection of Fe2p peaks around 700 eV on the modified monolayer that proved the successful of click reaction. Besides that, the electrochemical results obtained indicates that modification on azide monolayer by CuACC reaction act as a great platform for functionalization process and allow an efficient charge transfer reaction to the ethynylferrocene redox head group, in spite of the alkyl chain length head group based on the high reversibility of electron transfer behaviour of click monolayer. In short, the satisfactory properties shown by ferrocene-azide monolayer suggested that the modified surfaces have a great potential to be applied in development of sensor with great reversibility behaviour.

Acknowledgement

This work was in financially supported by Putra IPS Grant (GP-IPS/2016/9480600) Universiti Putra Malaysia.

References

1. Heise, A., et al., *Mixed silane self assembled monolayers and their in situ modification.* Thin Solid Films, 1998. **327**: p. 199-203.

2. Haensch, C., S. Hoeppener, and U.S. Schubert, *Chemical modification of self-assembled silane based monolayers by surface reactions.* Chemical Society Reviews, 2010. **39**(6): p. 2323-2334.

3. Such, G.K., et al., *Synthesis and functionalization of nanoengineered materials using click chemistry.* Progress in Polymer Science, 2012. **37**(7): p. 985-1003.

4. Collman, J.P., N.K. Devaraj, and C.E. Chidsey, *"Clicking" functionality onto electrode surfaces.* Langmuir, 2004. **20**(4): p. 1051-1053.

5. Martić, S., et al., *Ferrocene-peptido conjugates: From synthesis to sensory applications.* Dalton Transactions, 2011. **40**(28): p. 7264-7290.

6. Lutz, J.-F. and Z. Zarafshani, *Efficient construction of therapeutics, bioconjugates, biomaterials and bioactive surfaces using azide–alkyne "click" chemistry.* Advanced drug delivery reviews, 2008. **60**(9): p. 958-970.

7. Ho, M.Y., et al., *Detection of molecular interactions with modified ferrocene self-assembled monolayers.* The Journal of Physical Chemistry B, 2010. **114**(32): p. 10661-10665.

8. Ganesh, V., et al., *10 years of click chemistry: synthesis and applications of ferrocene-derived triazoles.* Chemistry, an Asian journal, 2011. **6**(10): p. 2670-2694.

9. Srivastava, S., et al., *A self assembled monolayer based microfluidic sensor for urea detection.* Nanoscale, 2011. **3**(7): p. 2971-2977.

10. Wang, M., *Fonctionnalisation des surfaces de diamant dopé au bore et applications en biosciences*. 2009, Lille 1.

11. Collman, J.P., et al., *Mixed azide-terminated monolayers: a platform for modifying electrode surfaces.* Langmuir, 2006. **22**(6): p. 2457-2464.

12. Fernández Landaluce, T., *Molecular motors: from solution to surfaces*. 2013: University of Groningen.

13. Spruell, J.M., *Heterogeneous Catalysis Through Microcontact Printing*, in *The Power of Click Chemistry for Molecular Machines and Surface Patterning*. 2011, Springer. p. 53-71.

14. Yeap, W.S., et al., *Boron-Doped Diamond Functionalization by an Electrografting/Alkyne–Azide Click Chemistry Sequence.* ChemElectroChem, 2014. **1**(7): p. 1145-1154.

15. Iimura, K.-i., Y. Nakajima, and T. Kato, *A study on structures and formation mechanisms of self-assembled monolayers of n-alkyltrichlorosilanes using infrared spectroscopy and atomic force microscopy.* Thin Solid Films, 2000. **379**(1): p. 230-239.

16. Schwartz, D.K., *Mechanisms and kinetics of self-assembled monolayer formation.* Annual Review of Physical Chemistry, 2001. **52**(1): p. 107-137.

17. Yang, L. and Y. Li, *AFM and impedance spectroscopy characterization of the immobilization of antibodies on indium–tin oxide electrode through self-assembled*

monolayer of epoxysilane and their capture of Escherichia coli O157: H7. Biosensors and Bioelectronics, 2005. **20**(7): p. 1407-1416.

18. Huang, N., et al., *XPS study of hydrogen permeation effect on SiC–C films.* Nuclear Instruments and Methods in Physics Research Section B: Beam Interactions with Materials and Atoms, 2003. **207**(4): p. 395-401.

19. Ciampi, S., et al., *Functionalization of acetylene-terminated monolayers on Si (100) surfaces: a click chemistry approach.* Langmuir, 2007. **23**(18): p. 9320-9329.

20. Yue, B., et al., *Hydrogen production using zinc-doped carbon nitride catalyst irradiated with visible light.* Science and Technology of Advanced Materials, 2011. **12**(3): p. 034401.

21. Carroll, G.T., et al., *Adhesion of photon-driven molecular motors to surfaces via 1, 3-dipolar cycloadditions: Effect of interfacial interactions on molecular motion.* ACS nano, 2011. **5**(1): p. 622-630.

22. Prange, J.D., *Development of Stable Metal Oxide Electrodes for the Conversion of Electricity to Chemical Fuels*. 2011, Stanford University.

23. Dementjev, A., et al., *X-ray photoelectron spectroscopy reference data for identification of the C 3 N 4 phase in carbon–nitrogen films.* Diamond and related materials, 2000. **9**(11): p. 1904-1907.

24. Ciampi, S., et al., *Optimization of Click Chemistry of Ferrocene Derivatives on Acetylene-Functionalized Silicon (100) Surfaces.* Electroanalysis, 2008. **20**(14): p. 1513-1519.

25. Ciampi, S., et al., *Tandem "click" reactions at acetylene-terminated Si (100) monolayers.* Langmuir, 2011. **27**(11): p. 6940-6949.

eISBN 978-967-344-778-7